

Measuring Joint Movement Through Garment-Integrated Wearable Sensing

A Dissertation
SUBMITTED TO THE FACULTY OF
UNIVERSITY OF MINNESOTA
BY

Guido Gioberto

IN PARTIAL FULFILLMENT OF THE REQUIREMENTS
FOR THE DEGREE OF
DOCTOR OF PHILOSOPHY/EDUCATION

Adviser: Lucy Dunne

April 2015

© Guido Gioberto 2015

Acknowledgements

This work was supported by the National Science Foundation under grant number IIS 1116719. A very special thanks to Dr. Lucy Dunne for her continuous supervision, and to all members of the Wearable Technology Lab for the support provided.

Dedication

To my lovely wife Kristin and daughter Sofia, and my family all

.....thank you for your love and support

Abstract

Wearable technology is generally interpreted as electronic devices with passive and/or active electronic components worn on the human body. A further sub-set of wearable technology includes devices that are equipped with sensing abilities for body movements or biosignals and computational power that allows for further analysis.

Wearable devices can be distinguished by different levels of wearability: wearable devices integrated into clothing, which are an integral part of the clothes; and wearable devices put on as an accessory. This thesis introduces a novel approach to truly wearable sensing of body movement through novel garment-integrated sensors. It starts from an initial investigation of garment movement in order to quantify the effect that garment movement has on sensor accuracy in garment-integrated sensors; continues with the development and detailed characterization of garment-integrated sensors that use a stitched technique to create comfortable, soft sensors capable of sensing stretch and bend; and ends with a final evaluation of the proposed wearable solution for the specific case of knee joint monitoring in both the stretch and bend modalities.

Table of Contents

List of Tables ...	p. ix
List of Figures ...	p. x
Thesis Overview ...	p. xiv
Ch.1 General Background on Wearable Technology and Smart Clothing ...	p. 1
1.1 Introduction ...	p. 1
1.2 Origins of Wearable Technology and Smart Clothing ...	p. 3
1.3 Wearable Sensing: Monitoring Body Motion ...	p. 7
1.3.1 Wearable Activity-Aware Systems ...	p. 7
Part I. Theory and Foundation: Garment Movement Measurement ...	p. 10
Part I. Introduction ...	p. 11
Part I. Background: Garment Movement Measurements ...	p. 13
Ch.2 Data Collection: The Method ...	p. 15
2.1 Experiment Setup ...	p. 15
2.2 Off-line MOCAP Tests ...	p. 16
2.3 Test Garments ...	p. 19
2.4 Mannequin Data Analysis ...	p. 21
2.4.1 Gait Cycle-based Method ...	p. 22
2.4.2 Garment Positioning Error and Drift Error Definition ...	p. 23

2.4.3 Movement Error ...	p. 25
<i>Movements Error: Size Analysis ...</i>	p. 25
<i>Movements Error: Fabric Analysis ...</i>	p. 26
Ch.3 Results and Discussion: Garment Error Analysis ...	p. 27
3.1 Euclidean Error Distribution ...	p. 27
3.1.1 Ease effect on Garment Noise ...	p. 28
3.2 Positioning Error and Drift Error: Fabric and Size Averages Analysis ...	p. 30
<i>PE Discussion ...</i>	p. 30
<i>DE Discussion ...</i>	p. 32
3.3 Movement Error Results ...	p. 38
<i>Movement Error by Size ...</i>	p. 39
<i>Movement Error by Fabric ...</i>	p. 40
Part I. Conclusion ...	p. 40
Part II. Application: Garment-Integrated Sensing ...	p. 42
Part II. Introduction ...	p. 43
Part II. Background: Garment-Integrated Stretch and Bend Sensing ...	p. 45
Ch.4 Stretch Sensing: The conductive Stitched Stretch Sensors Method ...	p. 49
4.1 Theory: Garment-Integrated Sensors Structures ...	p. 49
4.1.1 Sensor Fabrication ...	p. 51
4.1.2 Top-Thread Cover-Stitched Stretch Sensors Working Principle ...	p. 52

4.1.2.1 Anti-ladder Network Reduction ...	p. 55
4.1.3 Overlock Stitched Stretch Sensor Working Principle ...	p. 56
4.1.4 Bottom-thread Cover-Stitched Stretch Sensor Working Principle ...	p. 58
4.2 Experiment Design ...	p. 60
4.2.1 Testing method ...	p. 60
4.3 Initial Sensors Characterization: Results and Discussion ...	p. 62
4.3.1 Top-Thread Cover-Stitched Sensor Analysis ...	p. 62
4.3.2 Overlock Stitched Sensor Analysis ...	p. 65
4.3.3 Bottom-Thread Cover-Stitched Sensor Analysis ...	p. 66
4.4 Resistance Drift ...	p. 68
4.4.1 Initial Drift Characterization: 2 – 4 – 5 Ply Comparison ...	p. 71
2 – 4 – 5 Ply Discussion ...	p. 77
4.5 Stretch Sensor: Fabric Effect ...	p. 78
Fabric Results ...	p. 79
4.6 Insulated Stretch Sensor ...	p. 81
Insulation Results ...	p. 83
4.6.1 Wash Deterioration ...	p. 84
Wash Results ...	p. 85

Ch.5 Bend Sensing: The Bottom-Thread Cover-Stitched Sensor ... p. 87

5.1 Experiment Design ... p. 88

5.1.1 Sensor Structure and Experiment Setup ... p. 88

5.1.2 Insulated Sensor ... p. 90

5.1.3 Fold Morphologies ... p. 91

5.1.4 Testing Method ... p. 93

5.1.5 Data Analysis ... p. 93

5.2 Average Bends and Fabrics Relations ... p. 95

Insulation and Fold Types Effect Discussion ... p. 97

Fabric Effect Discussion ... p. 100

5.2.1 The Simple Fold case: Alignment and Hysteresis plots ... p. 101

Part II. Conclusion ... p. 106

Part III. Evaluation: Knee Joint Monitoring Through Garment-Integrated Sensing ... p. 110

Part III. Introduction ... p. 111

Part III. Background: Wearable Sensing of Joint Position and Movement, Application of Joint Sensing ... p. 113

Ch.6 Sensing Through Stretch: The Smart Stretchable Pants ... p. 116

6.1 The Bottom Thread Coverstitched Sensor Validation ... p. 118

6.2 Sample Garments and Sensors Location ... p. 119

6.3 Knee angle prediction: Maximum Knee Stretch-based Method ... p. 120

Angle Prediction Error Analysis: Sensors Location Example ... p. 122

6.4 Variability in Sensor ... p. 124

6.5 Variability in Size ...	p. 126
6.6 Human Tests ...	p. 128
<i>Human Tests Discussion</i> ...	p. 130
6.7 Potential Source of Error ...	p. 132
Ch.7 Sensing Though Bend: The Smart Jeans ...	p. 133
7.1 The Folding Method ...	p. 133
7.2 Jeans Preparation ...	p. 134
7.2.1 Source of Error ...	p. 135
7.3 Mannequin Tests ...	p. 135
<i>Mannequin Tests Discussion</i> ...	p. 137
7.4 Human Tests ...	p. 138
<i>Human Tests Discussion</i> ...	p. 140
Part III. Conclusion ...	p. 140
Final Conclusion ...	p. 144
Future Work ...	p. 145
Reference ...	p. 147

List of Tables

- Table 2.1. Fabric Weight Measurement ... p. 20
- Table 4.1. Sensor properties from literature - summary ... p. 46
- Table 4.2. 2 – 4 – 5 ply bottom-thread sensors basic parameters, precision and accuracy ... p. 76
- Table 4.3. Hysteresis Error (Ohms) at 10% elongation ... p. 81
- Table 4.4. Stretch Sensor - Insulation Results ... p. 84
- Table 5.1. Averages over simple-intermediate-complex bends, less stiff-more stiff fabrics - Insulated and Un-Insulated Sensors ... p. 96
- Table 5.2. Stitched Stretch and Bend sensors parameters summary ... p. 108
- Table 6.1. Knee bend prediction error ... p. 123
- Table 6.2. Knee Bend (pinned) – Between- and Within-sensors Error ... p. 125
- Table 6.3. Knee Bend – Within-sizes Error by Size ... p. 127
- Table 6.4. Knee Bend – Between-sizes Error ... p. 127
- Table 7.1. Sensor characteristic, mannequin tests ... p. 137

List of Figures

- Figure 2.1. MOCAP connection diagram (*BTS BioEng.*, IT) ... p. 16
- Figure 2.2. Normalized gait cycles of Marker 1 ... p. 18
- Figure 2.3. Test garment, mannequin, and markers location ... p. 19
- Figure 2.4. Test garment with nested size grade ... p. 21
- Figure 3.1. Normalized Euclidean distance over a gait cycles for markers 2-20. Markers location is shown in Figure 2.3 ... p. 27
- Figure 3.2. Denim jeans, over 5 different sizes ... p. 29
- Figure 3.3. PE of markers grouped by vertical levels, for all sizes: on the left pants 80833; on the right, Pants 52735 ... p. 31
- Figure 3.4. Best-fit line Positioning and Drift error, Marker 2 size +2 ... p. 33
- Figure 3.5. Best-fit line Positioning and Drift error, Marker 8 size +2 ... p. 34
- Figure 3.6. Best-fit line Positioning and Drift error, Marker 13 size +2 ... p. 35
- Figure 3.7. Total displacement (DE) during experimental period of markers grouped by vertical levels, for all sizes ... p. 37
- Figure 3.8. Average by level over 5 different fabrics for all sizes ... p. 38
- Figure 4.1. ASTM D-6193, ISO# 602 top- and bottom cover stitch ... p. 50
- Figure 4.2. ASTM D-6193, ISO# 514 overlock stitch structure ... p. 51
- Figure 4.3. Juki MF-7723 high-speed, flat-bed coverstitch machine ... p. 52

- Figure 4.4. Top-thread sensor and bottom-thread cover ... p. 53
- Figure 4.5. Top-thread stitched sensor: relaxed position on the left; stretched position on the right ... p. 53
- Figure 4.6. Top-thread stitched sensor, electric equivalent: relaxed and stretched position ... p. 54
- Figure 4.7. Basic stitch configuration: “closed”, “open”, “ladder” stitch ... p. 55
- Figure 4.8. Antiladder network equivalent resistance: (a) antiladder basic; (b) antiladder reduced; (c) $\Delta \rightarrow Y$ transformation; (d) series and parallel reduction ... p. 55
- Figure 4.9. Overlock stitched sensor, reduction: relaxed and stretched position ... p. 57
- Figure 4.10. Bottom-thread stitched sensor, reduction: relaxed and stretched position ... p. 59
- Figure 4.11. Stitched Stretch Sensor Test, initial flat fabric position ... p. 61
- Figure 4.12. Top-thread output: normalized resistance aligned with normalized extension and Resistance vs Elongation ... p. 63
- Figure 4.13. Overlock output: normalized resistance aligned with normalized extension and Resistance vs Elongation ... p.65
- Figure 4.14. Bottom-thread output: normalized resistance aligned with normalized extension and Resistance vs Elongation ... p. 67
- Figure 4.15. Bottom-thread sensor in stretched position for more than 40 minutes ... p. 69
- Figure 4.16. Bottom-thread consecutively stretched and relaxed for 100 cycles ... p. 70
- Figure 4.17. 2 – 4 – 5 ply Bottom-thread sensors ... p. 72
- Figure 4.18. 2 – 4 – 5 ply Bottom-thread sensors normalized responses for 25% stretch ... p. 73

Figure 4.19. 2 – 4 – 5 ply Bottom-thread sensors normalized responses for 35% stretch ... p. 73

Figure 4.20. 2 – 4 – 5 ply Bottom-thread sensors normalized responses for 50% stretch ... p. 74

Figure 4.21. Normalized peak-to-peak response range for each test fabric ... p. 80

Figure 4.22. Hysteresis magnitude for each test fabric ... p. 80

Figure 4.23. Insulated bottom-thread stretch sensor ... p. 82

Figure 4.24. Insulated bottom-thread stretch sensor output ... p. 83

Figure 5.1. Denim Sample with zoom of the stitched sensor ... p. 88

Figure 5.2. Denim Bend Test Setup: Denim sample clamped between INSTRON plates, and connected to Digital Multimeter ... p. 89

Figure 5.3. Insulation by Fusing technique: a strip of bonding film is fused on the stitched sensor ... p. 90

Figure 5.4. Denim Sample Layout for Controlled Bend: location of perforations for guide rods to control the number of folds ... p. 91

Figure 5.5. Fold Types drawing ... p. 92

Figure 5.6. Baseline Resistance normalized by fold length: Un-insulated case. Insulated case ... p. 98

Figure 5.7. Normalized alignment, Simple Inner Fold: Un-insulated case. Insulated case ... p. 102

Figure 5.8. Hysteresis, Simple Inner Fold: Un-insulated case. Insulated case ... p. 103

Figure 5.9. Normalized Alignment, Simple Outer Fold: Un-insulated case. Insulated case ... p. 104

Figure 5.10. Hysteresis, Simple Outer Fold: Un-insulated case. Insulated case ... p. 105

Figure 6.1. Stitched Stretch Sensor responses of 3" long sensors for 25% elongation (.75") ... p. 117

Figure 6.2. Tensile Evaluation of Sensor Response ... p. 118

Figure 6.3. Bottom-thread coverstitched sensors stitched on the frontal side of the left knee of a cyber mannequin ... p. 120

Figure 6.4. The polynomial model std error, for knee bend angle prediction ... p. 121

Figure 6.5. Model and maximum stretch region sensors responses ... p. 123

Figure 6.6. Human Squats, Knee Bend, and Sit for 5 knee bend repetitions ... p. 129

Figure 6.7. Human Walk @ 1MPH and 2MPH for 8 steps ... p. 129

Figure 7.1. Bottom-thread coverstitched sensor integration, and experiment setup ... p. 134

Figure 7.2. Aggregate responses of dorsal and lateral sensors, compared to true knee joint angle ... p. 136

Figure 7.3. Sensor responses and joint angle for human knee bend task, sit/stand task, and squat task ... p. 139

Thesis Overview

This dissertation develops a novel analysis, methodology and approach to body sensing through garment integrated sensors to detect body motion providing a better trade-off between sensing accuracy and wearer comfort. It is organized into 7 chapters. Chapter 1 introduces the research topic by defining wearable technology and smart clothing starting from its origins and providing more examples of wearable technology and wearable sensing solutions developed today for body motion. The following 6 chapters describe the novel contributions made in the Wearable Technology area, and are organized into three parts chronologically aligned to the research progress and discovery: Part I “Theory and Foundation: Garment Movement Measurements”; Part II “Application: Garment-Movement Sensing”; and, Part III “Evaluation: Knee Joint Monitoring through Garment-Integrated Sensing”.

Part I builds the theory of sensing through loose-fitting garments and defines some key fundamentals of the key variable under investigation: garment movement. An investigation of the garment noise introduced by garment movement and garment position on different areas of the lower body under different garment ease conditions is presented in Chapter 2, and discussed in Chapter 3. Feasible garment regions are identified for garment-integrated sensing.

Part II introduces a novel garment integrated solution for body sensing. Chapter 4 describes the stitched stretch sensing approach and covers all types of stitched stretch sensors implemented together with their comparison; similarly, chapter 5 focuses on the bend sensing modality with reference to one stitched sensor most capable of detecting bend due to its structural properties that provide bend sensing ability as well as stretch, as illustrated in the previous chapter 4.

Finally in Part III, based on the knowledge of garment movement and the novel garment-integrated sensors for garment sensing, the knee bend angle is predicted as an evaluation case of

the new approach to body sensing. Chapter 6 evaluates the accuracy of the knee bend angle prediction of a stretch sensor integrated on a pair of stretchable pants and the error introduced by variables of sensor fabrication tolerances and by the practical case of donning and doffing. Chapter 7 evaluates instead the accuracy of the knee bend angle prediction of a bend sensor integrated on a pair of un-stretchable jeans. Controlled and un-controlled scenarios for both types of sensors to predict the knee bend are considered.

In summary, parts I and II provide a basis and justification for part III: part I formulates a statistical method to analyze noise variables involved with garment sensing, in which the noise distribution over different garment locations is characterized and potential causes are identified. Part II introduces the core approach for garment sensing, based on the novel stitched sensors that allow measurement of garment movements while preserving comfort of the user. Finally, part III contains an evaluation of the theory presented in part I and the application developed in part II for the specific case of knee bend estimation, using truly wearable sensors. All three parts have the same structure with initial Abstract, Introduction and Background sections followed by chapters that describe in detail the contribution. More introductory details about each of the chapters are provided in the introduction sections specific to the chapter.

Chapter 1

General Background on Wearable Technology and Smart Clothing

1.1 Introduction

Smart clothes look and feel like normal clothes but with the addition of smart capabilities such as hands-free interactions with computing and information devices, and the potential to provide portable, continuous, convenient and comfortable assistance to the wearer for health, fitness, sports, gaming, entertainment and other everyday applications.

Smart clothing belongs to the broader area of wearable technologies that bring together computing power, electronics, e-textiles, and functional clothing. Wearable Technology has been presented as the interaction of two sub-groups [1]:

- Wearable Computers sub-group, defined as body mounted devices furnished with computational power, often used to enable the flow of information to and from the user;
- Smart Clothing sub-group, defined as garment-integrated devices that integrate electronics with fabric or garment functionality, for example to enable the sensing of garment movement [2].

Both sub-groups overlap with apparel functionality by making apparel functions dynamically adaptable depending on situational changes so as to improve perceived user comfort (physical, cognitive, or emotional comfort). In fact, reliability and accuracy are not the only factors that arise in the development of wearable technologies: comfort and perceptibility of the device by the wearer represent critical variables for the effective practicality of the wearable solution.

T-shirts, pants or any other fabric-based items that are worn follow the body movements, providing therefore a non-intrusive and accessible way to sense the body, specifically body movements. The correlation between body and clothes movement strongly depends on variables directly related to the garment: for example the amount of wearing ease in the cut of the garment (difference between the circumferences of the body and the garment), or the stiffness and hand of the textile, affecting folding or wrinkling behavior [25] [47]. Decreasing the ease defined as the difference in diameter between the same body and cloth section may bring the garment closer to the body decreasing relative garment fluctuations respective to the body, but at the same time can increase the number of folds and wrinkles during body movements, for example during a joint bend. In the same way, increasing garment ease increases body-garment fluctuations but decreases folds and wrinkles (favoring a few large folds rather than many small folds) [28]. Another fundamental variable that depends on the garment ease is wearer comfort, which can imply willingness to wear the smart sensing solution and employ a proper use of it. Thus appropriate sensing garment design and implementation are critical, and specific to the application case.

Body monitoring is an example of practical use for smart clothes. Body monitoring through electronics integrated into clothes allow for local collection and storage of data that can be then read and analyzed remotely: for instance, through ambulatory monitoring the number and duration of clinical visits could be drastically reduced and the specificity of treatment sessions improved because of the additional ability to consider data captured during daily activities of the

patient. In general, however, body monitoring is more accurate in full skin contact at the expense of minor comfort and reduced practical utility of the wearer (especially for long term monitoring).

The following section 1.2 is a general background on wearable technologies and smart clothing starting from its origins, underlining some key points of failure, and showing how clothes were part of the very first conception of wearable devices and the ability of bringing computers closer to the human body. The chapter then ends with a literature review wearable sensing for body monitoring, in order to provide an overarching general background and context for the work.

More introduction and background will be introduced in each of the following chapters as well, specific to the topic covered of each Part, specifically: Garment Movement in Part I; Garment-Integrated Sensing in Part II; Wearable Sensing of Human Joints in Part III.

1.2 Origins of Wearable Technology and Smart Clothing

“Wearable Technology” finds its root in the earliest wearable computing concept of body-worn technological devices. Mann’s Wearcam (MIT 1980) is one of the first examples of wearable prototypes that started to evolve, growing enthusiasm on the potentials of combining wearable electronic with computers computational power. Mann’s camera was a wearable photography equipment (camera + flashlight + battery) integrated onto a helmet. New electronic devices with wearable characteristics started to be introduced in the market: The Walkman (Sony, 1979) a portable music cassette player; The Polar heart rate monitor (Polar, 1982), was the first available heart rate monitoring system that could be worn unobtrusively with a wrist worn watch unit and a sensor belt around the chest.

In the late 1990s the idea of using electronic textiles to integrate electronic components by means of soft substrate was born at the MIT laboratories. With the aim of making wearable computing

truly wearable, Post et al. [3] describe the development of electronic embroidery to integrate technology directly into textile and clothing. These authors demonstrated that textile-based computing compares favorably to conventional printed circuitry and has advantages over existing flexible circuit substrates (i.e., in their design of a flexible multichip module fabric keypad readout) with respect to durability, conformability, and wearability. Examples of electronic circuits made out of conductive textiles (i.e. conductive threads and fabrics) were created at the MIT Media Lab in 1997¹. Conductive and non-conductive textiles were used in combination to create more robust and aesthetically pleasing solutions to light LEDs of various colors integrated on a dress (FireFly Dress) or to communicate using a simple touch of fabric covered buttons on a jacket messages through processors integrated on pants to an LCD mounted display integrated in the jacket (The Serial Suit). A few years later the Virginia Tech E-textile Laboratory started the development of hardware and software architectures for the design of “tailor made” e-textile fabrics, improving the wearability and ease of production of wearable technologies. Martin et. al. [4] presented a design framework with the goal of manipulating design variables such as number, type and location of components to optimize materials, manufacturing costs, comfort and accuracy of sensing applications.

In 1996, the Georgia Institute of Technology in collaboration with the research department of the United States Army started developing a versatile platform called The Wearable Motherboard, a smart shirt with integrated fiber circuitry with a “plug and play” interface for monitoring soldiers. Findings on comfort, versatility and un-obtrusiveness were important for medical applications such as EKG or body temperature monitoring, reducing healthcare costs and time spent at the hospital, and made it accessible to more people and professionals [5].

One of the first interdisciplinary projects that showed the difficulties and compromises faced in the design of a wearable system is the Reima Cyberia Survival Suit (launched at the Hannover

¹ <http://pubs.media.mit.edu/pubs/papers/a13.pdf>

World Expo, Germany May2000) [6]. The Cyberia is a snowmobile body suit designed to monitor body data through motion sensors that detect posture, movement and impact among other functionality of ECG or body temperature monitoring for example. This was a project shared between industry and academia: the clothing manufacturer Reima Ltd with expertise on outdoor clothing; the University of Lapland for industrial and clothing design; and, the Tampere University of Technology for electronics and body monitoring. The main academic goal was to explore how clothing and electronic fields align. The project showed the practical issues and the tradeoffs faced in designing a functional and working prototype:

- Circuitry and battery placement: heavy electronic packs with circuit boards and batteries had to be evenly distributed over a larger surface on the back so as to not restrict movements, leaving elbows, shoulders and knees joints free;
- Sizing: the vests had to be made with adjustable elastic bands, to accommodate small and larger sizes for both males and females;
- Washability: detachable electronics were necessary to allow the for the cleaning of the suit;
- Wiring: sensor layout was minimized so as to avoid unnecessary and uncomfortable wiring.
- Clothing and Electronic Domains: one of the major obstacles of the project was communication between people with extremely different backgrounds such as textile experts and electronic engineers: misunderstandings prolonged the duration of the projects whenever the subject was merging textiles and electronics.

Moreover, durability of the suit is another concern that arises: wires crossing the joint should be able to withstand hundreds or thousands of flexion cycles without breaking. The main limitations of the Reima Cyberial Suit product were the limited target population, high cost, limited comfort and size availability.

E-textiles use conductive fabrics to integrate electronics and enable wearable computing in interactive clothes. Smart clothing implements e-textiles to assist and simplify communication, health and safety applications during daily life, improving users' mobility, convenience of the wearable application, and quality of life in general [7]. E-Textiles offer the potential to develop more appealing wearable electronics, increasing the level of acceptance and comfort. The practicality of the wearable solutions is thus not just limited to the garment's aesthetics but also to emotional variables directly related to the user such as sensitivity and comfort as well as reliability of the e-application. Moreover, aesthetics, comfort and reliability of the wearable device have been found to be correlated in medical healthcare monitoring where an uncomfortable or attention-demanding device can change the behavior of monitored patients, with the result that the collected data does not reflect the patient's lifestyle [8]. Relationships between functionality and comfort of wearable devices for the case of an armband and a backpack show that the function of any wearable tool must overcome both physical and social discomfort in wearing it, and that the perceived functionality of the device influences its perceived wearability [9].

Nowadays wearable devices evolved in a technology of normal/daily use: for example, Mann's camera through the Go Pro Camera; the Walkman experience through digital players (including smartphones) like Ipods, iPhones, or Android phones; the Polar heart rate monitor implemented through a variety of skin-tight chest and wrist bands for example. The continuous evolution of

digital techniques and conductive fabrics and materials open to more accurate, reliable, and comfortable wearable devices as well as to novel applications and user experience.

1.3 Wearable Sensing: Monitoring Body Motion

The proximity of body worn sensors to the human body allows for increased data capture and tracking of human daily activity, so as to continuously learn (and, in some cases, eventually correct bad habits) behaviors or body postures and movements as in the case of activity-aware systems [10], under various contexts and situations. Edminson et al., design a cost effective, easy to use e-textile suit particularly suited for elder patients that provides an alternative method for gait analysis (or repeated motion analysis) which, at that time, was traditionally performed in a video-based locomotion laboratory [11]. A wave pattern in the fabric integrated on the suit a network of wires, sensors, and processors that provided the required level of accuracy (i.e. the same accuracy level computed by video-based gait analysis systems), fault tolerance, and energy consumption.

The comfort and invisibility of the integration of the wearable sensors is critical in order to minimize the perceptibility of the wearable device by the wearer and thereby increase its acceptance, leaving its effective use unbiased or unconditioned because the wearer does not draw the attention of others and the wearable device does not interfere with normal wearer actions.

1.3.1 Wearable Activity-Aware Systems

Activity-aware systems for body monitoring are employed to assist human needs and to measure static postures and dynamic body movement, in a variety of contexts. Dunne at al. designed a wearable body-monitoring device to detect seated postures [12]. A Plastic Optical Fiber (POF)

sensor integrated on the back of a shirt along the spine detected the overall spinal bend by measuring the reflected light traveling through the fiber which decreased as the fiber was bent. Einsmann et al., developed a wearable full 3D body motion system based on the time-of-flight between ultrasonic emitters and receivers to measure the distance between points on the body allowing an e-textile garment to sense its own shape [13]. Ultrasonic emitters on the torso located at stable reference points were connected to receivers on the limb through e-textile connections. Torso movements caused relative distance variation between reference points and torso rotations caused garment or body parts to block the signal transmitted through the textile or reduced the strength of the received signal. A more cumbersome solution for dynamic body movements and human posture monitoring was proposed by Yang et al. [14]. Dome shaped e-textile digital sensors capable to detect pressure points were attached on two sides of the elbow and knee joints, upper arms and buttocks of typical athletic apparel. A control box was clipped on the belt. Both the sensors and the clip were knitted onto the textile with conductive yarn fiber. Additional dome shaped sensors were embedded in the socks for plantar pressure sensing. Gait cycles of fast/slow walking, walking up/down the stairs, veering around as well as falling down were analyzed by monitoring the coordination between body and feet.

A traditional low cost system for gesture analysis relies on a sensing network of nodes wirelessly interconnected, with each node consisting of a 3-axis accelerometer, a 3-axis magnetometer, and a 3-axis gyroscope [15]. This latter example is constructed of identical interconnected circuit boards consisting of inertial measurements units, strategically attached at opportune body locations with little consideration of user comfort or aesthetics.

The common denominator between the different wearable solutions should be the comfort provided to the wearer that, however, has not always been prioritized because more attention is given to the technical performance rather than to the overall wearability of the system. A truly wearable device should always be wearable during body motion [16]. Gemperle et al. evaluated

the available real estate on the body surface and the relative advantage of different body locations in terms of wearability. They identified hip, waist, thigh, and calf body segments as comfortable and unobtrusive dimensional spaces in the guidelines for dynamic wearability. However this study has not provided support for the contemplated dynamic scenarios. Body movement is proportionally related to wearability, and vice-versa, but to capture the full body dynamics it is necessary to step one degree away from the body to a garment surface, preserving the wearability factor and making it possible to capture the full body dynamics.

The following chapters will start to gradually build and put together all the pieces for a new approach to body movement monitoring based on garment movement sensing as evaluated from the kinematics of the knee joint.

Part I. Theory and Foundation:

Garment Movement Measurement

The noise introduced into the signal of a wearable sensor due to slippage or movement of the garment housing the sensor over the body is frequently acknowledged as an important barrier to successful long-term body monitoring. Garment movement as a noise source has not previously been studied in depth. Awareness of the user is a key influence to the success or failure of a wearable sensor. Most wearable sensors seek to measure or monitor parameters of the body as accurately as possible, yet sensors are notoriously plagued by the error that may be introduced by the movement of the sensor over the body surface.

Quantifying the movement of a garment relative to the body surface presumes a measurement of the displacement of an hypothetical body sensor embedded in a garment which can be expressed as “error” or “movement noise” in some body sensing applications. Here an analysis of this error is developed through a controlled statistical approach based on the repeated gait cycle movement of an animatronic running mannequin (at slow speed motion) to extrapolate the garment movement noise in a pair of pants worn by the mannequin during the run gait cycles.

Part I. Introduction

Body sensing devices are used in a large variety of applications, from medical monitoring to human-device interface. The most reliable and accurate way to sense the body has traditionally been the second-skin approach, an approach that uses a skin-tight garment or suit to help the sensor to stay as close as possible to the body surface so as to maximize the accuracy of the sensed body signal and minimize potential misplacement or movements of the sensor during body motion which would add noise and disturbance to the sensed signal. It has become clear that the second-skin approach that characterized many early prototypes presents problems of physical and emotional comfort, as well as logistics in dressing and use, that are prohibitive to the ultimate success of the wearable system in everyday use due to reluctance on the part of users or observer effects of the technology [19]. It is often the case that variables that promote comfort and ease of use for the wearer are directly opposed to variables that improve the accuracy of the sensor. This tradeoff presents one of the most significant obstacles to widespread adoption of wearable sensor systems: sensing garments that are wearable and acceptable for everyday use can significantly limit the utility of the sensor, while sensing garments that produce high-quality data can limit the feasible user group and/or the expected compliance level. Measuring and analyzing the movement of garments of specific properties relative to the body surface is an essential component in overcoming the comfort/accuracy tradeoff of wearable sensing. In addition, traditional sensing techniques often rely on components and approaches developed for sensing outside of the wearable environment, and consequently do not often prioritize the physical comfort of the component parts. This gap in available options has led to the development of textile-based sensing techniques that integrate the comfort properties of fibers, yarns, and textiles with electrical properties to yield sensing abilities.

The following sections discuss the prior work that has been conducted in the area of measuring and analyzing garment movement. A novel method for analyzing the error introduced by garment properties in garment-integrated wearable sensors during body movement is then implemented. The method aggregates successive gait cycles method and computes a measurement of the garment movement relative to the body in terms of the linear distance of the garment from the body over time, by measuring through motion-capture the movement of garments worn by an animatronic mannequin and comparing that movement to the movement of the mannequin itself. The results of two preliminary evaluations measuring the movement of a skin-tight bodysuit and a pair of denim pants are presented. Two fundamental error metrics are computed: the errors introduced by donning and doffing of a garment (named garment Positioning Error) and by garment drift during the gait cycle (named Drift Error). These are assessed in detail in order to quantify the movement of the garment. Two additional sources of error are then investigated in detail: repetitive garment movement due to garment ease defined as the difference in circumference between body and garment dimension; and, repetitive garment movement error due to differences in textile properties, specifically in weight variation of textiles with identical fiber content and weave structure.

Predictability and distribution of the noise are factors that must be taken in account to improve the accuracy of garment-integrated sensors to capture body movement when the garment is used as an infrastructure for body sensing.

Part I. Background: Garment Movement Measurements

The error introduced into wearable sensor signals by garment-related parameters is a problem in many application areas. Sensor misplacements or movements affect most types of wearable sensors by adding attenuation or distortion to the input data, for example in the case of electrodermal sensors [20] that sense heart and muscle activity, in which case the signal itself can be interrupted due to electrode slippage on the skin, or in the case of inertial sensing units [21] like accelerometers, magnetometers, and gyroscopes which sense position and movement, in which case the signal continues but presents inaccurate information about the body movement. If the movement or slippage of the sensor is originated by body motion, then the distortion in the sensor output is referred as motion artifact. The most common approach to reduce movement noise and minimize the effect of motion artifact in wearable sensors is motion prevention or minimization, by attaching the sensor tightly to the body using elastic, straps, adhesive, or a skin-tight garment (e.g., [22]).

Motion artifacts have been recognized as a major limitation for wearable monitoring solutions [20]. Motion artifacts lead to a degradation of the observed signal quality, making impossible to satisfy the clinical requirement. In the study by Such and Muehlsteff, ECG signals captured by two different embodiments are compared: a belt (in direct contact with the skin); and underpants (a normal pair of men underwear) which waistband integrates the same circuitry as in the belt. The belt showed more error caused by motion artifacts and variable positioning on the body, with an average value of good signal coverage between 60-80% compared to the 80-90% of the underpants, during 24h. In another clinical application, a wearable ECG device constituted of conductive fabric sensor was compared with the traditional Ag-AgCl electrode ECG device under motion artifacts showing similar performance [18].

In cases where improving mechanical coupling in surface sensors is not sufficient to reduce or remove motion artifacts (for example when the garment cannot apply sufficient force to the body, or where the wearer's movement is sufficiently vigorous), other countermeasures have been investigated, such as arrays of redundant sensors [23]. Harms et al. have undertaken significant study of the impact of garment movement on sensor signal quality, both in measuring the effects [24], and in modeling the impact of sensor orientation and textile folds using a simplified model of textile and garment properties [25] [47]. Their work focuses primarily on the effects of movement and fabric wrinkles on inertial sensors. Previous work established a method of measuring the movement and position of a garment relative to the body surface [26], and employed this method to explore the variability in error measured over the lower body [27].

Dunne [28] explores an experimental approach in garment design to address style and fit as to provide an alternative to skin-tight garments for spinal posture sensing using an optical bend sensor constituted by a rigid optical fiber integrated in a shirt along the spine. The impact of garment ease (or fit) is investigated. Contrary to what should be expected in a skin-tight garment, increasing the garment size in this case led to the sensor responses having a higher correlation with a test spine bend reference signal, showing smaller garment-interference with the sensor response. Since the output of the optical fiber sensor is related to the curvature of the fiber, this opposite trend is justified by the inextensibility of the optical fiber which causes it to buckle more for smaller sizes so that the output signal is less representative of the spine curvature.

Chapter 2

Data Collection: The Method

To initially explore the potential effect of garment movement on sensor signals, experiments were conducted to analyze the garment movements of a pair of pants during a walk/run. To capture the garment movement an IR (infrared) motion capture system was used. 25 pairs of custom made denim jeans were tested, consisting of: 5 fabrics of different weight and stiffness, and for each fabric 5 jeans sizes (basic, +1, +2, +3, +4: each with a 1” increase at the waist and hip, tapered down to a ¼” circumference increase at the ankle).

2.1 Experiment Setup

An animatronic running mannequin (Cyberquins, UK), comprised of an electro-mechanical skeleton with a self-skinning urethane foam shell that is mechanized to reproduce a human run, was positioned in the middle of 6 infrared cameras. Retro-reflective markers were strategically attached to the mannequin surface and the garment surface (in separate trials) in the areas of interest so that each marker can be “seen” by (is visible to) at least three cameras in order for the data point to be captured. The motion capture system (BTS Smart-E, BTS Bioengineering, IT) collected position samples from the retro-reflected IR ray and mapped them on a 3D coordinate space (X, Y, Z), with nominal sampling rate of 60Hz. The retro-reflective markers are of negligible weight, thus were assumed to not introduce motion artifacts in the garment. Raw data were then sent to and stored in a Windows PC data file using the BTS proprietary software.

Figure 2.1 illustrates the actual camera layout from a top view. Given the symmetry of right-left

sides of the mannequin, the retro-reflective markers were placed only on one side of the mannequin closer to the cameras, and the 6 cameras were placed so to cover 180deg around it preserving visibility of all markers.

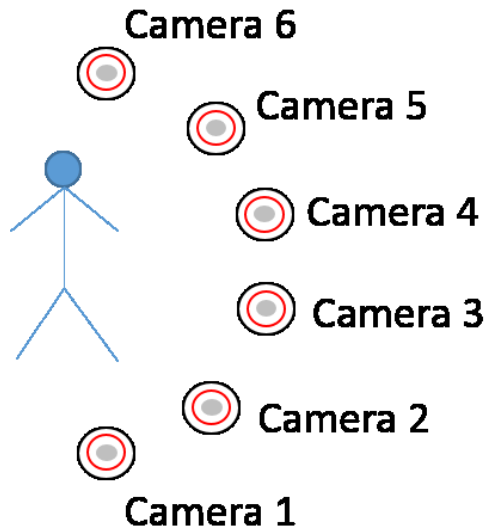


Figure 2.1. MOCAP camera setup, top view

2.2 Off-line MOCAP Tests

The objective of the first experiments is to analyze the garment movement of a pair of pants during running. Two parallel experiments were conducted: markers were strategically placed on the mannequin's skin-tight suit, and the location in 3D space of each marker was captured at each time instant during the mannequin run. Subsequently, markers were placed in the same locations on top of a pair of pants worn by the mannequin (figure 2.3), and the positions of these markers were captured in the same way. The movement of markers on the garment surface was then compared to the movement of the corresponding markers on the mannequin surface. Because the

mocap system relies on line-of-sight, it was necessary to capture these two layers separately and compare them off-line. The mannequin precise gait cycle insures the same “input signal” for both tests.

The mannequin run describes a repeated gait cycle over time by alternating flexion and extension of right and left leg which for each marker is represented by a periodic function, where one period corresponds to one gait cycle along each direction, either X, Y, or Z. This property is exploited for the marker alignment of the two parallel experiments mentioned above (aligning the periods of body and garment markers), by using a gait cycle reference marker placed on the heel (right foot, figure 2.3), labeled as Marker 1. The marker alignment is a key step to compare sample values of markers on pants and markers on the mannequin’s body at the same spatial location (in the following, markers on pants are referred to as *pants*, and markers on the mannequin’s skin tight suit as *body*). Marker 1 gait cycles captured during the experiment are shown in figure 2.2: the plot on the left shows the normalized position coordinates of marker 1 movements during both experiments, while the plot on the right show the normalized position coordinates for the same experiments along each coordinate separately. Comparing the position coordinate of figure 2.2 with the mannequin movement, when $Mkl.X$ and $Mkl.Y$ increase the right heel goes up and goes back down when $Mkl.X$ and $Mkl.Y$ decrease; $Mkl.Y$ represents the right knee bend when decreases; $Mkl.Z$ position coordinate is a factor 10 smaller than the other two so that it shows the mannequin oscillations during the run, and it is out of phase since Z axis is almost perpendicular to the 2D plane (i.e., (X, Y) plane) of the run movement.

It is important to notice that because Marker 1 is located on the mannequin’s foot, it is not affected by the presence or absence of a garment, and follows the same path for both body and pants experiments. From the plots on the right in figure 2.2, it is also clear that the X component ($Mkl.X$) has the most regular wave. The alignment of the two experiments is therefore done by

synchronizing Marker 1 along the X coordinates, at each time instant, by detecting the peak position, relative to the gait cycle period, of the waveform.

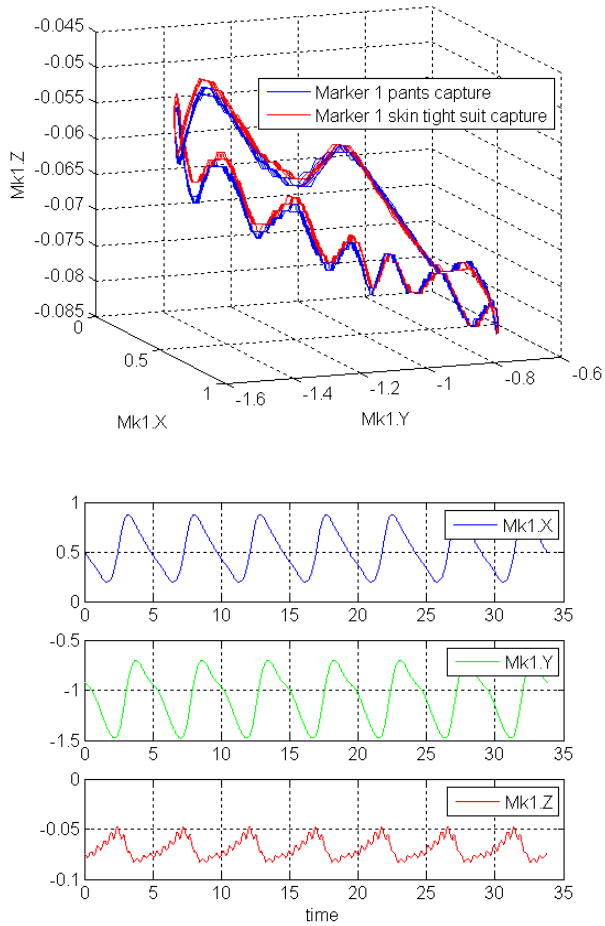


Figure 2.2. Normalized gait cycles of Marker 1. On the top, the gait cycles are a function of all three spatial coordinates X, Y, and Z. The red line refers to the skintight suit while the blue one refers to the pants. On the bottom, the same gait cycles are shown along each spatial coordinate, separately, for a 35 second experiment

Additionally, another reference marker, called Marker 0, is considered in order to compensate the mannequin oscillations, located on the waist above Marker 4 in figure 2.3 directly attached on the

mannequin. The mannequin is connected to a metal arm that keeps it suspended, as shown in figure 2.3. During motion, the articulations of the legs generate oscillations of the arm that propagate in the signals reflected to the IR cameras, resulting in a small deviation of the captured samples from their actual value. Such oscillations are visible along the Z coordinate of Marker 1 in Figure 2.2, above. To correct the oscillations, the coordinate system origin is moved to the location of Marker 0, by subtracting the position of Marker 0 from all other markers along each coordinate individually. Marker 0 is affixed directly to the mannequin, and it is unaffected by the presence or absence of a garment.

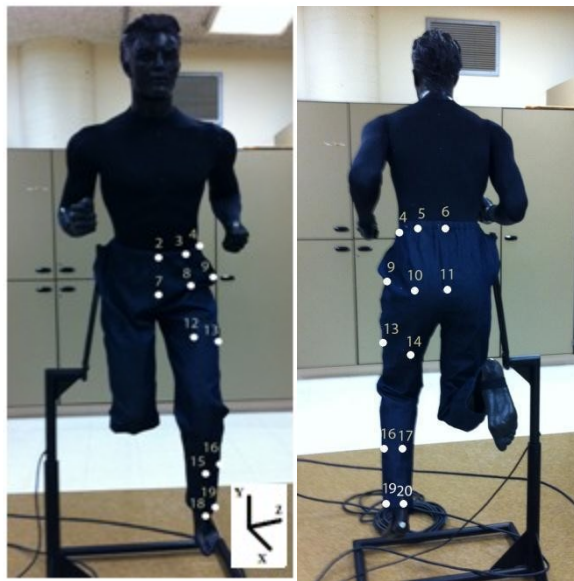


Figure 2.3. Test garment, mannequin, and markers location

2.3 Test Garments

A total of 5 fabrics different in weight and stiffness are used to study the garment movement. The sample stiffness was measured according to the ASTM D 1388 standard: a strip of fabric is

placed on a tool that has a flat part that then falls away at a 45 deg angle; the strip slides along the flat part until it bends down and touches the incline. The Inch measurement is how far the strip went down before touching the incline, with higher values corresponding to stiffer fabrics. For the fabrics tested, the following approximated stiffness listed on Table 2.1 was measured.

Table 2.1. Fabric Weight Measurement

Item No.	Manufacturer's specified weight (oz/yd ²)	Stiffness - ASTM D 1388 (cm)
80270	14.50	10.47
81415	13.75	11.17
80833	12.75	12.00
81814	12.50	10.60
52735	9.75	6.00

This is an initial experiment, it uses only one of the available fabrics used later. The test garments used in this experiment are all constructed from the same bolt of denim (100% cotton twill, 12.5 oz) with intermediate stiffness properties, listed on table 2.1 with no. 81414. A base pattern, fitted to the mannequin, was initially developed (size "base") using a common drafting procedure for men's trousers. This pattern (depicted in figure 2.4), was modified to include extra rise/fullness in the posterior, to allow the mannequin's hip to flex unimpeded (impeding the motion of the mannequin significantly can damage its mechanism). The base pattern was then graded into five sizes using a custom grade, which increases the waist and hip circumference by 1" for each successive size. This increment is tapered down to a ¼" circumference increase at the ankle to

maintain the garment style. These sizes are named for their ease increase from the base size at the waist/hip: Base, +1, +2, +3, and +4.

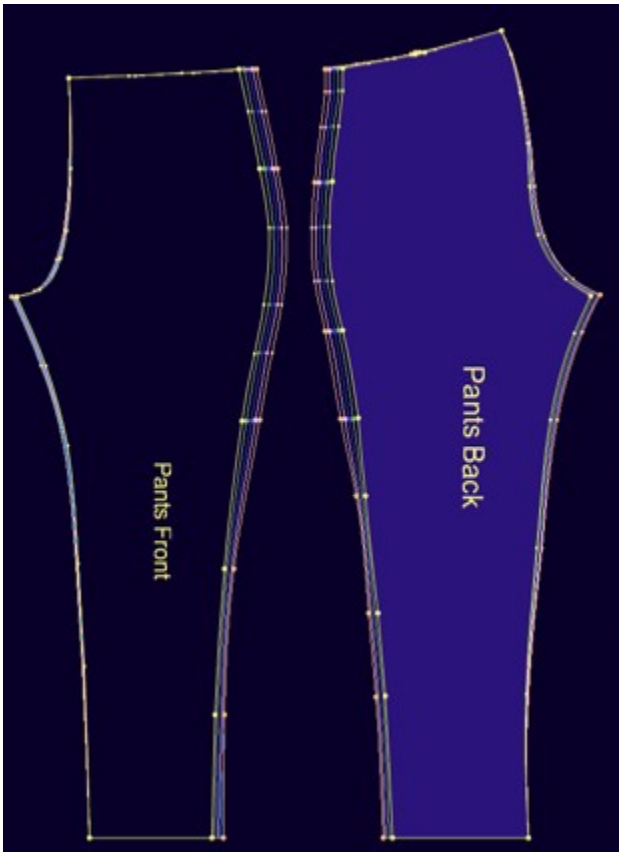


Figure 2.4. Test garment with nested size grade

2.4 Mannequin Data Analysis

Data analysis is done per gait cycle. The *periodicity property* allows the extraction of all gait cycles available in the experiment, along X, Y, and Z coordinates. The approach used to first extract and then align the gait cycles of the skin tight suit and pants experiments, overlaps samples over the same relative position within the gait cycle of body and pants cycles, where the reference position for defining the cycles is detected corresponding to the peak value of Marker 1

along the X axis, as described previously. The sample relative position in the gait cycle is easily determined because of a constant sampling rate, therefore equally spaced samples, and that the reference Marker 1 utilized for the alignment is only affected by small precision error, due to the camera's limited capabilities.

The intent of this experiment was to characterize the garment movement relative to the body. The Euclidean distance between body and garment (described in the following section) is the primary metric used to quantify the amount of garment movement at specific points. Additional noise variables such as positioning error and drift error are discovered and properly identified so to allow complete knowledge and understanding of the effects of garment movement on garment-integrated sensor which will be covered in Part II.

2.4.1 Gait Cycle-based Method

The motion-capture of the skin-tight bodysuit and of a pair of denim pants for markers placed in the same locations for each of the two experiments was recorded for 10 gait cycles. This description is part of the initial experiment introduced in paragraph 2.3 and it uses the same one fabric (100% cotton twill, 12.5 oz) in the available 5 sizes. Gait cycles of duration T were determined and correctly aligned. The Euclidean distance mean $d_{e_k}(t)$ later called as *Euclidean error*, for each Marker $k \in K$ on pants $m_{p_k}(t)$ and on body $m_{b_k}(t)$, labeled as

$$(1) m_{p_k}(t) = [x_{p_k}(t) \quad y_{p_k}(t) \quad z_{p_k}(t)] \quad m_{b_k}(t) = [x_{b_k}(t) \quad y_{b_k}(t) \quad z_{b_k}(t)]$$

was computed at each time instant $t \in T$ by averaging overall cycles,

$$(2) d_{e_k}(t) = E_{cycles} \left[\|m_{p_k}(t) - m_{b_k}(t)\|_2 \right]$$

Formula (2) is a sample-by-sample average over all the gait cycles. The average is considered over all available samples in each position: if the t -th sample of the n -th cycle for Marker k is not captured (i.e., NaN in Matlab notation), then the n -th cycle is excluded from the t -th sample average of Marker k . This approach of averaging sample by sample relies on the intuition given by the Law of Large numbers, wherein performing the same experiment a large number of times, the average result should be close to the actual expected value. Considering that repeated gait cycles of the mannequin are identical and having observed for each marker the consistency of the Euclidean error over the cycles, just 6 cycles were enough to obtain valuable average results, for each sample value.

In order to characterize how the average Euclidean error is distributed in the different body locations, the average Euclidean error $d_{e_k}(t)$ over the gait cycle for each marker $k \in K$ is averaged again over all samples in the gait cycle,

$$(3) \quad d_{e_k} = E_t[d_{e_k}(t)]$$

2.4.2 Garment Positioning Error and Drift Error Definition

The garment movement error quantified on average by formula (3) includes the error caused by garment positioning (initial placement on the mannequin) and drift (movement or slippage of the garment on the mannequin that is not cyclical) is isolated [17]. To quantify the effects of just garment movement between garments of different sizes and fabrics, positioning and drift errors are identified and defined so that they can be extracted from the overall error.

The *Positioning error*, also indicated as *PE*, is computed as the initial (X,Y,Z) difference in position or Euclidean Distance between markers on pants and markers on body, that at the beginning of the first gait cycle of a test trial should ideally be close to identical. The Y component of the positioning error is on average larger than the X and Z components, because in the experiments pants are subject to more vertical sliding than in other directions, over the cycles. Thus, straight left leg position is the most intuitive choice for the reference of the first sample of each gait cycle.

The variation of the positioning error between two consecutive cycles is called *Drift error*, *DE*, and it is defined as

$$(4) \text{ drift error} = \nabla_T(\text{positioning error})$$

where now the PE is redefined for each consecutive run gait cycles of the test trial.

In the experiments, PE and DE are measured for 10 consecutive donning and doffing trials of 10 gait cycles each: PE is computed as the initial (X, Y, Z) difference in position between a marker placed in a given location on pants and on body, for the first gait cycle of each donning and doffing trial; the DE is computed as the (X, Y, Z) difference in position between markers on pants and markers on body of consecutive gait cycles of the same trial, after redefining the PE at the beginning of each gait cycle for “straight leg” position.

Tests are focused on two different fabrics of 100% cotton denim jeans, characterized by two opposite fundamental textile properties: thickness and stiffness. In particular, one fabric, textile

no. 80833², is more thick and stiff than the other, textile no. 52735³. Five different sizes (i.e., Base, +1, +2, +3, and +4, as above) of each fabric are tested.

For each pair of pants (10 total pants, with the 5 sizes of fabric 52735 and the 5 sizes of fabric 80833), 10 Independent donning and doffing trials of 10 cycles are tested and both PE and DE computed.

2.4.3 Movement Error

To characterize the error introduced by garment movement more comprehensively, 3 additional fabrics in 5 sizes each with intermediate stiffness properties between fabric 52735 and fabric 80833 were considered. A total of 25 pants are now tested. As before, for each pair of pants 10 donning and doffing trials of 10 gait cycles each were considered. Initial pants positioning (PE) and pants drift (DE) over the cycles were quantified and removed (or subtracted) from the Euclidean error calculated according to formula (2), so to have the garment movement error alone in formula (3) for each of the markers. However, the analysis of all 20 markers for 5 sizes of 5 different fabrics yielded unwieldy and noisy results. To simplify this analysis, markers were grouped by vertical levels (i.e., 2-6, 7-9, 10-11, 12-14, 15-17, 18-20) according to their body location. Consistent relations between markers locations were found.

Movement Error: Size Analysis

The standard five sizes (basic, +1, +2, +3, +4) of five different fabrics with intermediate textile properties between fabric 52735 and 80833 (previously analyzed), were tested. The data collected for each marker are averaged over all fabrics for the same size. The average Euclidean error of

² 14.50 oz/yd², company measurement

³ 9.75 oz/yd², company measurement

each marker, given by formula (2), is averaged over markers on the same level, as specified above.

Movement Error: Fabric Analysis

The same simulation as in the previous paragraph is considered here. Markers are no longer grouped, and the different fabrics are initially compared respective to the average Euclidean error over all sizes.

Chapter 3

Results and Discussion: Garment Error Analysis

Data analysis exploits the repeated gait cycle movements of the mannequin. Data and metrics are calculated on a gait cycle basis and then averaged over the total number of gait cycles captured. Results and discussion of all the error metrics defined in Chapter 2 are presented: initial Euclidean Error; Positioning Error; Drift Error; and Movement Error. Size and fabric effects are considered.

3.1 Euclidean Error Distribution

A normalized version of the Euclidean error in formula (3) is presented in the following diagram (figure 3.1), which describes the general distribution of overall movement error for fabric 80833.

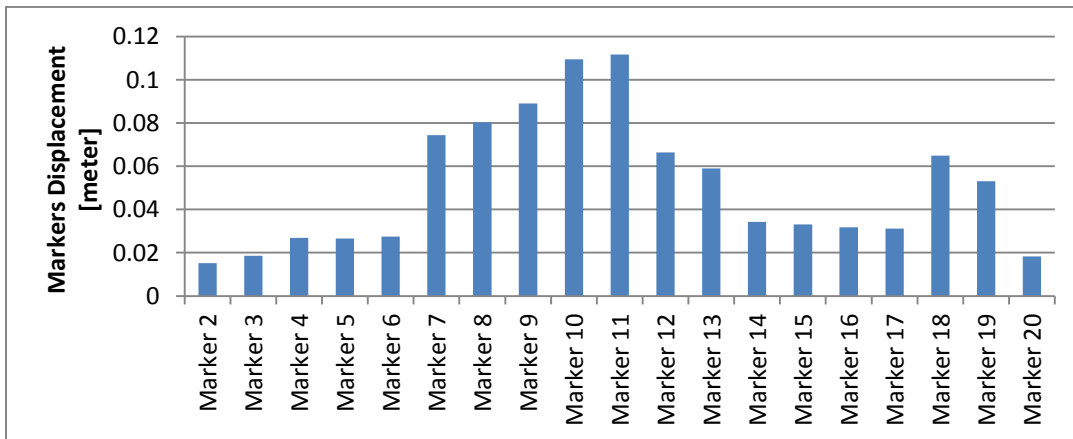


Figure 3.1. Normalized Euclidean distance in meters over a gait cycles for markers 2-20. Markers location is shown in figure 2.3

Markers located in the same area have similar error distribution, showing a consistent pattern over the trial tested: the error is minimal around the waist; becomes maximum around the hip; gradually decreases down to thigh and calf; and increases and decreases again around the calf. Specifically, Markers 2-6 have a small and about constant error, because they are on the waist area, which is tight on the mannequin and held in place with an elastic waistband. The error increases for Markers 7-11 around the hip, and this is to be expected since the hip area has more wearing ease to allow the mannequin's hip to swing freely (constricting the hip joint will damage the mannequin's mechanism), and therefore it folds more during movement. The calf area has almost the opposite properties from the hip area because the garment never folds, but instead slides up and down on the calf. Markers 14-16 thus have low error. The ventral part of thigh, Markers 12-13, and ankle, Markers 18-19, show higher error, due to the force of gravity and geometry of the garment/body relationship during the gait cycle that holds the jeans in more constant contact with the dorsal side of the leg, displacing the wearing ease to the ventral side. Marker 20, right above the heel, and Marker 14, on the dorsal side of the thigh are less affected by error than the others markers on the same area.

3.1.1 Ease Effect on Garment Noise

In a more detailed analysis, the error over different sizes of the same pair of jeans is assessed [24]. As already described, there are 5 different sizes with 1" circumference increase at waist and hip, and $\frac{1}{4}$ " circumference increase at the ankle, for each successive size. At the beginning, a deterministic proportional increase of the average Euclidean error in formula (2) should be expected, corresponding to the increase in size. The simulation results reveal instead that the error has a random component associated with it. The error is more like a random variable

approximately distributed over the markers according to figure 3.1. Such behavior is reproduced in the following picture over 5 different sizes.

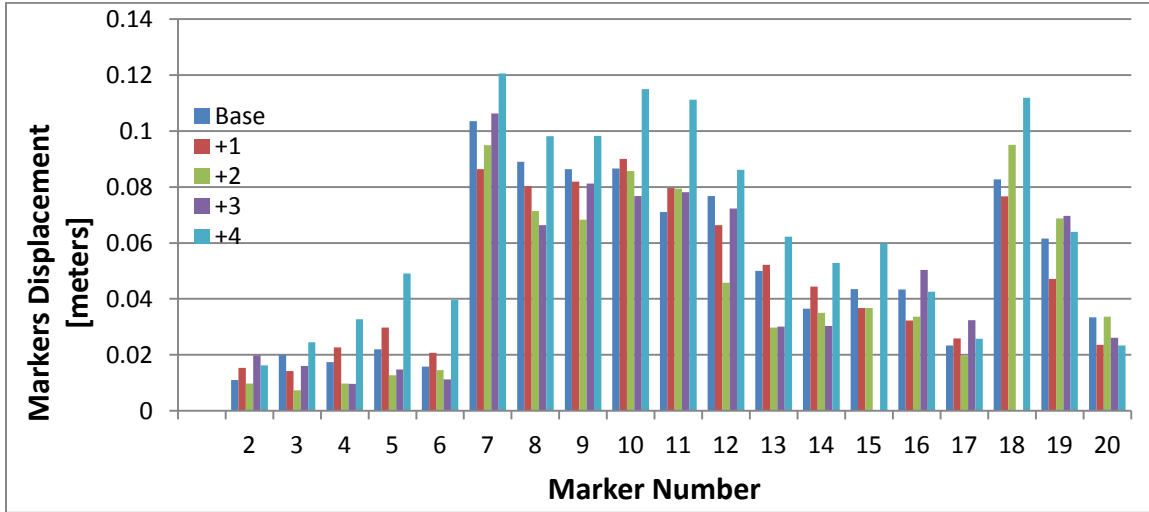


Figure 3.2. Denim jeans, over 5 different sizes

In figure 3.2, all sizes follow a similar pattern with markers around the waist and around the calf that show lower average error than hip, ankle and thigh. For most of the markers, size +4 has the highest error, but this does not happen with regularity. Unexpected is the error of the base size that is the lowest for Marker 11 only, while size +1 has the lowest error for Markers 7, 15, 16, 18, 19, and 10; size +2 the lowest error for Markers 2, 3, 5, 9, 12, and 17; and, size +3 the lowest error for Markers 4, 6, 8, 10, 13, and 14. The last observation emphasizes the random behavior of the Euclidean error.

3.2 Positioning Error and Drift Error: Fabric and Size Averages

Analysis

Preliminary results show that both errors have a similar distribution for the stiffest and least stiff fabrics no. 80833 and no. 52735 respectively that did not change by increasing the size.

PE Discussion

From a comparison with initial results based the Euclidean error calculation, the distribution of the positioning error over the markers shows correlation with the Euclidean error of Figure 3.1 and 3.2, following the same pattern, on average, for all fabrics and sizes. The PE gets smaller around the waist (*10-30mm*); larger on the hip (*100-130mm*); decreases on the thigh and calf (*40-80mm*); increases on the front side of the ankle (*70-100mm*), and decreases again on the back side (*30-50mm*). Both types of jeans have the same distribution, with the average error over all markers of fabric 52735 smaller than fabric 80833. Fabric 52735 is less thick and stiff, so it in general moves and folds more in such a way that on average the error over all markers is greater than fabric 80833.

Since markers on the same vertical level show a variable deviation, in the following analysis markers are grouped on the same level by averaging over their individual values.

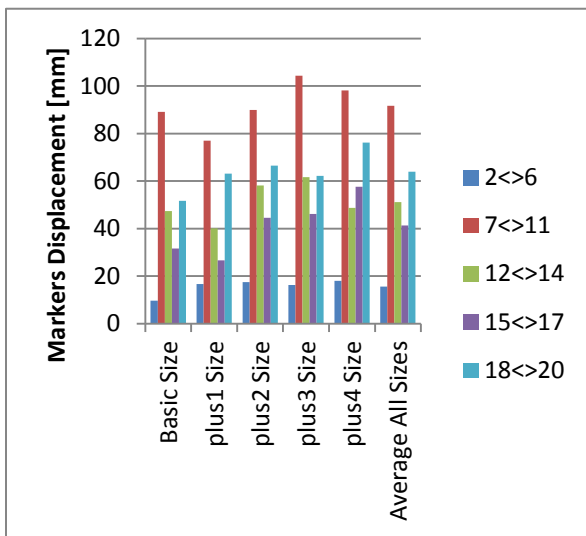
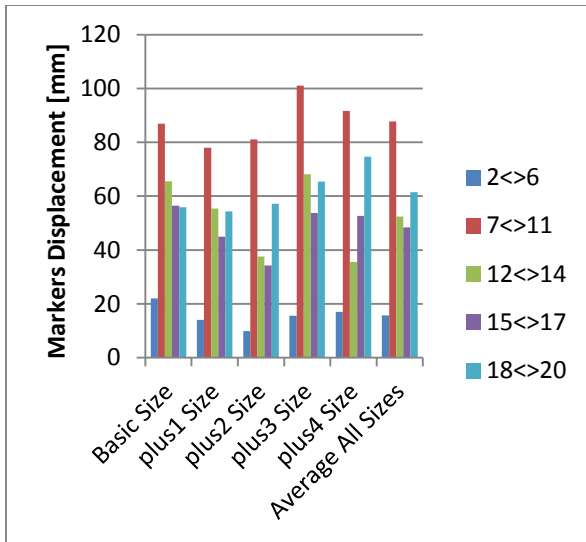


Figure 3.3. PE in millimeters of markers grouped by vertical levels, for all sizes: on the top pants 80833; on the bottom, Pants 52735

Figure 3.3 shows the group average for the 5 vertical levels, where the bar plot on the top refers to fabric 80833, while the bar plot on the bottom to fabric 52735. The PE pattern of the two fabrics is similar, as well as their average values are close: Markers 2<>6 (located on the waist) have the smallest PE error over all sizes; Markers 7<>11 (located on the hip) have the larger PE over all sizes; Markers 12<>14(on the thigh), 15<>17(on the calf), and 18<>20(on the ankle)

values are in between with Markers 18<>20 and Markers 15<>17 that show more correlation between each other than with Markers 12<>14. The position error is a quantification of the “human error” introduced by donning/doffing. PE tends on average to be worst for larger sizes, especially for Markers 7<>11.

DE Discussion

The distribution of the drift error is similar to the distribution of the positioning error, following the same pattern on average for all fabrics and sizes. The DE gets smaller around the waist (*0.1-1.5mm between cycles*); larger on the hip (*1-3.5mm*); decreases on the thigh (*0.5-1.5mm*); increases on calf and ankle (*1.5-3.5mm*). Both types of jeans have the same distribution, with the critical difference that the Base size DE of fabric 80833 (more thick and stiff) is on average greater than the average DE of sizes +1, +2, +3, +4; while the Base size DE of fabric 52735 (less thick and stiff) is on average lower than the average DE of sizes +1, +2, +3, and +4. The garment of fabric 80833 moves and folds more as the amount of ease increases, in such a way that the DE, on average, tends to be smaller.

Figures 3.4-3.6 show the DE in each gait cycle of Marker 2, Marker 8, and Marker 13, located on the waist, hip, and thigh, respectively, reported in figure 3.3. The horizontal axis indicates the gait cycle’s ordinal number while the corresponding vertical coordinate (*mm*) is the measured drift error. To better visualize the behavior of the drift across the cycle, a polynomial curve is used to interpolate the points at each cycle. Plots on the left of each figure are of fabric 80833 and plots on the right of fabric 52735. In fabric 80833, the DE decreases exponentially in the initial gait cycles and drastically reduces the variation in the next cycles. The DE settles by the 3rd gait cycle, showing the largest negative slope of the DE. In fabric 52735 the DE instead does not show settling behavior, while the DE of the stiffest fabric 80833 settles.

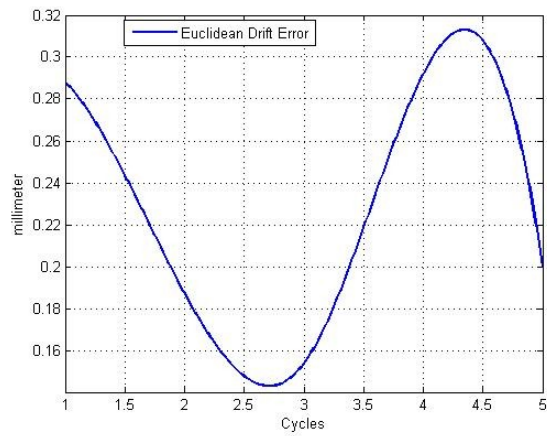
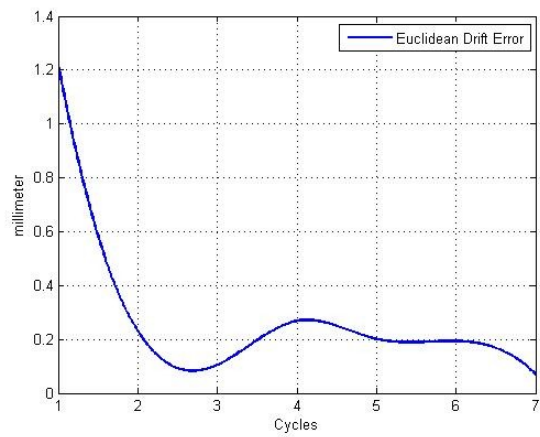


Figure 3.4. Best-fit line Positioning and Drift error, Marker 2 size +2: Fabric 80833 on the top, Fabric 52735 on the bottom

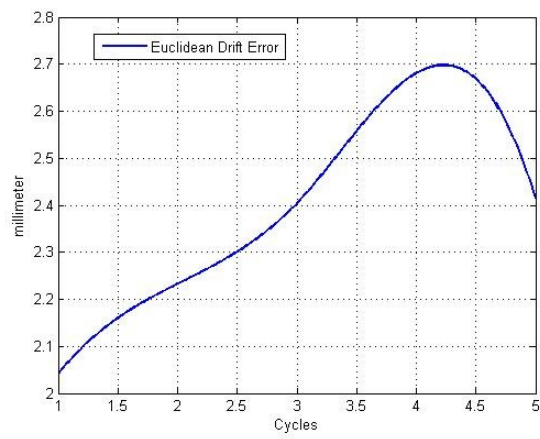
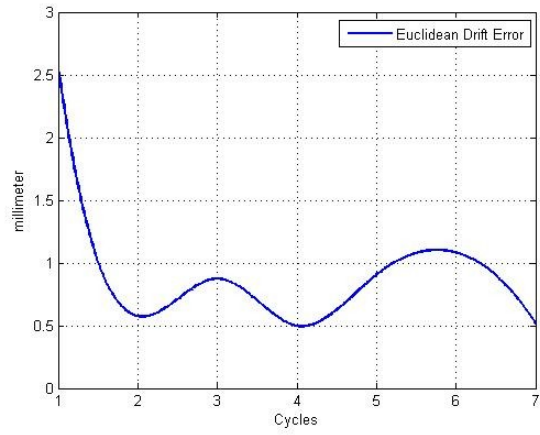


Figure 3.5. Best-fit line Positioning and Drift error, Marker 8 size +2: Fabric 80833 on the top, Fabric 52735 on the bottom

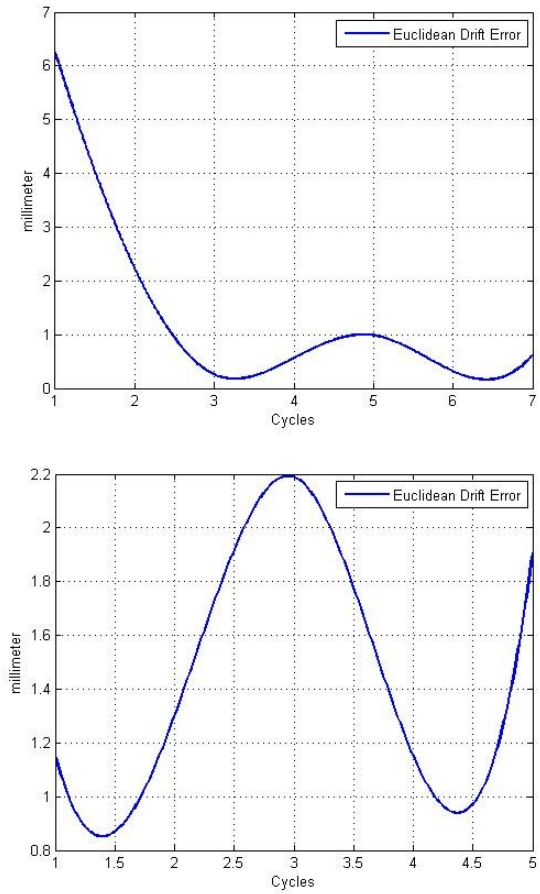


Figure 3.6. Best-fit line Positioning and Drift error, Marker 13 size +2: Fabric 80833 on the top, Fabric 52735 on the bottom

Effects of thickness and stiffness on the convergence of the DE error are thus observed. From Figures 3.4-3.6, fabric 80833 DE settles after few gait cycles DE settles while fabric 52735 does not. The flexibility of fabric 52735 introduces more randomness in the garment movement, and therefore becomes hard to predict in the short time frame what value the error of fabric 52735 will settle to or if it will settle at all.

Restricting the analysis to the DE of jeans 80833, markers on the same body area generally have similar DE. However, this is not always true for the hip area where the garment moves more,

toward more random directions. Another exception is given by Marker 12 that has larger drift than the other two markers at the same vertical level (Markers 13 and 14). This is expected because the articulation of the leg lets the jeans slide more on the front side of the thigh, rather than on the rear side – the mannequin’s knee traps the fabric during full flexion of the joint and remains wedged for much of the gait cycle, preventing it from sliding freely.

For size +2 of fabric 80833, 82% of the markers experience the largest DE rate of change by the end of the 3rd gait cycle, with an average maximum rate of $\sim 2.5mm$ for all Markers 2-20.

Averaging the DE ratio over the two smaller sizes (i.e., base size, and size +1), both sizes experience on average $\sim 2.2mm$ of maximum DE variation by the 3rd gait cycle of their markers, but this is the maximum variation rate overall gait cycles observed for the 76% of the markers of the two sizes combined. Size +3 and size +4 are not considered because both sizes experience the largest DE variation after the third gait cycle, for most of the markers, so that the observation window considered is not large enough to characterize such bigger sizes. Results show that the average DE rate of change does not vary much with the size for a thick and stiff fabric, as long as the ease in the garment is on the smaller size. It is more likely that the smaller sizes experience more consistent forces, where the forces in a larger size are more random.

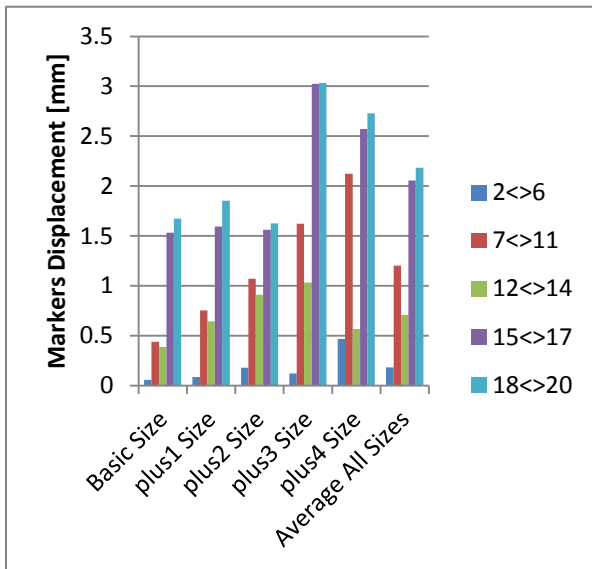
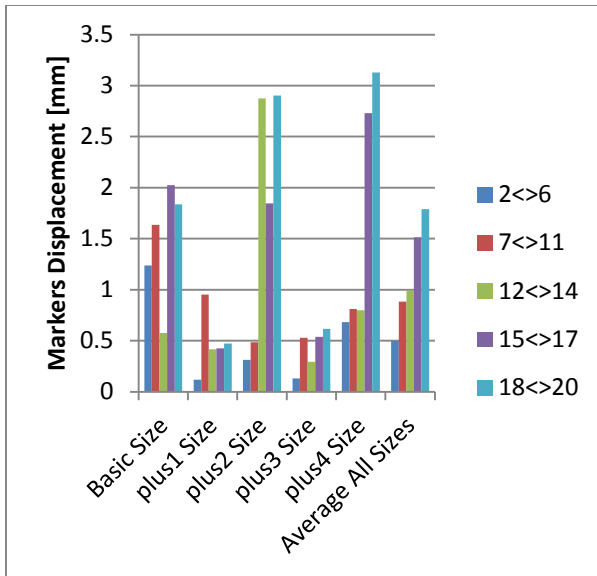


Figure 3.7. Total DE displacement in millimeters during experimental period of markers grouped by vertical levels, for all sizes: on the top pants 80833; on the bottom, Pants 52735

Figure 3.7 shows the total DE displacement during the experimental period for all markers, grouped by 5 vertical levels (as previously done for the PE) where the bar plot on the left refers to pants 80833, and the bar plot on the right to pants 52735. The DEs do not follow the same pattern for the two fabrics, with fabric 80833 on average having larger DE for Markers 2<>6 (on the

waist) and 12\diamond14 (on the thigh), while fabric 52735 has larger DE for Markers 7\diamond11 (on the hip), 15\diamond17 (on the calf), and 18\diamond20 (on the ankle). Markers 15\diamond17 and 18\diamond20 have usually the largest DE, with the exception of size +1 of fabric 80833, while Markers 12\diamond14 of size +2 of the same fabric is hypothesized to be an outlier due to a bad capture from the incoherent large value of Marker 12.

3.3 Movement Error Results

Unwieldy and noisy results of the absolute error at each marker required grouping the markers by location (i.e. waist, hip, thigh, calf and ankle) to capture consistent relations between the markers. By averaging the movement error of markers over different fabrics of the same size, a repeated pattern shown in the figure below is found, as shown in figure 3.8.

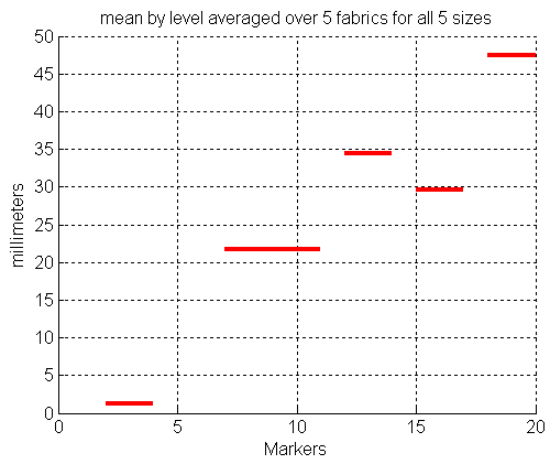


Figure 3.8. Movement Error average by level of markers grouped by location (i.e. waist, hip, thigh, calf and ankle) over 5 different fabrics for all sizes

Comparing the error levels of figure 3.8 with the distribution found for the PE of figure 3.3 and the initial Euclidean error of figure 3.1 (which include both PE and DE), it appears clear how the PE corrupts more markers around the hip than markers around the thigh and calf. Markers around the waist are tightly secured with an elastic band around the mannequin waist thus their error value is about the same; at the same time, the error of the markers around the ankle is likely constrained by the fact that the mannequin never straightens his leg fully, which results in the jeans always hanging on the posterior side of the ankle bending forward, trapping the markers and limiting their movement.

As the size (amount of ease) in the garment increases, the Euclidean distance between the same levels (level defined as in figure 3.8) on skin tight suit and pants increases almost linearly, for all levels. An analysis by level (level defined as in figure 3.8) for each of the fabrics finds a consistent pattern between sizes, with the larger sizes that show greater error.

Movement Error by Size

For all sizes, the group error relative position results are identical to the average ones shown in figure 3.8. Increasing the size, the group average increases of some millimeters, and such increment is more evident for the markers around ankle, calf, and thigh, where shows the largest increment of $7-10mm$ between size +3, and size +4. Markers around the hip show the maximum increment of $\sim 3.5mm$ between size +3, and size +4, while markers around the waist have an error that does not change significantly with the size.

Movement Error by Fabric

All fabrics have the same error variation between adjacent markers. Markers are therefore not grouped by levels as done in the previous 2 sections. Starting from the ankle and moving up to the waist the error relations between adjacent markers are analyzed: for markers around the ankle, the error is maximum at Marker 18, decreases to Marker 19, and decreases again to Marker 20; for markers around the calf, the error increases from Marker 15 to Marker 16, and decreases to Marker 17 where it is minimum; for markers around the thigh, similarly to the markers around the calf, the error increases from Marker 12 to Marker 13, and decreases to Marker 14 where it is minimum; for markers around the hip, the error is maximum at Marker 8, so it decreases to both Marker 7 and 9, then from Marker 9 decreases to Marker 10 (Marker 9 and 10 have the highest error after Marker 8), and from Marker 10 decreases again to Marker 11 where it is minimum; for markers on the waist, the error variation between adjacent markers is not significant.

Considering the individual contribution given by each size to the average error analyzed above, size +4 usually gives the largest contribution, particularly for those markers with the largest error on each level (ankle, calf, thigh, hip, and waist). The waist area reflects the largest variance in generated noise/error of the variables considered so far.

Part I. Conclusion

Part I presents a detailed analysis of one of the crucial obstacles that separates wearable technology integrated in everyday clothing from reliable and accurate estimates. This area is an emerging focus for wearable sensing, and is not yet well investigated. Because of this, the investigation as presented here reflects the exploratory nature of early research. Through

experimental investigation, a novel method for measuring the error introduced by the cloth movement is provided, based on the 3-dimensional Euclidean space. Initial results show the distribution of the noise that would be experienced from a garment embedded sensor at specific locations over the body surface: higher noise was estimated around the hip and smaller noise on thigh and calf. The impact of varying the size was evaluated: pants of size +4 exhibited larger noise compared to all other smaller sizes.

A more detailed analysis is developed comparing 5 pants sizes of two fabrics with opposite textiles properties, and the error is described as drift and positioning variables. Results show that the initial PE due to donning and doffing was found to affect more marker around the hip rather than markers around thigh and calf. The DE was found to settle after first few cycles. Both DE and PE error follow a similar pattern for the two fabrics, and it does not change with an increase in garment size. Fabrics and sizes did not have a noticeable effect on the noise if compared to the markers location.

This preliminary study suggests the best locations for body sensing and the potential noise effects for garment integrated sensors: garment-integrated sensors need to be located so that the garment movement experienced is minimal; fabric and garment fit need to be chosen so to minimize errors due to initial positioning and garment drift during body motion, but preserving wearer comfort in order to avoid too stiff or too tight garments that could constrict body movements.

The next Part II introduces and characterizes in detail novel garment-integrated sensors to sense garment movements preserving fabric properties, aesthetics, and wearer comfort.

Part II. Application:

Garment-Integrated Sensing

Garment-integrated body sensing is an approach to measuring body movements in wearable sensing. Textile-integrated sensors have the potential to equip everyday clothes with smart capabilities, making the detection of body movements accessible during normal activities. The practicality of this solution preserves variables directly related to the wearer's needs such as Comfort, Perceptibility, and Awareness that must be equally prioritized with Accuracy and Precision of the sensor data. Using sensors already embedded in clothes removes the effort of putting on the device; if the sensor looks and feels like a part of the clothing itself, then acceptance and willingness to wear the device become almost unbiased variables. The central contribution of this approach is to improve the quality of wearable sensing while preserving user comfort.

A novel approach to garment-integrated sensing is proposed which directly sense fabric stretch and bend without adding complexity to existing apparel production methods, textile aesthetics, or general garment wearability.

Part II. Introduction

Garment-integrated sensors represent an approach to create passive sensor components at the apparel level, bringing electric components closer to the body. The development of textile based sensing techniques increases user comfort by adopting yarns, textiles, and fibers with electrical properties to build smart clothing, thereby reducing the hard components in circuitry. Garment-integrated sensing also represents an approach to directly sense the body without the requirement for the user to put on or take off an extra device, because it is already embedded in the garment, therefore simplifying the donning/doffing process.

Wearable technology and integrated systems have demonstrated significant advantages in the last two decades for body sensing for example in terms of biosignals like heart rate or respiratory rate to monitor physical activity so to prevent or identify health risks [29]. The main strength of garment-integrated wearable technology has already been recognized as its close integration with daily activities. However, a significant practical limitation to widespread commercial use is the difficulty garment-integrated technology poses for manufacturers, because of the need to reconcile electronics fabrication processes with apparel production processes. Apparel production operates on very short production cycles with complex machinery and processes. It is not amenable to large-scale changes in manufacturing processes. A novel garment-integrated sensor that does not require changes in the existing apparel production machinery and cycles is here presented.

Garment-integrated sensing in wearable technology often faces the barrier of user comfort. Bulky or burdensome wearable devices constrain and condition the wearer's behaviors. The appearance of the device can be limiting to their usage and application. Bulky, uncomfortable, or unappealing devices are difficult to integrate with the wearer daily life and activities. If the objective is to monitor body movements for example for a post-surgery rehabilitation period or to

monitor athletic performance and training then limiting or conditioning the movement of the wearer can have a critical impact on the quality of the data monitored. For instance, an athlete may underperform, and a patient in rehabilitation may not move as he/she normally would without the wearable sensing monitoring solution.

Logistics in the manufacturing process is another key barrier for wearable technologies. Smart clothes are the hybrid results of separate and sometimes parallel developments in garments and electronic circuit boards. An additional, and probably the most critical and expensive step for the final assembly is the requirement of integrating these parts together. The final assembly requires a complete understanding of the wearable solution as a whole to build a robust, fully functional and durable smart garment. The lack of precision in cut-and-sewn methods that may affect the fabrication and integration of the sensors will be covered with more detail in Part III.

The following two chapters characterize novel garment-integrated stretch and bend sensors made by re-using existing standard stitches common in apparel, but with the addition of conductive properties. A rigorous characterization in terms of the working principle and sensor output for three types of sensors different for sensor response behavior and field of application is here presented. The stretch sensor's working principle is based on the looped conductor method: a looped conductor of specific resistance per unit length, in which the loops of the conductor pass in and out of contact as the textile structure is stretched and relaxed. When loops are in contact, the electrical length is shortened and resistance is decreased. Conversely, when the loops are separated, the electrical length is lengthened and the resistance increases. The bend sensors are a generalization of the stretch sensors for un-stretchable fabrics. Sensors' reliability in terms of drift, durability by means of insulation and fabric effects on the sensors' output are investigated.

Part II. Background: Garment-Integrated Stretch and Bend Sensing

Traditionally wearable sensing devices are developed outside the wearable environment, paying attention to the accuracy and reliability of the wearable device without prioritizing user comfort. An example where accuracy and reliability are prioritized at the expense of comfort is provided in a commonly-used motion capture technology for Kinematic analysis, which uses a set of rounded and flat shaped rigid sensor units housing inertial sensors, attached with Velcro bands around limb, arms, and legs [30]. While such a system provides a reliable and accurate output, it is not wearable in the sense that the average person would not be willing to wear it continuously in everyday life.

E-Textiles are made with conductive fabrics that intrinsically prioritize user comfort. There are a number of e-textile methods currently in use or in development that measure stretch or bend. These methods generally fall into three categories: 1) piezo-electric, 2) electro-active polymer materials 3) coatings that respond to stretch, bend, or compression with a corresponding change in resistance [36][37][38].

In a critical review of wearable electronics and smart textiles, textile materials composed of self-intersecting conductive fibers have been recognized as functioning as stretchable sensors when their properties change during and after deformation: i.e. the number of self-intersecting contact points (shorts within the structure) may change; textile fibers could extend; fiber cross-sections can decrease [32]. A thermoplastic elastomer combined with carbon black particles has been used to measure large strain in textile (up to 80%) for extension and retraction cycles [33]. The sensor was bonded on the textile using a silicone film protecting the sensor against water while preserving the elasticity property. Atalay et al. presented knitted strain sensors comprising silver-plated nylon looping yarns with 20 Ω /cm linear resistance insulated by elastomeric yarns is used

to investigate the effect in the sensing mechanism of different linear yarn densities [34]. Fabric extension of 40% was chosen to capture the typical human extension. Sensors were characterized for decreasing yarn densities (800-570-156 dtex). Rovira et al. presented the characterization of a three piezoresistive fabric sensors to detect breathing patterns (2mm extension). Sensors are distinguished based on the resistance range of operation: “Grey” sensor operates between 20KOhm-100KOhm; “Black” sensor between 20KOhm-30KOhm; “Brown” sensors between 12MOhm-25MOhm. The following table 4.1 summarizes some of the results from testing three alternative approaches to textile-based strain sensors for extension and recovery cycles:

Table 4.1. Textile-based strain sensor properties from literature - summary

Sensor Properties	Thermo Plastic w/ Carbon [33]	Knitted Silver Plated [34]	Piezoresistive sensors [38]
Linearity	the output resistance of the sensor showed good linearity for strain above 20%, working reliably up to 80% strain;	The linear working range decreased with the sensors' dtex: 8%-40% for the 800dtex sensor; 2%-40% for the 570dtex sensor; more than 2%-less than 40% for the 150dtex sensor, due to a lower density sensor;	pre-extension is required for the sensors to behave linearly: 10% pre-extension for Black sensor; 25% for Grey sensor; 30% for Brown sensor;
Drift	the sensor was kept in steady positions at 20% and 80% strain for 2min, showing an inaccuracy of 8.8% due to a decreases of the resistance value over the 2mins; testing the sensor for 8 hours showed a marginal resistance increase less than 1KOhm due to fabric deformations, therefore the sensors properties can be assumed constant with time;	the electrical resistance at zero strain (prior extension) increased up to 170Ohm for higher yarn knitted tension;	consecutive extensions of about 20% for about 2 ½ hours showed a drift of about 5KOhm for Black and Gray sensors; drift results on Brown sensor are not available
Speed	strain speed was increased from 50 to 600mm/sec showing a marginal rise in resistance;	sensing fabrics were tested between 0% and 40% strain levels at an extension speed of 2	N/A

		mm/sec with no dwell times for the lowest or the highest strain levels;	
Peak to Peak	2cm of sensor length for strain between 20-80% showed a peak-to-peak of 17KOhm, and sensitivity of 1.25 KOhm/mm;	N/A	for 5% stretch at 0.143Hz, a peak-to-peak of 2.5KOhm is measured for Black sensor
Response	for stretch lower than 10% sensor stop responding cause fabric deformations due to excessive stretch;	increasing the number of conductive course increased the possibility for the yarn to buckle describing on average a lower starting working point;	N/A
Hysteresis	small hysteresis with maximal error between extension and recovery strain cycle of 7%;	the maximum hysteresis increased up to 5.20% strain for 150 dtex sensor; 4% for 570 dtex sensor; 3.45% for 800 dtex sensor;	N/A
Washability	washing the sensor 8 times using a conventional detergent at 30C did not affect the sensors properties;	N/A	N/A
Durability	no ageing effects evaluated by checking the sensor output once a week over two months; confirming the long term stability of the sensor;	N/A	N/A

Tables 4.2 and 5.1 report the same parameters summarized in table 4.1 but for the novel stretch and bend stitched sensors topic of the next chapters. The conclusion provides a summary and a comparison of them in table 5.2.

Piezoelectric materials have been used to implement an e-textile based glove prototype able to sense hand typing movements; specifically finger flex and tap motion [31]. Piezoelectric materials are available in a variety of form factors, good sensitivity to almost any type of physical stimuli including pressure, tensile force and torsion, low power consumption, reasonable costs

and development complexity so to make them well suited for e-textile sensing. Dunne et al. propose piezo-resistive foam pressure sensors integrated on a torso worn garment to measure breathing, shoulder and neck movement, and scapula pressure, using a total of six sensors [35]: one sensor per shoulder was integrated in the corresponding garment area to detect motion; one on each scapula area to detect pressure; one along the neutral spine on the upper thoracic beginning of cervical part between the scapulae to detect posture; and, one on the frontal side of the torso to detect breathing. They have found that the increased pressure on the sensors exhibited a positive linear conductance response providing useful information to describe the status of the wearer.

Wearable stretch and bend sensors have shown to reliably work with good linearity properties. The use of piezo-electric or piezo-resistive materials has been employed to develop stretch and bend sensors through e-textiles. Wearable sensors simplify the ease of use and open to new sensing scenarios at the expenses of a noisy output due to the sensor movement.

In e-textiles, sensing stretch requires extension and retraction of the sensor while sensing bend requires some sort of pressure applied to the sensor in order for the sensor to flex. For both cases, the input stimuli generate the electric response of the sensor, i.e electric resistance. The ability of capture stretch and bend makes the sensor well suited to directly sense body movements, while comfort, bulkiness, ease of integration and manufacturing, and durability are shortcomings for such e-textile sensors. Stitched methods for example, as illustrated in the next chapters, integrate directly in the garment soft sensors made out of textile materials preserving user comfort and simplifying manufacturing, compared to conductive rubber or elastomer -based solutions which physical properties make the sensors bulky and potentially uncomfortable to the wearer.

Chapter 4

Stretch Sensing:

The Conductive Stitched Stretch Sensors Method

Garment stretch is captured by integrating conductive stitches on stretchable fabrics. A stretch or elongation deforms the fabric as well as the attached stitch, which results in a change in the structure of the stitch, which causes a variation of the overall resistance of the stitch. Three types of stitched stretch sensors are here presented, together with their properties. More attention is given to the best-performing sensor for the final evaluation of Part III. An investigation of the fabric substrate's effect on the sensor response is also covered.

4.1 Theory: Garment-Integrated Sensor Structures

Coverstitches and Overlock stitches are commonly used in apparel production for seaming and finishing knit garments [39] [40]. The coverstitch is formed by top and bottom thread loops which intersect with two to three needle stitches that keep the thread in place as specified in several of the standard ASTM D-6193 600- and 400-class stitches. The coverstitch is depicted in figure 4.1

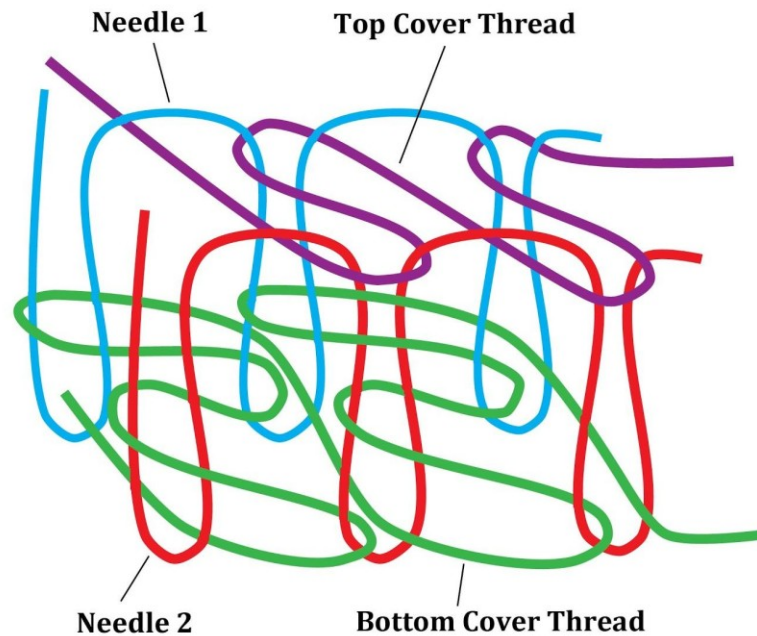


Figure 4.1. ASTM D-6193, ISO# 602 top- and bottom cover stitch

The bottom-thread coverstitch alone (the stitch structure with two needles and a bottom-thread loop, without the top-thread loop) is the most common stitch for hemming t-shirts, while the top thread (the stitch structure with both bottom- and top-thread loops, with two or three needles) is used for low-profile, flat and lapped seams like flatlocked seams on performance sportswear. The overlock stitch instead is used for standard superimposed seams (right-sides-together seams) and finishing edges, and cannot be applied in the middle of a piece (the machine cuts the fabric edge as it sews). The overlock stitch forms loops on both sides of the edge/seam that intersect with one or two needles that keep the thread in place as specified in many of the ASTM D_6193 500-class stitches. The overlock stitch is depicted in figure 4.2.

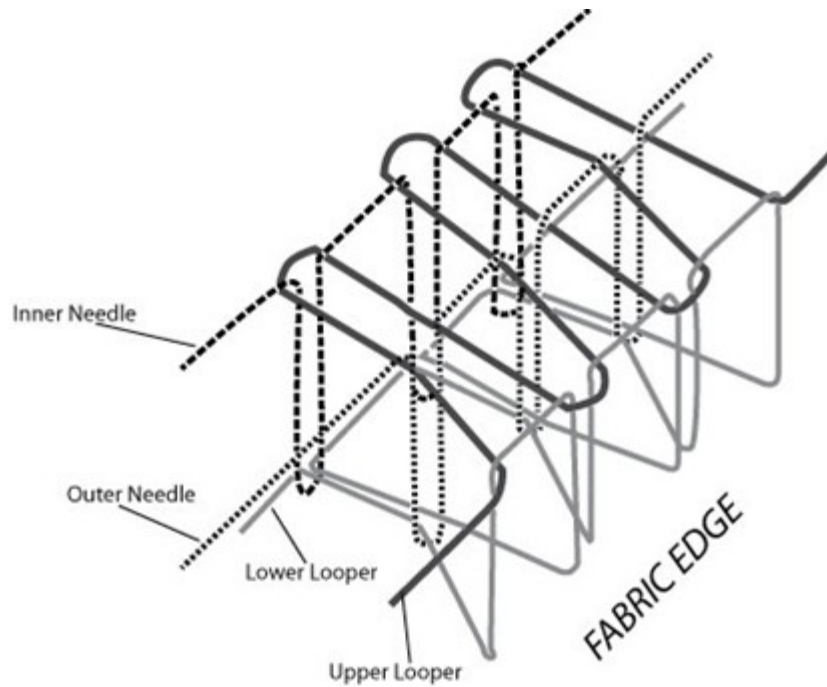


Figure 4.2. ASTM D-6193, ISO# 514 overlock stitch structure

The following paragraphs describe the use of Top-Thread coverstitch, Bottom-Thread coverstitch, and Overlock stitches to develop stitched stretch sensors, together with the theory of operation and analysis of their output responses.

4.1.1 Sensor Fabrication

All three types of stretch sensors are made using a traditional stitching machine with a silver coated Nylon conductive yarn used to sew the main thread describing the stitch. This allows for sensors with tactile and physical properties similar to everyday clothing to be quickly and easily produced. As an illustrative example, figure 4.3 shows the Juki MF-7723 high-speed, flat-bed coverstitch machine used to create the top- and bottom-thread coverstitched sensors discussed here.



Figure 4.3. Juki MF-7723 high-speed, flat-bed coverstitch machine

Stretching can either bring loops out of contact or more in contact depending on the architecture of the structure as illustrated in the following working principles and theory of Top-Thread, Bottom-Thread and Overlock stitched sensors.

4.1.2 Top-Thread Cover-Stitched Stretch Sensors Working Principle

The Top-Thread sensor is implemented in the coverstitch on the elastomeric fabric of figure 4.4, constituted by both top (horizontally, on the left side of the picture) and bottom thread (vertically, on the right side of the picture), with only the top looping thread being conductive.



Figure 4.4. Top-thread sensor horizontally folded on the left in gray, bottom-thread cover vertically on the right in blue on elastomeric fabric

The top-thread sensor working principle is illustrated by the following serpentine structure in figure 4.5.

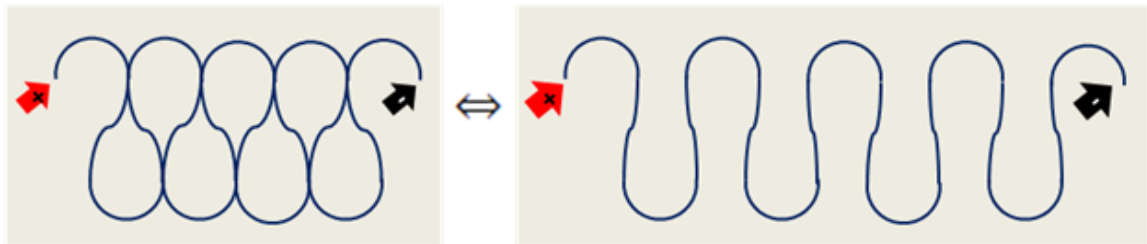


Figure 4.5. Top-thread stitched sensor: relaxed position on the left; stretched position on the right. Red and black arrows indicate the connection points of the sensor for the DMM probes.

The Stitched Sensor is a direct implementation of the looped conductor method, in which a resistance response is originated by two stretching modalities: extension and recovery.

Implementing the looped-conductor method in a stitched sensor generates a resistance increase when the stitch is in extension mode and a resistance decrease when the stitch is in recovery mode. Segmenting the stitch loops in the equivalent resistors as in figure 4.6: when the stitch is in full recovery mode the equivalent resistance is an anti-ladder network of resistors (figure 4.6, left) with smaller equivalent resistance than when the stitch is in full extension mode and the equivalent resistance is the series of resistors (figure 4.6, right).

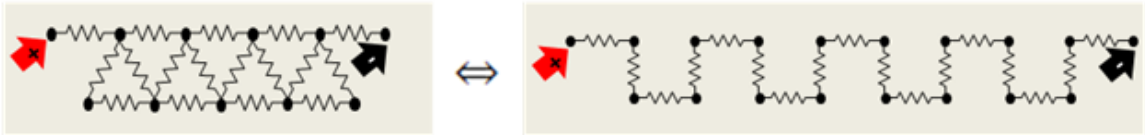


Figure 4.6. Top-thread stitched sensor, electric equivalent: relaxed position on the left; stretched position on the right.

For instance, the equivalent of 8.91 Ohm of series resistors (i.e. fully stretched sensor) was measured reduced to 0.96 Ohm when same resistors were put in an antiladder configuration (i.e. fully recovered sensor).

By visually inspecting the stitch when in relaxed mode, not all adjacent conductive loops are in contact. This imperfection can be related to the fabrication process as well as to fabric elongation after repeated stretches. The possible configurations of the looping yarn were modeled in terms of three basic stitch configurations: “ladder” stitch, where resistors are in anti-ladder topology; “open” stitch, where resistors are in series; “closed” stitch where a ‘resistor Delta’ is shorted. Figure 4.7 illustrates such basic stitch configurations that will be used in the top-thread sensor model in the analysis of the following section 4.1.2.1.

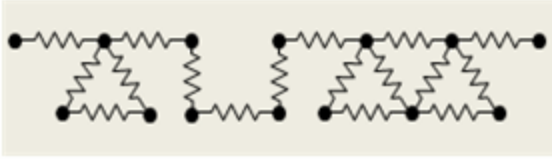


Figure 4.7. Basic stitch configuration: “closed”, “open”, “ladder” stitch, from left to right.

4.1.2.1 Anti-ladder Network Reduction

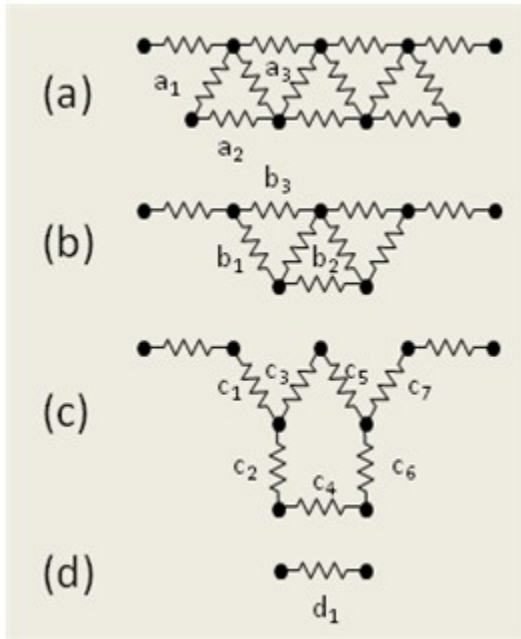


Figure 4.8. Antiladder network equivalent resistance: (a) antiladder basic; (b) antiladder reduced; (c) $\Delta \rightarrow Y$ transformation; (d) series and parallel reduction.

The equivalent electric resistors network of the top-thread sensor in relaxed position is associated with an anti-ladder network of resistors as in figure 4.8 (a). The total equivalent resistance depends on the number of loops or upside/downside deltas, equal to 5 in the circuit of figure 4.8

(a). A series/parallel of the resistors on both sides results in the anti-ladder reduced form of figure 4.8 (b):

$$b1 = \frac{1}{\frac{1}{a1 + a2} + \frac{1}{a3}}$$

The reduced anti-ladder is then simplified using a $\Delta \rightarrow Y$ transformation on the downside delta, equal to two deltas in figure 4.8 (b), obtaining the simplified network of figure 4.8 (c):

$$c1 = \frac{b1 * b3}{b1 + b2 + b3}$$

$$c2 = \frac{b1 * b2}{b1 + b2 + b3}$$

$$c3 = \frac{b2 * b3}{b1 + b2 + b3}$$

The simplified network of figure 4.8 (c) has resistors in series and parallel only that can easily combined in the network equivalent resistor in figure 4.8 (d):

$$d1 = \frac{1}{\frac{1}{c3 * c5} + \frac{1}{c2 * c4 * c6}} + c1 + c7 + \dots \text{ (series resistance)}$$

4.1.3 Overlock Stitched Stretch Sensors Working Principle

The Overlock sensor has the same looping structure as the top-thread sensor [40], but (in our case) with the addition of a needle on the inner side of the sensor (i.e., on the fabric side) that

keeps the inner facing adjacent loops in contact at all times, as more clearly illustrated in the picture on figure 4.9 for relaxed and stretched position.

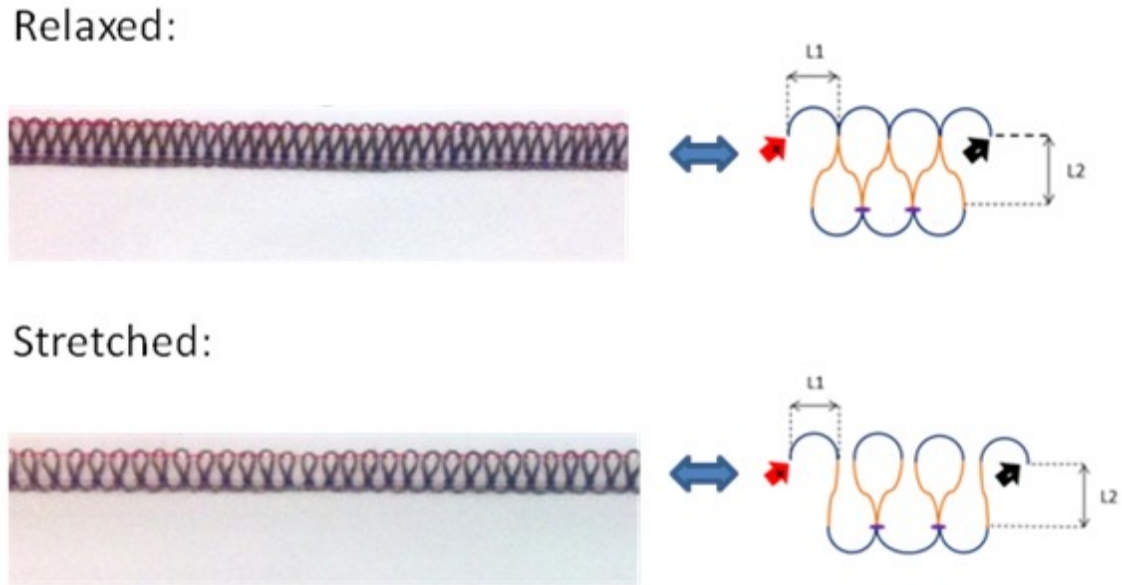


Figure 4.9. Overlock stitched sensor, reduction to equivalent: relaxed position on the top; stretched position on the bottom

When the overlocked sensor is in the relaxed position, it is equivalent to an anti-ladder configuration of resistors; and when the sensor is stretched the output resistance is a series of resistors similarly to the top-thread sensor. Referring with n to the total number of inner and outer loop halves ($n = 5$ loops in the diagram of figure 4.9), and with $R1$ and $R2$ to the equivalent electric resistance corresponding to $L1$ and $L2$ in figure 4.9, the total resistance is equal to

$$R_{total} = \left(\frac{n+1}{2} + 2 \right) * R1 + 2 * R2$$

which is smaller by a factor

$$\frac{n-1}{2} * (2 * R2 + R1)$$

respect to the total resistance of the equivalent top-thread stitched sensor [39]. The crossing thread holds the adjacent downside loops together in contact during stretch. Theoretically, this determines an isolated triangle configuration shorted from the series of resistors. Practically, the fabric extends during the stretch and the inner needle constraint loses contact between adjacent loops depending on the elasticity of the fabric. Thus different fabrics can have different resistance increase during the stretch.

4.1.4 Bottom-Thread Cover-Stitched Stretch Sensors Working

Principle

The Bottom-Thread Coverstitch was shown in figure 4.4. Sewing the bottom thread using a conductive yarn makes the bottom-thread coverstitched sensor.

The bottom-thread can be modeled as resistors in series, whether the stitch is stretched or relaxed. Such stitch can theoretically be modeled by a series of basic z-shaped serpentine of resistors interconnected between each other by another resistor. Practically the resistors on the bottom edge of the basic z-serpentine are shorted because the conductive thread in the actual stitch overlaps, thus the resistor in relaxed configuration can be further simplified (figure 4.10, left). When the sensor is stretched the resistors on the top edge of the basic z-serpentine are shorted as

well because the edges of the top loop come together in contact. As the sensor keeps stretching the length of the top edge loops increases, thus the value of shorted resistance increases, while the value of the remaining resistors in series (i.e., the length of the crossing yarn in the middle of the stitch) decreases. The length of the bottom edge yarn has relatively small variation; therefore it is assumed to not change during the stretch. The image below illustrates the two stitch configuration just discussed in the equivalent electric model.

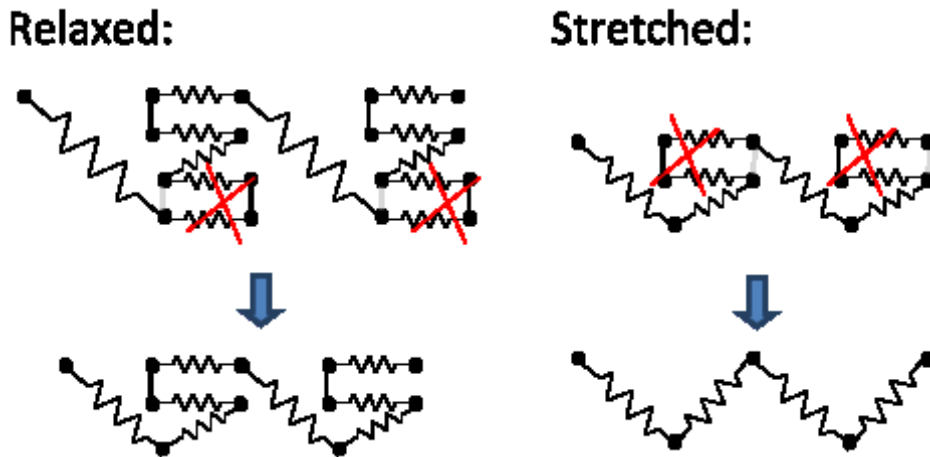


Figure 4.10. Bottom-thread stitched sensor, reduction to equivalent: relaxed position on the left; stretched position on the right. The light gray lines indicate the shorted points in the stitched, while the red crosses indicated the shorted loops from the equivalent series reduction

Continued stretching of the sensor generates a continuous decrease of the resistance until eventually either the stitch or the fabric breaks, depending on the tension used to stitch the sensor thread. Increasing the stretch increases the length of the shorted yarn in the top loop of the bottom-thread, decreasing the length of the un-shortened zig-zag yarn (figure 4.10, right).

The simplicity of this stitch model allows a computation of the theoretical resistance by a simple sum of the equivalent resistors that partition the stitch.

4.2 Experiment Design

All three sensors introduced in the previous section 4.1 were repeatedly and consistently stretched using an INSTRON Tensile machine. A Digital Multimeter (DMM) connected at the sensor extremity was used to capture the resistance change output of the sensor during extension and retraction (or relaxation) of the sensor. The following section starts with a method section that outlines the whole set of experiments, the experiment setup adopted for each of the sensors, and then covers in more depth the experiment and the analysis of the test results for each of the sensors. Sensors were applied to 98% polyester 2% lycra jersey knit fabric using standard cone thread in all other threads of the coverstitch.

4.2.1 Testing Method

Each Sensor was tested for 10 consecutive stretch and recovery cycles. In relation to the sensor structure and characteristics previously described:

- A top-thread sensor 4.75" long was repeatedly stretched for about 0.9" (~18% stretch);
- An overlock sensor 4.50" long was repeatedly stretched for 2" (~44% stretch);
- A bottom-thread sensor 2.25" long was repeatedly stretched for 1" (~44% stretch).

Over the 10 cycles, linear correlation, normalized sensor output and hysteresis were computed.

An INSTRON Tensile testing machine (Mod. 5544) was used to consistently stretch and relax a stitched stretch sensor sewn in an elastomeric fabric. The sensor was clamped tightly between the two pairs of INSTRON plates to allow for fabric stretch and recovery as the INSTRON arm was moving the top plates up and down, starting from an initial flat but not pre-stretched fabric between top and bottom plates. The length of the sensor tested was considered in terms of the initial distance between the INSTRON top and bottom plates. Each plate is about 2” high, thus at least an additional 4” length for the sensor is needed to clamp the sensor. The two sensor terminations on the outer sides of the plates were then connected to DMM probes to measure the electric resistance response of the sensor. Figure 4.11 shows a typical stitched sensor stretch test.

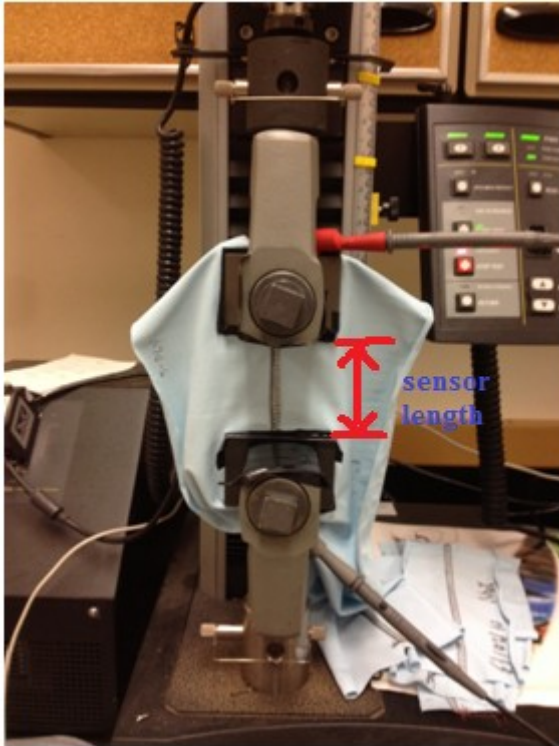


Figure 4.11. Stitched Stretch Sensor Test, initial flat fabric position

The sensor clamped between the plates was trapped due to the compression applied by the plates, adding a constant bias in the DMM readings that is removed from the output readings. To insulate the sensor from the conductive clamp plates, a layer of non-conductive neoprene was applied on both side of the sensor to minimize the contact between conductive thread and plates.

The DMM (BK-precision 2821-E) was connected via USB to a windows PC, where a Matlab script was used send a query and listen to the continuous data streaming to the DMM COM port:

```
fprintf(serial_port, ':FETCh?', 'async');  
fscanf(serial_port);
```

The DMM sampling rate was set to Fast, allowing for an average sampling rate of the data collected on the windows PC equal to 3.3Hz. The INSTRON sampling rate for the measured extension distance was set to 10Hz. Both extension [inch] and resistance [ohm] from INSTRON and Resistance DMM, respectively, were stored in a binary file with the corresponding time stamps. The time stamp was used to align and overlap the two sources of data for post-processing analysis.

4.3 Initial Sensors Characterization: Results and Discussion

4.3.1 Top-Thread Cover-Stitched Sensor Analysis

This subsection covers details about the test of the top-thread sensor, and develops the analysis of the test results.

Figure 4.12 shows raw sensor data normalized to align with the extension cycles (on the top) and the sensor hysteresis (on the bottom), at an average of 7.27 cycle/min.

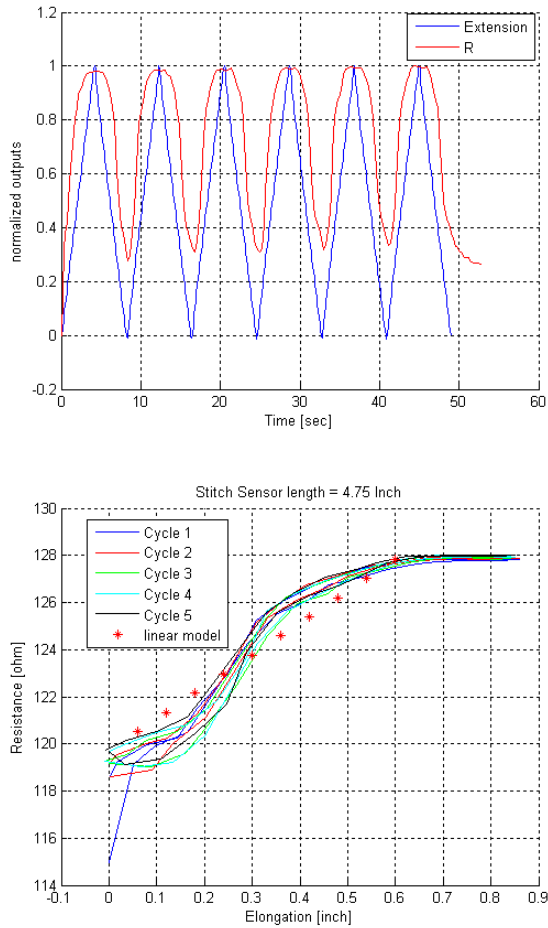


Figure 4.12. Top-thread output: normalized resistance aligned with normalized extension on the top; Resistance vs Elongation on the bottom. Pearson correlation Resistance vs Elongation 0.93

The output resistance shows the maximum variation between 0.2-0.6” elongation; it settles between 0.6-0.9”, when all loops are out of contact and the maximum resistance has been

achieved. Between 0-0.2” the variation is slower because the sensor is relaxed to its natural length and there are not many loops opening during the stretch or many loops closing during the recovery. The amount of contact between the fibers of adjacent loops during the stretch determines a non-binary sensor response, i.e. not all loops open and close at the same time. The filaments slide over each other and more or less filaments are touching as the strain increases. Moreover, the stitch tension used in the stitching machine determines the amount contact between the filaments of adjacent loops, i.e. how much in contact are adjacent loops between each other. The small Elongation allows the fabric to quickly recover and follow the sensor Resistance response with correlation coefficient $\rho = 0.93$, where

$$\rho = \frac{cov(Resistance, Elongation)}{std(Resistance) * std(Elongation)}$$

The very first resistance value is smaller than the following resistance values at 0” elongation. After the first stretch of the un-conditioned fabric, the fabric substrate does not completely recover its original length before the second cycle start. This generates less contact of the loops in the conductive thread which translates in a higher resistance value, as shown in figure 4.12. Subsequent extensions show a return to a more regular baseline resistance.

Using the model and basic stitch configurations introduced in the working principles section 4.1, a linear model for the sensor is generated and overlaid on the sensor raw data in the hysteresis plot on the right in figure 4.12. The model is based on an empirical calculation: the same number of “closed” stitches is gradually opening at equi-spaced extension points, between 0-0.6” [39]. By comparison, in practice the sensor stitches open during stretch and close during recovery at a

faster rate around 0.3” elongation than at the beginning of the extension where the stitches are “closed” or before saturation where most of the stitches are “open”. When the resistance saturates all stitches are “open” and the rate becomes zero.

4.3.2 Overlock Stitched Sensor Analysis

Similarly to the previous subsection, details of the test and test results are here provided for the overlock sensor. The cycle rate is on average 3.125 cycle/min.

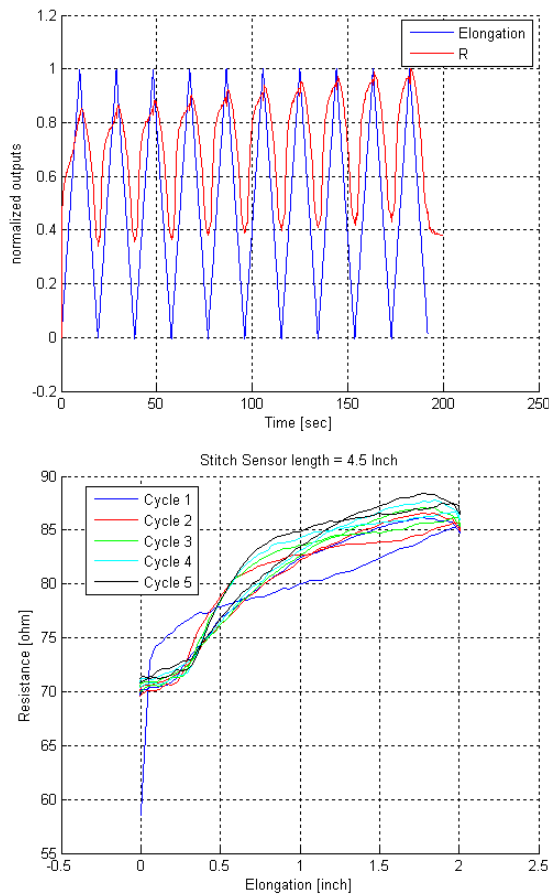


Figure 4.13. Overlock output: normalized resistance aligned with normalized extension on the top; Resistance vs Elongation on the bottom. Pearson correlation Resistance vs Elongation 0.91

The overlock output resistance never completely saturates, but the sensor's output response keeps increasing with elongation but at slower rate due to the inner loops constraint, illustrated in figure 4.13. Specifically, as the fabric stretches and the outer loops come out of contact, adjacent inner loops are still pulled together by the crossing needle. Depending upon the tension of such crossing needle, overstretching the fabric will cause compression of the crossing needle on the yarn conductive filaments of the two adjacent loops which will be shorted, causing a decrease of the resistance. The latter is visible closer to 2" elongation in figure 4.13.

The small Elongation allows the fabric to quickly recover and follow the sensor Resistance response with correlation coefficient $\rho = 0.91$. Stretching the fabric required more time for the fabric to recover, thus for the outer loops to come back into contact as visible by the non-overlapping hysteresis curves: in the stretch phase, the conductive yarn loops come out of contact at a faster rate than when they come back into contact in the recovery phase of the same cycle. As also observed for the top-thread case, the un-conditioned fabric does not fully recover from the first stretch influences the sensor response.

4.3.3 Bottom-Thread Cover-Stitched Sensor Analysis

This subsection concludes the experiments discussion providing details of the test and test results for the bottom-thread sensor.

As in the previous sections, figure 4.14 shows raw sensor data normalized to align with extension cycles and the sensor hysteresis. The cycle rate is on average 6.25 cycle/min.

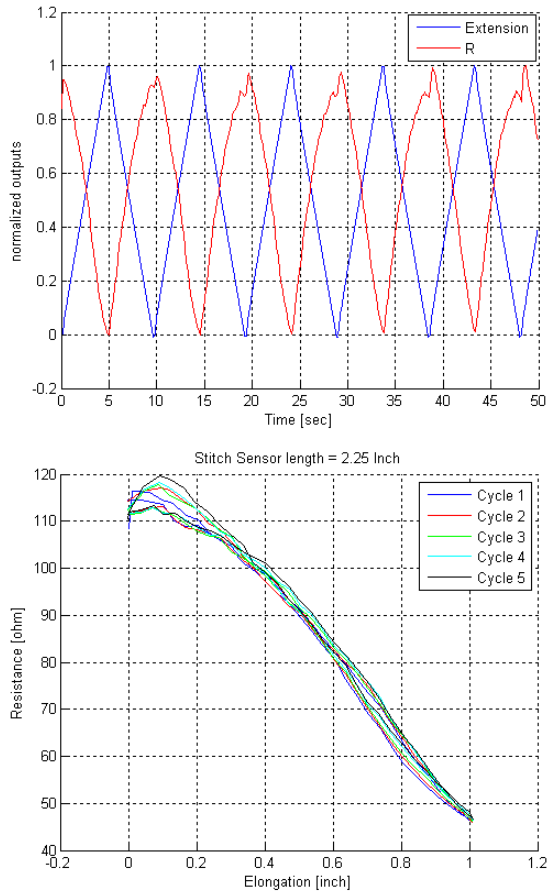


Figure 4.14. Bottom-thread output: normalized resistance aligned with normalized extension on the top; Resistance vs Elongation on the bottom. Pearson correlation Resistance vs Elongation 0.98

The resistance almost linearly decreases during the stretch phase and increases during the recovery phase. After the very first stretch, the resistance value slightly increases at 0” extension. This is likely an effect of “bending artifacts” in the response of the elongated sample: after the first cycle, the stretched-out sample buckles in the middle in relaxed position. As will be explained later, this sensor is also sensitive to bending deformations, and this change in the

relaxed-position response is likely an effect of the stretched-out (un-recovered) part of the sample buckling when in the relaxed position.

The bottom-thread stitched sensor benefits from a wider sensor response and better linearity properties such as Pearson's correlation compared to both top-thread and overlock stitched sensors. The small elongation allows the fabric to quickly recover and follow the sensor resistance response with correlation coefficient $\rho = 0.98$. The bottom-thread sensor responds to larger stretches compared to both top-thread and overlock sensors, and it is in general less affected by the fabric recovery properties (it shows very little hysteresis). The sensor would keep responding until the thread and/or fabric breaks. Although it was not rigorously evaluated in this study, anecdotally for the same stitch length loosening the tension on the conductive thread during fabrication allows the sensor to stretch to the detriment of a more noisy sensor response for a very small tension.

4.4 Resistance Drift

Textile-based conductive sensors are commonly known to show drift of the electric resistance [40]. This problem adds uncertainty in the interpretation of the resistance of the textile based sensor, if for example the output resistance is used to map the physical input that actuated the sensor [58]. Anecdotally, it was found that the deterioration over time of the conductive material certainly contributes to the baseline resistance increase of the sensor: for example, silver coated nylon based fibers (like the conductive yarns considered here) show silver particles and in some cases entire silver fragments (depending on the quality of the bond between nylon and silver) that come off after repeated mechanical stress of the fiber, for example after stretch or bend. However this may not be the only reason for the resistance drift, but the limitation of the method used to

measure it as well as variables of the yarn coating process could also influence drift properties, as discussed below and in the subsequent section.

All sensors' raw data of figures 4.12-14 exhibited drift of the resistance values measured over the cycles. For sake of generality among the sensors, the most responsive sensor identified by the bottom-thread sensor is reported in this analysis. To check the drift condition, the sensor was measured for over 40 minutes while INSTRON Tensile machine was holding it stretched. Figure 4.15 shows the sensor output.

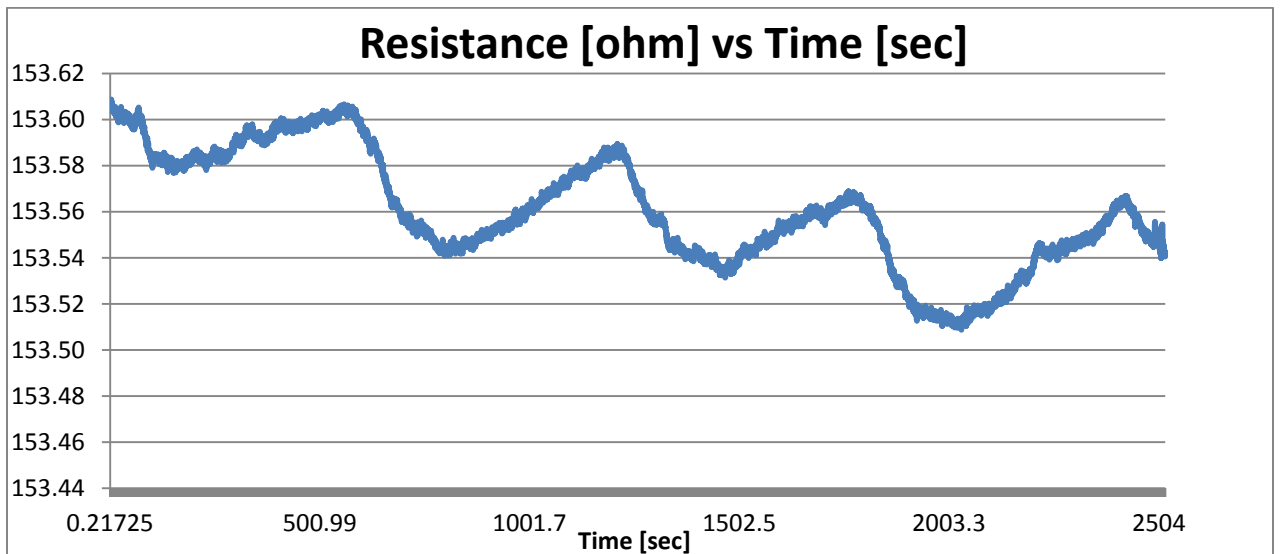


Figure 4.15. Bottom-thread sensor in stretched position for more than 40 minutes

The DMM generates an irregular oscillation of the measured resistance values that decreases over time, recalled as a biasing effect of the DMM. The constant sensor resistance corresponds to a downward drift of the resistance readings.

In another test, a 1” long bottom-thread sensor was stretched for 1” (100%) and relaxed for 100 consecutive cycles. The alternate variation of the sensor resistance now causes an overall upward drift of the resistance readings where the mechanical stress on the yarn is predominant. One hypothesis for this behavior relates to variables of the coating process used to produce the silver-plated yarn. The yarn used here is coated in a 2 ply structure, in which two bundles of Nylon filaments with opposite twists are twisted together into a 2-ply yarn, which is then plated with silver. Because the plies are in contact with each other at various points in the twist, the silver coating develops “shadowed” areas where less silver is deposited. One hypothesis is that as the yarn is repeatedly stretched and relaxed, these “shadowed” areas of crossing filaments stabilize, causing a decrease of the yarn conductivity thus an increase of the measured resistance. Figure 4.16 shows the corresponding sensor response.

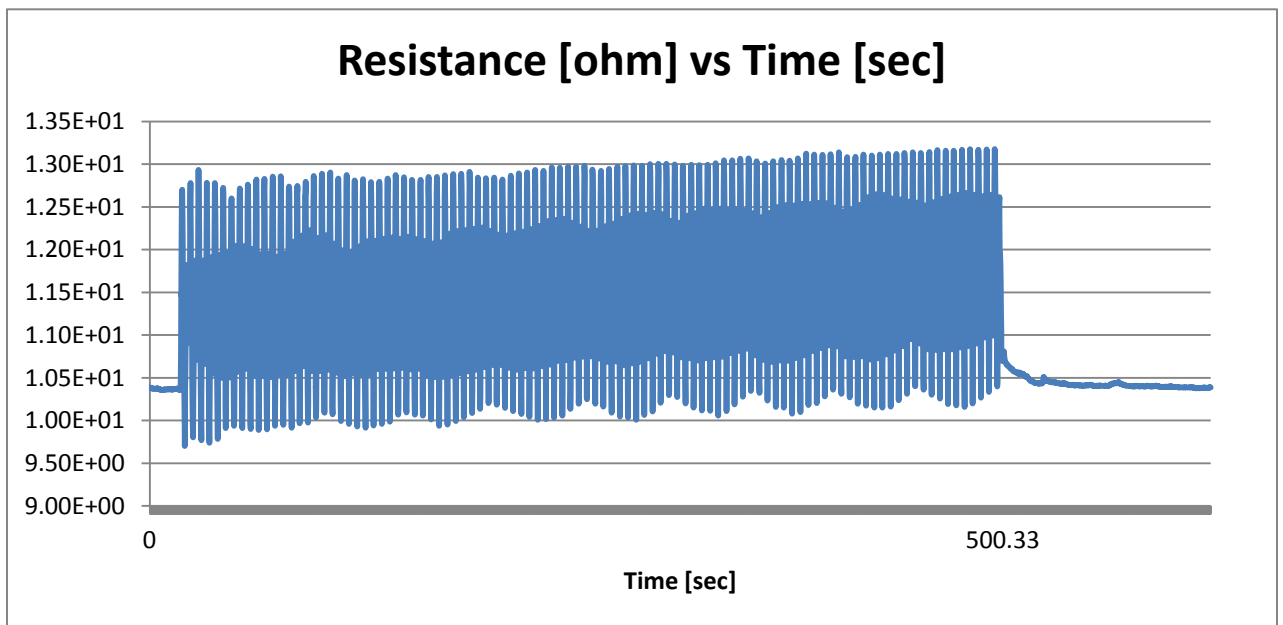


Figure 4.16. Bottom-thread consecutively stretched and relaxed for 100 cycles

An infinite number of cycles would be characterized by upward drift of the resistance due shadowing that will tend to settle, and by deterioration of the silver coating which will eventually result in a complete loss of conductivity.

To test such hypothesis on the yarn drift illustrated in figure 4.16, the following section 4.4.1 analyzes and justifies the mechanical effect on the yarn conductivity due to stretch, by comparing yarns made out the same silver coating material but with different number of plies twisted together. The effect of the number of plies in the yarn conductivity is investigated.

4.4.1 Initial Drift Characterization: 2 – 4 – 5 Ply Comparison

In order to better understand and minimize the overall drift effect, three Shieldex silver-coated nylon yarns were tested: 177/17 dtex 2-ply sewing thread; 235/34 dtex 4-ply⁴ sewing thread; and a custom fabricated 5-ply sewing thread. Plies are coated in 2-ply yarns. The 4-ply yarn is 2 2-ply yarns that have already been coated twisted together. Similarly the 5-ply yarn is 2 2-ply and 1 1-ply that have already been coated twisted together. Both 4-ply and 5-ply yarns have better conductivity because there is less “shadowing” or lack of silver coating since the outsides (un-shadowed areas) of coated plies are in contact between plies.

One bottom-thread sensor length was made for each conductive yarn. Figure 4.17 shows the three sensors.

⁴ <http://www.shieldextrading.net/pdfs/23534x4hc.pdf>



Figure 4.17. 2 – 4 – 5 ply Bottom-thread sensors, from left to right

All three sensors were evaluated using INSTRON and a DMM as described in section 4.2. For both 4-ply and 5-ply yarn sensors, 3” long sensors were tested, while for the 2-ply sensor only 1” long sensor was tested due to the very high resistance per unit length of the 2-ply yarn that exceeded the upper limit of the DMM for longer sensors. In separate experiments, each sensor was first stretched and relaxed 20 consecutive times for 25% stretch; followed by another 20 stretch-relax cycles at 35% stretch; and finally the last 20 stretch-relax cycles at 50% stretch, respectively.

Figure 4.18-4.20 illustrate the normalized response of the three sensors for 25% stretch, where the 2-ply thread appears as the most noisy while the 5-ply shows the least drift if compared to both 4-ply and 2-ply threads.

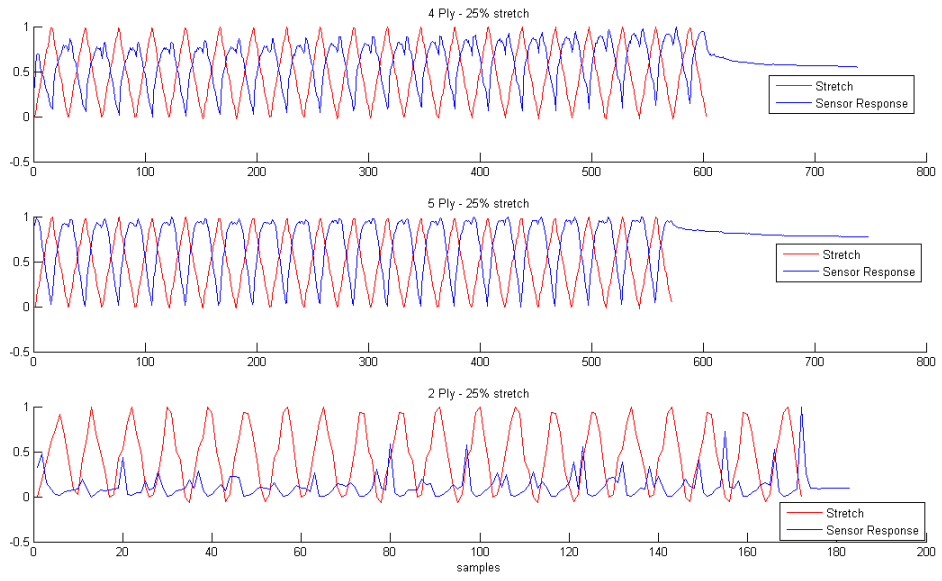


Figure 4.18. 2 – 4 – 5 ply Bottom-thread sensors normalized responses for 25% stretch, at approximately 3.3Hz sampling rate

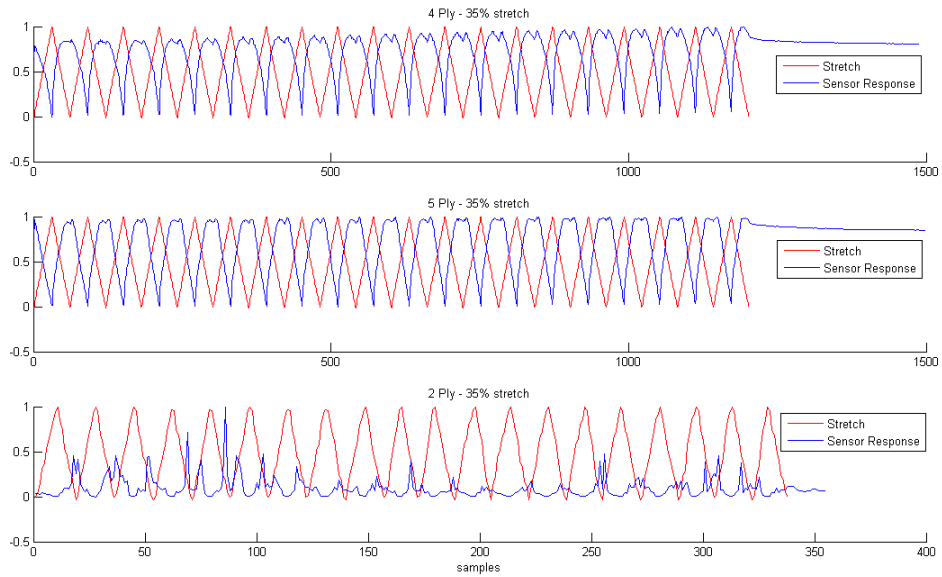


Figure 4.19. 2 – 4 – 5 ply Bottom-thread sensors normalized responses for 35% stretch, at approximately 3.3Hz sampling rate

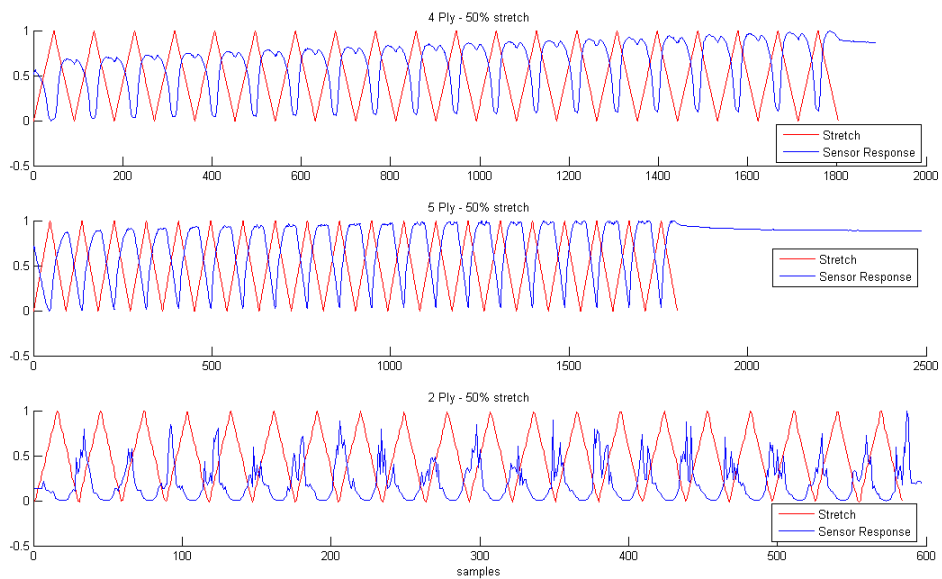


Figure 4.20. 2 – 4 – 5 ply Bottom-thread sensors normalized responses for 50% stretch, at approximately 3.3Hz sampling rate

For each cycle, sensor responses were assessed for nominal and baseline resistance value at 0° extension, sensitivity, base and peak drift, peak-to-peak response, hysteresis area, and response to fabric bend regions during both stretch and recovery phases. The following definitions are used:

Nominal resistance: the nominal resistance represents the theoretical resistance for each inch of sensor in the relaxed position (no extension), and it was measured by rounding a coarse average value of ~10 consecutive measurements of 1-inch sections on different areas of the sensor;

Baseline resistance: the baseline resistance is computed as the resistance in the relaxed position (no extension) of the second stretch cycle, after the first full extension;

Sensitivity: the sensitivity is the ratio between the absolute maximum resistance change $|\text{MAX}(R)-\text{MIN}(R)|$ and the amount of elongation, where R refers to the sensor output resistance at the maximum relative extension (i.e., 0.75" for a 25% stretch of a 3inch long sensor).

Sensitivity is expressed as a change in Ohms per unit length of the sensor;

Average Base Drift: the approximate derivative of the baseline resistance, base drift is calculated as the average difference between consecutive maxima in the sensor response, corresponding to minimum extension (or fully relaxed sensor);

Average Peak Drift: peak-drift is calculated as the average difference between consecutive minima in the sensor response, corresponding to maximum extension;

Total Base Drift: total base drift is defined as the difference between minimum and maximum values of the resistance value at minimum extension (or fully relaxed sensor);

Total Peak Drift: total peak drift is defined as the difference between minimum and maximum values of the resistance value at maximum extension (or a fully stretched sensor);

Peak-to-peak response: the peak-to-peak response is computed as the absolute difference between minimum and maximum values of the resistance in each cycle, averaged over all cycles;

Hysteresis area: the hysteresis area is defined as the area comprised between extension and recovery curves of the same cycle, averaged over all cycles;

Bend region: the difference between the initial resistance value at minimum extension and the maximum resistance before resistance begins decreasing, averaged over all cycles.

These values were averaged over all cycles. The mean values are reported on table 4.2 in the next page. Long term repeatability parameters indicate an increase in drift of the 2-ply yarn and a

much smaller drift of the 5-ply yarn compared to the 4-ply yarn, supporting the hypothesis of better conductivity and less “shadowed” areas of crossing filaments brought into contact, and less chance of shadowed areas stabilizing (increasing conductivity) over time through mechanical stress. The 2-ply sensor shows more Peak-to-Peak variability, due to a more noisy response. By contrast, both 4-ply and 5-ply sensors showed consistent, repeatable, and reasonably comparable performance.

Table 4.2. 2 – 4 – 5 ply bottom-thread sensors basic parameters, precision and accuracy

Relative Stretch – yarn Ply’s	Basic Parameters			Precision and Accuracy							
	Nominal R per unit length [Ω /in]	Baseline R [Ω /in]	Sensitivity S [Ω /in]	Long Term Repeatability						Hysteresis Area [Ω *in]	Bend Region [Ω] @ Extension – Recovery
				Average Base Drift [Ω]	Average Peak Drift [Ω]	Total Base Drift [%]	Total Peak Drift [%]	Peak-to-Peak Mean [Ω]	Peak-to-Peak Var [Ω]		
25% stretch – 2 Ply	2K	1.48K	0.47K	24.92	4.92	95.75	6.44	0.8K	0.29M	2.33K	1.94K – 1.25K
25% stretch – 4 Ply	16	16.88	5.52	0.02	0.02	1.34	1.47	4.16	0.02	12.63	1.14 – 0.73
25% stretch – 5 Ply	8	9.59	3.78	0.01	0.02	0.72	1.93	3.79	0.03	9.12	0.30 – 0.15
35% stretch – 2 Ply	2K	3.3K	7.34K	76.33	2.02	112.3	5.70	1.3K	0.43M	7.09K	1.47K – 2.95K
35% stretch – 4 Ply	16	17.48	15.02	0.07	0.02	3.23	1.74	16.04	0.14	80.10	1.47 – 1.72
35% stretch – 5 Ply	8	9.67	7.87	0.01	0.01	0.98	1.21	8.34	0.01	32.38	0.42 – 0.30
50% stretch – 2 Ply	2K	2.37K	2.9K	18.97	-0.43	197.69	134.88	3.3K	2.7M	25.4K	2.99K – 1.32K
50% stretch – 4 Ply	16	18.90	16.79	0.61	0.20	17.40	8.48	29.25	5.18	229.01	2.31 – 2.88
50% stretch – 5 Ply	8	8.90	6.76	0.06	0.018	3.60	1.81	10.71	0.04	69.42	0.31 – 0.33

2 – 4 – 5 Ply Discussion

The 4-ply sensor has double the nominal resistance of the 5-ply sensor, but a factor 100 smaller than the 2-ply sensor. For each sensor, the baseline resistance shows consistent values with a small variability among the trials at 25%, 35%, and 50% due to the cumulative effect of deforming the fabric repeatedly. Both sensor types show a larger sensitivity increase between 25% and 35% stretch than between 35% and 50%. If the sensor response were perfectly linear, sensitivity would be consistent regardless of the amount of extension. Instead, there is a larger change between 25% and 35% stretch than between 35% and 50%. However, because the bending artifact is encompassed in the beginning of the stretch period, it comprises a relatively larger portion of the 25% stretch response than the 50% stretch response.

The 5-ply sensor has better long term repeatability properties than the other two threads, exhibiting smaller drift and smaller variance. However, the 4-ply sensor showed similar performance, especially for 25% and 35% stretch, and both sensors show drift on the order of less than 4% for 25% and 35% stretch. Increasing the amount of stretch in both the 4-ply and 5-ply sensors correlates with a predictable increase in the peak to peak mean responses, while average drifts stay about the same, except in the case of the 4-ply sensor (that shows a larger increase, particularly at 50% stretch). The 4-ply shows increase of both total drift and peak to peak variance with increase in extension; the 5-ply shows a smaller increase compared to the 4-ply of the total base drift with the extension, while the total peak drift and peak to peak variance oscillate around closer values for 25%, 35%, and 50% stretch. The hysteresis between the extension and recovery curves increases as the stretch increases for both types of threads. This is consistent with the behavior of elastomeric fabrics. In all our tests the fabric was never pre-conditioned (pre-stretched).

The 5-ply thread exhibits the best sensor behavior. However there are other practical considerations that affect the choice of thread for fabricating sensors. For example the 4-ply

thread is commonly used, easily available, and relatively low cost while the 5-ply thread must be custom-fabricated and is higher-priced. While this factor is feasibly overcome, the 5-ply yarn is also thicker and bulkier than the 4-ply yarn, as seen in figure 4.17. This has two key consequences: it is more difficult to handle in the machine, and it creates a bulkier, more noticeable appearance in the finished stitch. Therefore given the similarity in performance parameters between the 4- and 5-ply threads, the 4-ply thread is the preferred choice.

4.5 Stretch Sensor: Fabric effect

The fabric on which the sensor is stitched potentially has a significant effect on the response of the sensor. To test this, the overlock sensor presented in section 4.1.3 was stitched on fabrics with different physical properties and its output response was recorded to measure the effect of fabric property on the sensor response [42]. The initial theoretical consideration was that if the textile has poor recovery capabilities, meaning it “stretches out” rather than returning to its initial length prior the stretch, the sensor response will follow this physical behavior and fail to return to the baseline level. The conductive thread used here is the 4-ply described in section 4.4. Sensors were stitched on five different fabric substrates with different elongation and recovery properties: 100% polyester jersey knit, 60% cotton/40% polyester jersey knit, 94% cotton/6% spandex jersey knit, 90% polyester/10% spandex jersey knit and 82% nylon/18% spandex jersey knit. Each of these textiles uses the same knit structure, with variations in fiber content.

An INSTRON tensile machine was used to stretch the test sensors by 40%, adopting the same methodology as in 4.2. For each fabric, approximately 20 stretch and recovery cycles were completed and then averaged. Because samples were all previously un-stretched, the first extension cycle for each sample is discarded as a “conditioning” sample. A DMM connected to the sensors extremity during the stretch and recovery cycles measured the resistance output of the

sensor that was then aligned and overlapped with the extension points measured by INSTRON machine.

To evaluate the characteristic of this sensor implementation with respect to fabric substrate, the following properties were measured: baseline resistance of the stitch in the relaxed position, peak-to-peak resistance of the sensor response, hysteresis of the sensor response between elongation and relaxation of the stretch cycle, and linear response range with respect to elongation. Sensor responses were characterized for the following metrics: Peak-to-peak and Hysteresis.

Fabric Results

The measured peak-to-peak response for all sensors is between 2 and 14 ohms. Figure 4.21 shows the average peak-to-peak sensor response range for each fabric, normalized with respect to baseline resistance measured at the trough of each elongation cycle (representing the minimum-load of each cycle and corresponding to the minimum resistance). Sensors integrated on fabrics with elastomeric components (i.e. spandex) show the largest values with maximum average range for the poly/spandex equal to 22.97% of its baseline resistance.

Figure 4.22 shows the sensors hysteresis trends for test fabric, while table 4.3 shows the hysteresis error defined as the maximum difference between the sensors output during the extension and during the recovery phases at 10% of the total elongation input. Also in this case, spandex fabrics show the highest hysteresis in the sensor responses.

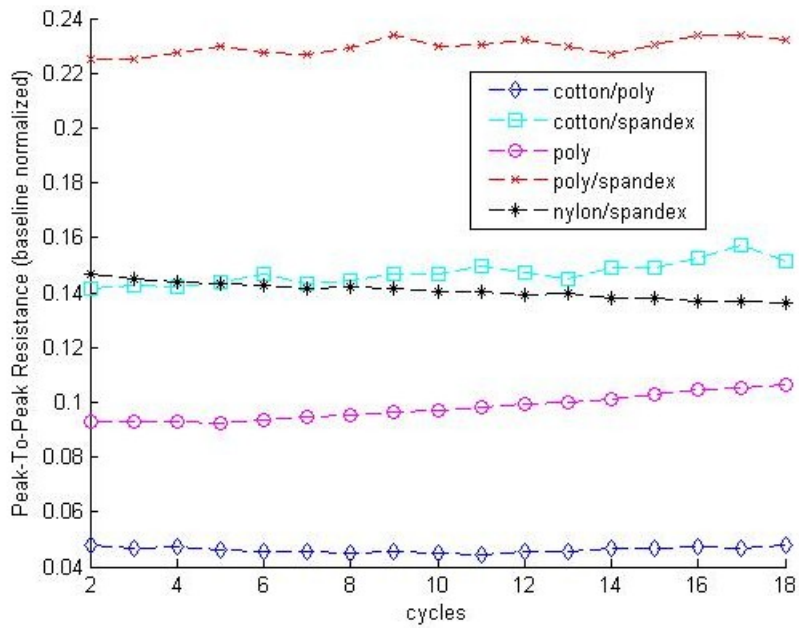


Figure 4.21. Normalized peak-to-peak response range for each test fabric

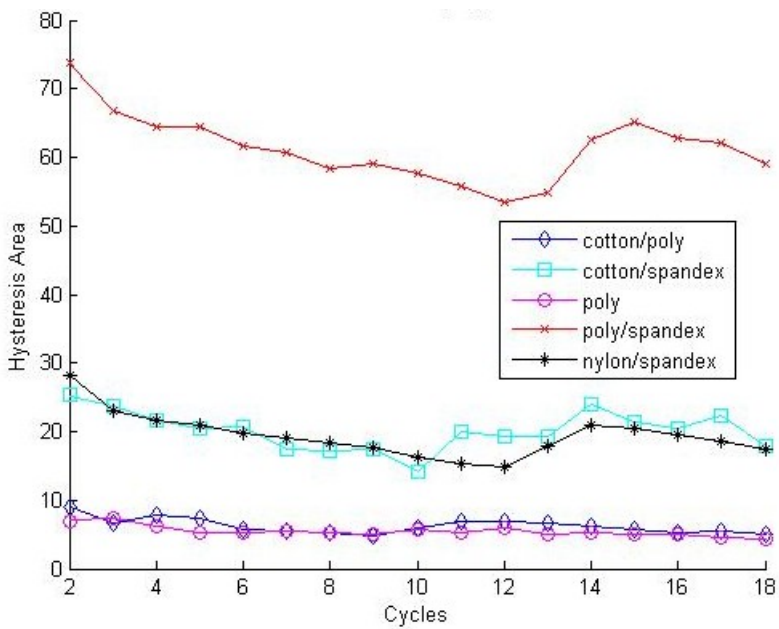


Figure 4.22: Hysteresis magnitude for each test fabric

Table 4.3. Hysteresis Error (Ohms) at 10% elongation

Hysteresis Error	Cotton/ Poly	Cotton/ Spandex	Poly	Poly/ Spandex	Nylon/ Spandex
@10% Elongation	0.35 Ω	1.15 Ω	0.19 Ω	3.04 Ω	0.82 Ω

Textile-based sensors can provide comfort benefits to wearable sensing, but are often difficult to construct and manufacture so to preserve the mechanical properties of the textile. The overlock thread was chosen because optimize wearer comfort and minimize manufacturing cost which hold true for the other two industrial coverstitches presented here.

Clear influence of amount of elastomeric content is not observed. However fabrics with spandex content generated larger output range, while fabrics without spandex but with polyester and cotton content generated smaller hysteresis between sensor stretch and recovery phases.

Additional sensors output parameters, for example the drift, are likely influenced by additional variables such as thread properties that however were not properly controlled. Fabrics are a good choice for sensing in clothing because allow to meet the wearer aesthetic or more practical needs based on their fabric content providing comfort, and sensing capability through stitched sensors.

4.6 Insulated Stretch Sensor

The stitched sensors are in many ways like normal stitches in our clothes with the additional property of being conductive. The conductivity of the sensor, however, requires protection from external agents (like water or sweat) that could interfere with the working principle of the sensor or generate shorts. The un-insulated nature of the conductive yarn is essential to the sensor's

working principle, but can present practical problems of implementation. To avoid the sensor being exposed (and subject to shorting) while preserving its stretchable and flexible properties, a strip layer of stretchable 3M 7012 stitchless bonding film (fusible polyurethane film) was fused directly on top of a 4-ply bottom-thread sensor integrated on a stretchable fabric, as shown in figure 4.23. The thin film provides electrical insulation of the sensor: for instance, applying the DMM probes between two points of the sensor on top of the bonding film measures 0 Ohms.

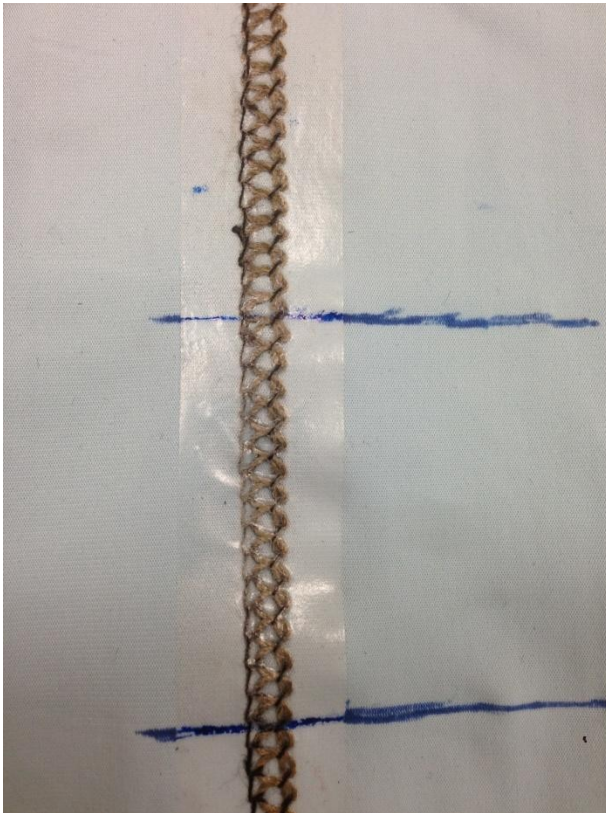


Figure 4.23. Insulated bottom-thread stretch sensor, on 98% polyester 2% lycra jersey knit fabric

The Insulated sensor was tested with INSTRON and a DMM, using the same methodology described in 4.2. The two blue marks in figure 4.23 indicate the space between the INSTRON

plates so the sensor length that was stretched was approximately equal to 2". The sensor was stretched for 12.5%, 25%, 37.5% and 50%. Figure 4.24 shows the insulated sensor output.

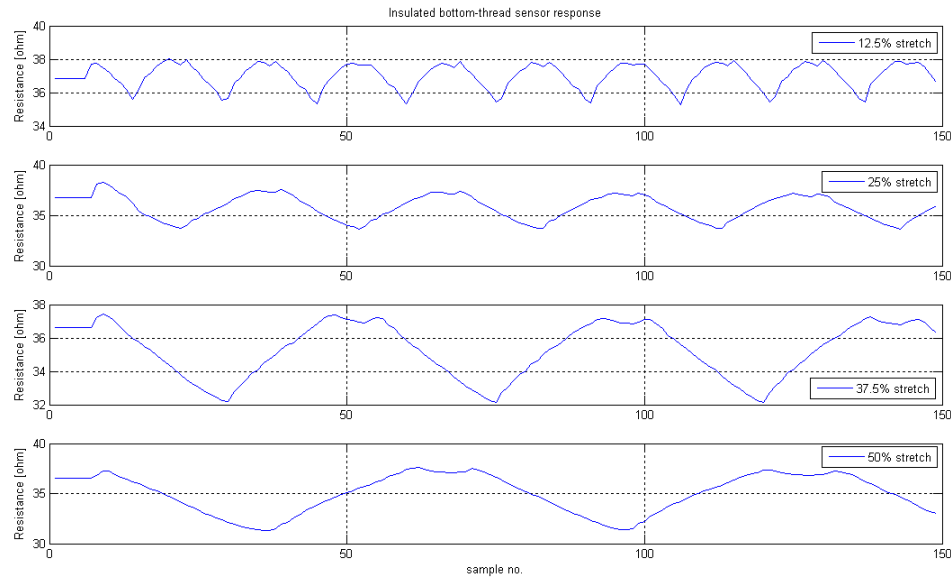


Figure 4.24. Insulated bottom-thread stretch sensor output

Insulation Results

The response of the insulated sensor is comparatively smaller than without insulation, likely because the sensor thread move less during the stretch (according to the working principle described in 4.1.4) because the insulation layer fused on top of the stitch tends to keep the thread structure in place. Thus, insulation increases the durability of the sensor by protecting the sensor from environment factors like water or sweat for example, but simultaneously decreases the amplitude of the sensor output for larger stretch amount. Table 4.4 approximate the peak-to-peak values of the experiments illustrated in figure 4.24 with the peak-to-peak values of experiments reported in table 4.1 for the 4-ply yarn

Table 4.4. Stretch Sensor - Insulation Results

	peak-to-peak @25%	peak-to-peak @35%	peak-to-peak @50%
Insulated	3Ω	6Ω	7Ω
Un-Insulated	4Ω	16Ω	30Ω

The insulated sensor is 1” shorter than the un-insulated one, in the comparison above. However, the length of the sensor does not remarkably affect the peak-to-peak but bias the initial output value measured for the sensor.

Insulation thus decreases the sensor output range making the sensors more stiff and potentially less comfortable to wear, to the advantage of sensor protection.

4.6.1 Wash Deterioration

(NB: This experiment was conducted in collaboration with Mary Ellen Berglund, an undergraduate UROP student in the lab, who contributed significantly to the testing and analysis.)

Insulation provides a solution to protect the sensor from the environment. In order to find how practical this solution is, the durability of the insulation layer was investigated by putting the sensor through regular wash and dry cycles.

3” long Insulated bottom-thread sensors with the fusible polyurethane film and 3” long un-insulated sensors were washed (cold) and dried 5 times consecutively either with air or machine dry (delicate). Three samples were tested under each condition for the un-insulated case, while only one sample was tested under each condition for the insulated case. For the un-insulated sensor, peak-to-peak and baseline resistance were measured using a DMM and an INSTRON Tensile machine; for the insulated sensors, the delamination of the insulation layer was measured after each dry cycle by marking the delaminated areas on the film with a marker. Marked samples were then photographed in a standardized position. Using the magic wand selection tool with 5% sensitivity of Adobe Photoshop, the marked areas were selected and the pixel count of the marked areas was recorded as a measure of delamination. Before measuring the delamination, all three samples were stretched by 25% using the same method described in 4.2.1. Both samples are then compared with a reference sensor that is never washed or dried [41].

Wash Results

- The delamination of the bonding film increases with the number of cycles, and larger delamination is observed for tumble dry cycles. The delamination increases 149% from the initial delamination area for the reference sensor never washed or dried; 177.9% for the sensor washed and air-dried; 246.6% for the sample washed and machine dried;
- The baseline drift increases after washing the sensor, and more drift is observed after tumble dry cycles. The drift increases an average of 14.7% of the initial resistance for the reference group; 20.1% for the wash and air-dry group; and 30.6% for the wash and tumble dry group;
- The peak-to-peak deteriorates with washes and at a higher rate with tumble dry cycles. The peak-to-peak decreases an average of 22.1% of the initial value for the reference

group; 30.3% for the wash and air-dry group; and 44.6% for the wash and tumble-dry group.

In summary, tumble dry cycles contribute more significantly to the delamination of the insulation and have a greater effect on the sensor's properties than just washing alone. Insulation is shown to preserve the sensor's working principle and to be sufficiently durable during washing.

Therefore insulation represents a practical way to protect the sensor from external factors, for example sweat or accidental shorting which could happen if the sensor is integrated on the garment and left exposed.

Wash and dry cycles however deteriorate sensor insulation and conductivity. A large enough number of wash and dry cycles is expected to destroy the sensor.

Chapter 5

Bend Sensing:

The Bottom-Thread Cover-Stitched Sensor

A fabric that stretches can also bend; a fabric that bends does not necessarily stretch. To characterize in general the garment movement, it is key to be able to sense movements of those fabrics that do not stretch but fold or bend, during body movements. The bottom-thread coverstitched sensor has been revealed to be the most responsive sensor with a larger number of self-intersecting points in the stitch structure. It can generate a resistance response when bent, due to shifts in contact points between self-intersections in the conductive thread and the stitch structure. Specifically, when the sensor is bent the self-intersecting conductive threads come closer together increasing their conductive contact. This ability makes the sensor best suited to detect bend originated by fabric folding behavior. In a controlled scenario, the effects of fold types and fabric structures on the bend sensor response are investigated.

The looper thread of the bottom-thread coverstitched sensor has the most complex structure and it is the most responsive to bend if compared to the other stitched sensors analyzed here, due to a larger number of crossing yarns of the conductive thread. A larger number of crossing yarns correspond to a more responsive sensor with the additional benefit of larger amplitude of the stitched sensor response during bend [43].

5.1 Experiment Design

The five samples of un-stretchable denim jeans with different fabric stiffness properties listed on Table 2.1 of Chapter 2 were considered.

5.1.1 Sensor Structure and Experiment Setup

The bottom-thread sensor was stitched down the center of circularly shaped samples, as depicted on figure 5.1.

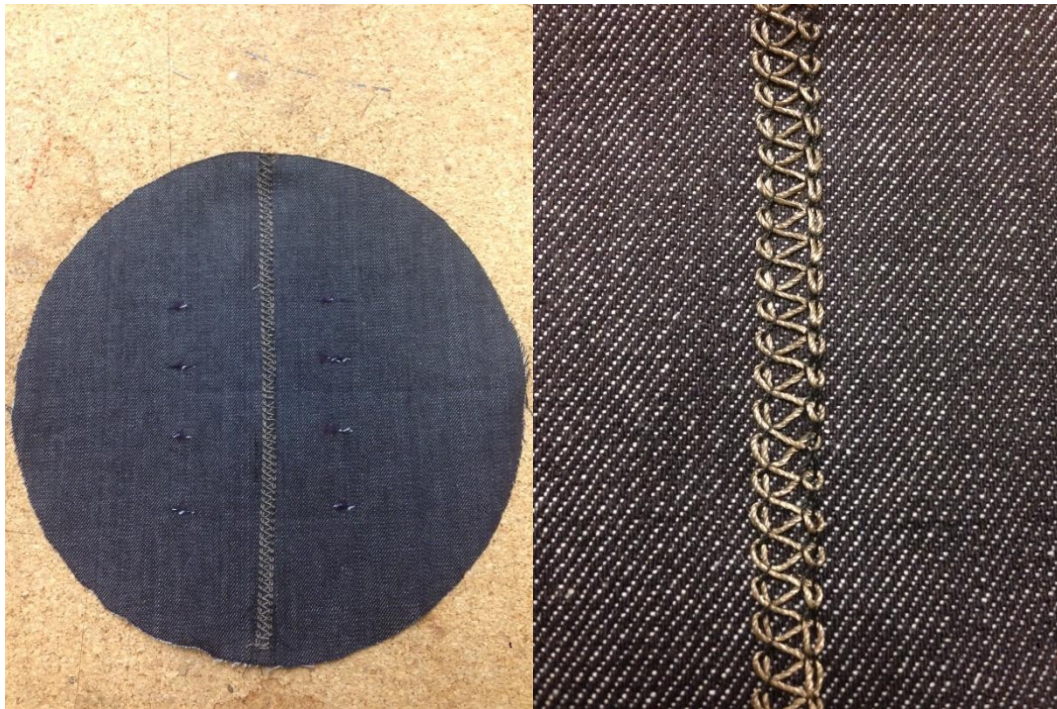


Figure 5.1: Denim Sample (on the left) with zoom of the stitched sensor (on the right)

Similarly to the stretch experiments of section 4.2, the sample was symmetrically placed between the INSTRON clamps, and a layer of neoprene material was added between each clamp plate and the sample to prevent shorting between the metallic plates and the sensor. Given the tendency of the fabric to produce a single fold in the middle of the sample when the INSTRON clamps are brought together, controlled bend was introduced to produce specific fold morphologies. Folds were induced in specific spots by inserting two straight, rigid rods passing through equally spaced perforations on both sides of the sensor, with each rod placed about 2.5” away from the sensor. By changing the orientation of the fabric as the guide rod was inserted, induce folds in either direction above and below the perforation can be induced. The diameter of the perforation allowed the fabric to slide along the guide rod as the INSTRON clamps (4” wide, 2” high) moved during flexion and extension. Figure 5.2 shows our bend testing setup.

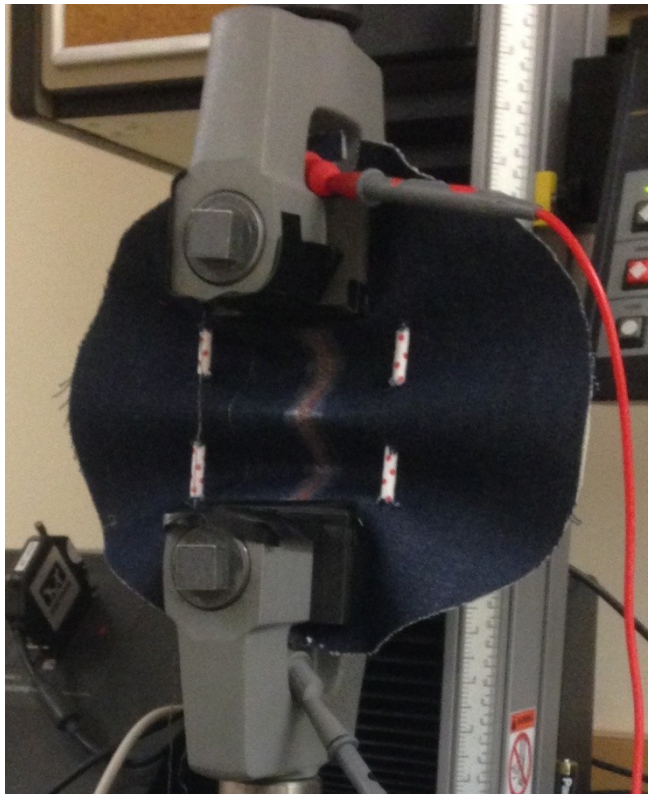


Figure 5.2 Denim Bend Test Setup: Denim sample clamped between INSTRON plates, and connected to Digital Multimeter

Top and bottom perforations were spaced about 4” from the sensor extremes to allow room for the INSTRON clamps and to connect the DMM probes, and 1” was left between perforations as depicted in figure 5.4. All denim samples have 11” diameter.

5.1.2 Insulated Sensor

In the un-insulated case, the inner folds at maximum bend cause shorts of the stitch with itself, due to the fact that the conductive thread of the stitch is exposed. In order to insulate the sensor, the same methodology used for the insulated stretch sensor of paragraph 4.6 was used: a thin layer of transparent glue is directly fused on the sensor, preserving sensor response and fabrics bending properties.



Figure 5.3 Insulation by Fusing technique: a strip of bonding film is fused on the stitched sensor

The insulated bend sensor is illustrated in figure 5.3. Its response is originated by self-intersecting yarns of the conductive looping thread: when the sensor is bent, the self-intersecting yarns come closer to contact introducing additional shorting within the sensor, generating a decrease of the measured resistance.

5.1.3 Fold Morphologies

Different combinations of perforations were used to create the desired fold morphology in each test.

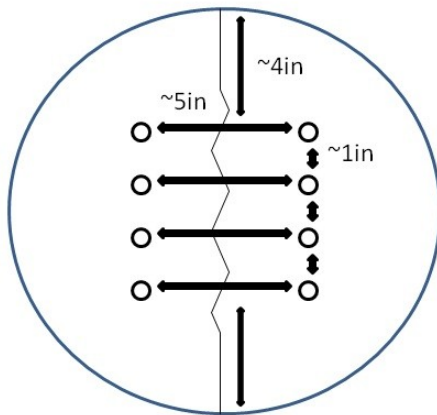


Figure 5.4 Denim Sample Layout for Controlled Bend: location of perforations for guide rods to control the number of folds.

Five types of fabric bend morphology were tested, depending on the number and direction of folds generated. Folds were generated in three categories: Simple Fold; Intermediate

Fold; Complex Fold. Simple Fold bend type is characterized by one fold (a C shape); the Intermediate Fold type by 2 folds (or 2 Simple Folds in opposite directions, resulting in an S shape); the Complex Fold type by 3 folds (or 3 alternating-direction Simple Folds, resulting in a sinusoidal wave). All folds for all bend types have equal length: Complex folds can be seen as a combination of 3 simple folds; while, intermediate folds can be seen as a combination of 2 simple folds.

For each fold type two separate cases of sensor along the inner (or convex) surface and the outer (or concave) surface of the fold were considered, to investigate the effect of folding direction. The Intermediate Fold case is considered in only one direction, given the fold's symmetry, as depicted in figure 5.5.

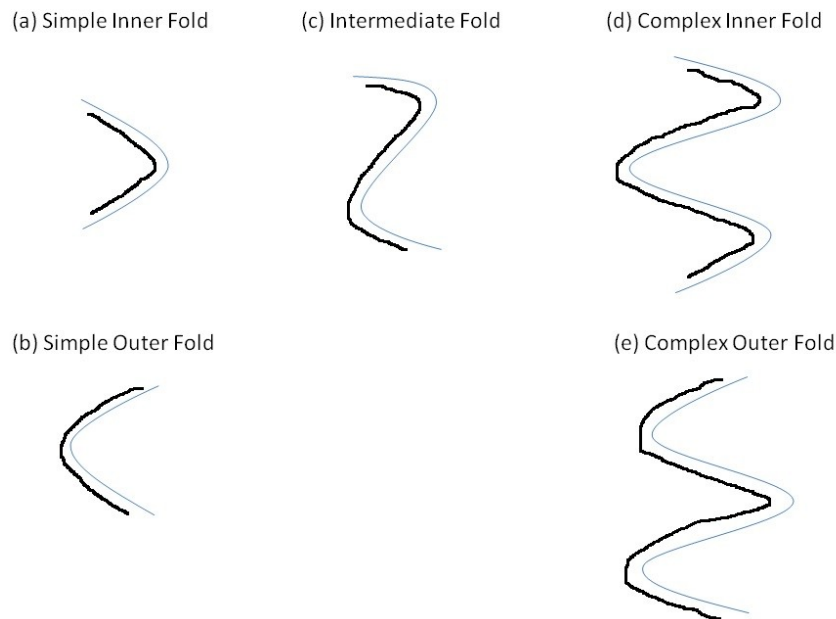


Figure 5.5 Fold Types (the dark line represents the sensor).

5.1.4 Testing Method

For each test, each denim swatch was bent and straightened for 10 consecutive cycles, where one cycle includes bending plus recovery (straightening) phases. Specifically, for each bend cycle Complex Fold bend started from an initial length of 5" (equivalent to 5" distance between INSTRON clamps) and bent the fabric 4.5" (down to 0.5" distance between INSTRON clamps plates). The INSTRON clamps were then returned to their original position, straightening the fold; on the same way, Intermediate Fold bend started from an initial length of 3.5" and bent the fabric 3"; Simple Fold bend started from an initial length of 2" and bent the fabric 1.5". Systematically, for each fabric the test session started by testing Complex Inner Fold, followed by the Complex Outer Fold test. INSTRON bottom plates were then unclamped and the top plates were lowered from 5" to 3.5" to test the Intermediate Fold. Finally, INSTRON bottom plates were unclamped again and top plates lowered from 3.5" to 2" to test Simple Outer Fold first and Simple Inner Fold after. The length of the sensor between INSTRON clamps (and the corresponding displacement during bending) was chosen so that all folds had similar diameters and curvature when the fabric was fully bent. Minimum separation distance for the INSTRON clamps was calibrated to prevent clamps from touching in order to avoid compression (thus distortion in the output) of the sensor.

Controlled bends were tested for all fold types, with and without sensor insulation.

5.1.5 Data Analysis

In order to characterize the sensor response, 8 parameters were computed: Baseline Resistance; Sensitivity; Base Drift; Normal Drift; Peak-to-Peak Mean and Variance; Hysteresis Area;

Linearity, for both Bending and Recovery phases. Similarly to the measured parameters of section 4.4,

- The Baseline Resistance (*BR*) is defined as the first peak in the sensor response (corresponding to a straight sensor) R_{M1} for the insulated case, and for the un-insulated case R_{M1} minus the bias introduced by the two sections of sensor between the INSTRON clamp plates: $BR = R_{M1} - bias$;
- Sensitivity (*S*) is the absolute average difference between minimum and maximum of the sensor output R_{ci} for cycle i normalized by the maximum bend length l_x : $S = abs(mean(MIN(R_{ci}) - MAX(R_{ci}))) / l_x$, for all i 's;
- Base Drift (*BD*) is the average difference between consecutive maxima (corresponding to the fully straightened sensor position) of the sensor resistance cycles: $BD = ((R_{M2} - R_{M1}) + (R_{M3} - R_{M2}) + \dots + (R_{MN} - R_{MN-1})) / (N-1)$, where N is the number of cycles averaged;
- Peak Drift (*PD*) is the average difference between consecutive minima (corresponding to the fully bent sensor position) of the sensor resistance cycles: $PD = ((R_{m2} - R_{m1}) + (R_{m3} - R_{m2}) + \dots + (R_{mN} - R_{mN-1})) / (N-1)$, where N is the number of cycles averaged;
- Peak-to-Peak (PtoP) is the difference between minimum and maximum sensor output for each cycle i : $PtoP = MIN(R_{ci}) - MAX(R_{ci})$;
- Hysteresis Area (*HA*) is computed as the area between bending and recovery curves of the hysteresis plot, using the trapezoidal numerical integration;
- Linearity (*L*) is the slope of the sensor response approximated to a straight-line passing between maximum and minimum of the sensor response at minimum and maximum bend, respectively.

Baseline resistance and base drift were calculated for the maxima of the sensor output in order to capture the reference resistance of the sensor in the straight position. Peak drift instead refers to the minima, and captures the effect of the fabric in generating drift in the amplitude of the sensor response when fully bent. The peak-to-peak is here defined for the generic cycle i . It will be referred to as mean and variance over all N cycles i of the trial.

5.2 Average Bends and Fabrics Relations

The sensors' responses preserved on average the relations between the folds between fabric types, even though the variability that exists in the garment movement does not allow the expression of more complex folds as a composition of simple ones for all fabrics and insulated/un-insulated cases tested. For each fold type and fabric, relationships are captured by averaging over all fabric and fold types, respectively. Table 5.1 summarizes such averages.

Table 5.1. Averages over simple-intermediate-complex bends, less stiff-more stiff fabrics - Insulated and Un-Insulated Sensors

Insul.	Simple Inner Bend	Simple Outer Bend	Inter-mediate Bend	Compl. Inner Bend	Compl. Outer Bend	Fabric no. 80833	Fabric no. 81415	Fabric no. 81814	Fabric no. 80270	Fabric no. 52735
Un-Insul.										
Baseline [Ω]	62.4 43.7	63.7 43.7	64.6 64.2	64.9 84.3	65.2 84.8	73.3 63.1	64.1 65.6	60.5 64.1	58.3 68.2	64.9 59.7
Sensitivity [Ω /in]	1.8 12.9	1.9 2.5	2.2 10.1	2.0 13.4	2.3 7.4	2.1 9.1	2.7 11.0	1.7 9.2	1.9 9.6	1.7 7.3
Base Drift [Ω]	.03 -.00	.06 .03	.06 .08	.07 .13	.09 .13	.09 .09	.04 .11	.09 .10	.07 .06	.02 -.00
Peak Drift [Ω]	.03 .11	.03 .04	.05 .25	.05 .24	.11 .07	.07 .08	.02 .12	.07 .09	.05 .35	.07 .08
P2P mean [Ω]	2.9 19.6	3.0 3.7	6.5 29.5	9.1 59.8	10.7 33.4	7.1 29.3	8.4 34.0	5.3 29.2	6.2 30.0	5.3 23.6
P2P var. [Ω^2]	.06 .36	.05 .05	.05 .83	.06 1.2	.30 .26	.20 .12	.16 .30	.04 .20	.03 1.7	.09 .35
Hysteresis [Ω *in]	13.2 46.8	9.5 17.9	37.1 191	92.3 772	116.2 265	43.4 216	78.0 352	45.7 281	38.6 216	62.6 226
Bend (- slope)	.98 .66	.97 .95	.95 .65	.94 .42	.92 .69	.95 .67	.92 .62	.96 .68	.95 .68	.97 .73
Recovery (+ slope)	.98 .66	.98 .96	.95 .65	.93 .41	.91 .70	.94 .67	.92 .62	.97 .68	.95 .68	.97 .73

Insulation and Fold Types Effect Discussion

Over all fold types and fabric types the insulation layer limit and constrain the movement of the conductive thread resulting in a more predictable sensor, as shown by the smaller range and variability of the parameters computed. Repeatability and reliability of the sensor appeared to be more strongly related to the type of fold rather than the fabric property. Insulated sensors showed variability in baseline resistance for the same fabric (same sensor) over all bends that was 4 or more times smaller than in the un-insulated case. Baseline resistance is a raw measure of the resistance of the individual sensor. Because the different bend types measure a different length of a single sensor, it is expected that the baseline resistance reflects considerable variability. The un-insulated sensor showed a more consistent baseline over the different fabrics for the same type of bend, cases in which the same length is measured for all sensors. However, if the baseline resistance is divided by the length of the sensor tested (i.e.: 5" for Complex Folds; 3.5" for Intermediate Folds; 2" for Simple Folds) a consistent pattern between the type of folds is found, where more complex folds show lower Ohm/Inch values and a maximum difference for the same fabric (same sensor) of about 20Ohm/Inch for the insulated case and about 60Ohm/Inch for the un-insulated case, as shown in figure 5.6 below. This is likely due to the slight bend introduced into the insulated sensor by the guide rods, even in the straight position. The higher the number of bends, the more total bend is present in the straight position.

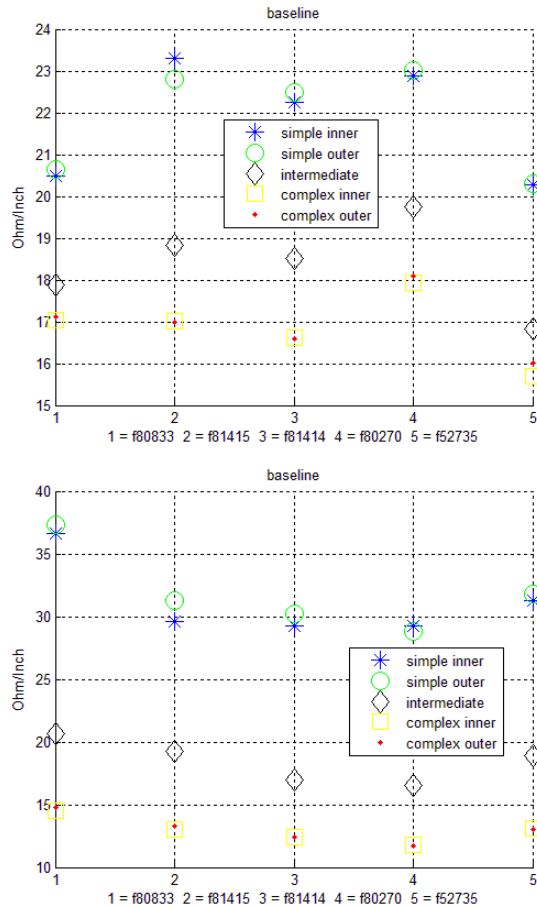


Figure 5.6: Baseline Resistance normalized by fold length: (top) Un-insulated case. (bottom) Insulated case

The sensitivity variability for the same fabric (same sensor) over all bend types became about 6 times bigger for the un-insulated case (where self-intersecting folds produce dramatic changes in resistance due to the shorting of the sensor). Base drift even in the worst case is less than $|0.3|\text{Ohm}$ and does not show evident differences between the insulated and un-insulated scenarios, indicating a stable sensor with little base drift. The largest peak drift was in the order of 0.1Ohm for the insulated case and increased about a factor 10 in the un-insulated case. For both drift cases the drift values appear to be of the same order, both reflecting a very small amount of drift that is not consistently related to fold type or fabric type. Peak-to-peak sensor responses of $2\text{-}11\text{Ohms}$

were observed for the insulated case, but increased in magnitude and variability to 4-60Ohm in the un-insulated case. However, it is important to note that the un-insulated sensor experiences shorting across the sensor during inner-direction self-intersecting folds, which explains the extreme difference in peak-to-peak response. The peak-to-peak variance is on average larger for the un-insulated case. Normalizing both base and peak drift of each fabric by the corresponding peak-to-peak mean value, for both un-insulated and insulated scenarios the drift is a small fraction of the peak-to-peak, between 0.01% and 2.1% for the various bends tested. The maximum hysteresis variability for the same fabric (same sensor) over all bend types was 116 [Ohm*Inch] for the insulated case, and almost a factor 7 larger for the un-insulated case. However, it is interesting to point out how hysteresis values among all fabrics for the simplest bends and particularly for the Simple Outer Fold are close for both insulated and un-insulated sensors. Linearity variability for the same fabric (same sensor) over all bend types for both bending and recovery phases were within 0.07 for the insulated case and within 0.5 for the un-insulated case, indicating a strongly repeatable response.

The direction of bend did change the response of the sensor. On average, outer bend showed slightly higher sensitivity for the insulated case and smaller sensitivity for the un-insulated case; smaller peak drift in the un-insulated case (while in the insulated case the relation was almost inverted, particularly for Complex Folds); smaller peak-to-peak mean and variance (particularly for the un-insulated case); smaller hysteresis; and larger slope for both phases (particularly for the un-insulated case). Baseline resistance and base drift did not show consistent changes in the response between outer and inner folds.

Insulation had a larger impact on the inner type of folds, as expected, since it is an effective solution to prevent shorts. For example, with insulation the sensitivity of both Simple and Complex Inner Folds become very close to the sensitivity of the corresponding Outer Folds (as would be expected). The same applied to the relative baseline values, for peak-to-peak mean and

variance (particularly for Complex Inner Fold), peak drift, hysteresis and linearity regions. Base drift was not affected by the direction of the fold. In general, for all other types of bends and fabrics, insulation improves linearity of the sensor response, acting like a sort of guideline or shell that limits the movement of the stitch. Such limitation decreases peak drift, hysteresis, baseline resistance values, and peak-to-peak mean and variance. Although a larger response may be useful in some scenarios, (where, for instance, the self-intersecting short may be used to detect in a binary way that a fold has occurred, rather than measuring the degree of bend) a cleaner, less noisy response may be more important in others. Peak drift in the insulated case is no longer influenced by stitch shorting. Sensor response to complex bend, on average, changes the most after insulation, since it is the type of bend where the yarn in the sensor experiences the most folds. In this case, the “guiding” effect of the insulation patch is magnified by the multiple folds. In general, the insulated case shows much closer values for almost all parameters calculated.

Hysteresis values are strongly correlated with the type of fold, (Complex, Intermediate or Simple). More complex bends show the largest hysteresis due to a larger length of fabric being folded by more folds.

For the same reason, more complex bends have on average more base and peak drift, smaller baseline resistance per unit length, higher sensitivity (particularly for the un-insulated case), larger peak-to-peak response (more in terms of mean than variance), and worst linearity (particularly for the un-insulated case).

Fabric Effect Discussion

It is also observed that in the insulated case the stiffest fabric no. 80833 is the most responsive with the largest average baseline in the insulated scenario for all fold types because of the more

rigid structure. It seems that the insulation patch added proportionally less stiffness to the stiffest fabrics, making its output resistance closer to the un-insulated case. Stiffer fabrics have also on average the largest sensitivity, the largest peak-to-peak (in terms of mean in the un-insulated scenario), and the smallest linearity for both bending and recovery phases. The heaviest fabric no. 80270 showed the largest peak drift and peak-to-peak variance for the complex intermediate and inner complex folds of the un-insulated case while in the insulated case the all fabrics values become closer together with magnitude related to the complexity of the bend.

5.2.1 The Simple Fold case: Alignment and Hysteresis plots

The least stiff and lightest fabric (no. 52735) showed on average for simple bend the largest linearity for both bending and recovery phases and the smallest hysteresis, for both the insulated and the un-insulated case. This fabric is therefore used to show the best-case scenario for the sensor response and hysteresis plot used for the calculation of the parameters mentioned above, shown in Figures 5.7-5.10.

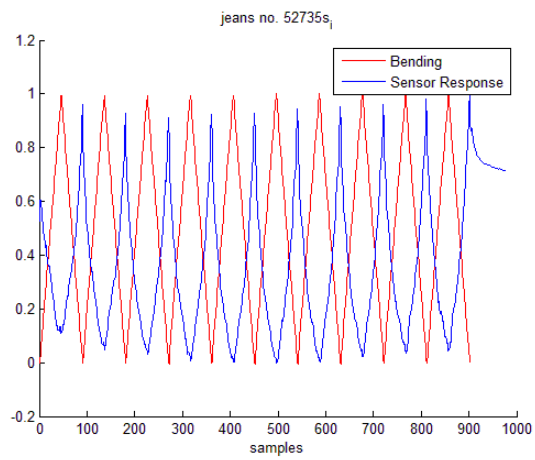
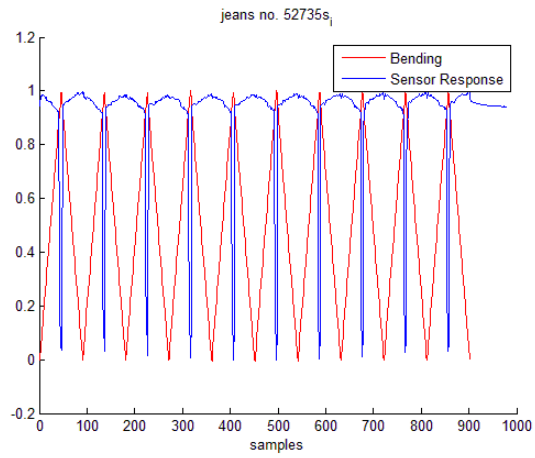


Figure 5.7: Normalized alignment, Simple Inner Fold: (top) Un-insulated case. (bottom) Insulated case

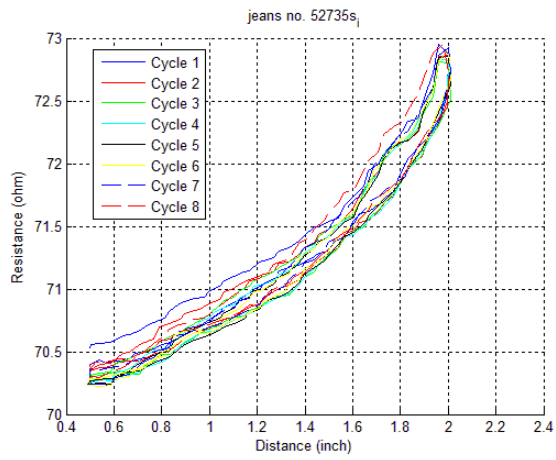
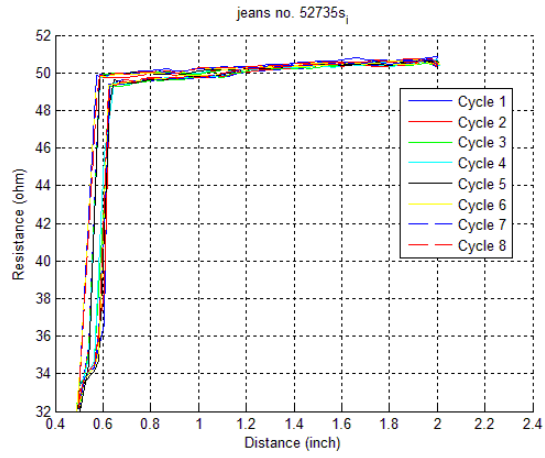


Figure 5.8: Hysteresis, Simple Inner Fold: (top) Un-insulated case. (bottom) Insulated case

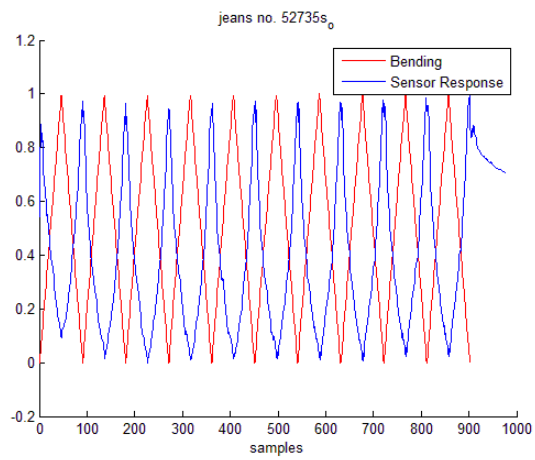
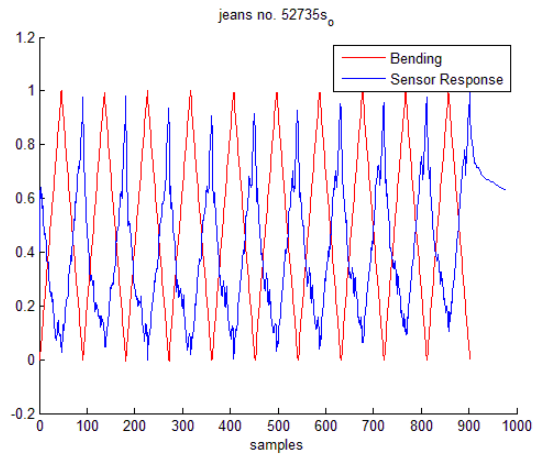


Figure 5.9: Normalized Alignment, Simple Outer Fold: (top) Un-insulated case. (bottom) Insulated case

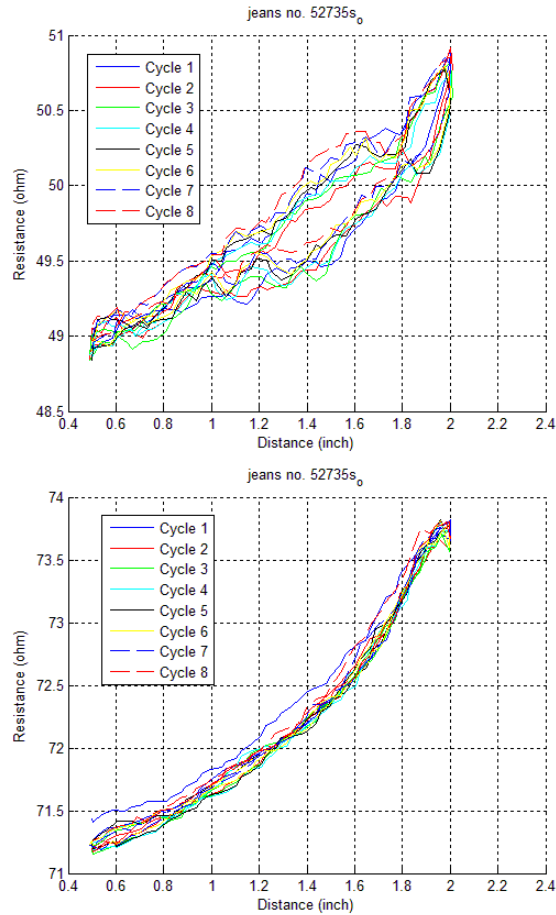


Figure 5.10: Hysteresis, Simple Outer Fold: (top) Un-insulated case. (bottom) Insulated case

From figures 5.7-5.10 it appears clear how linearity benefits from insulation, for both bending and recovery phases. The transition 0-1 of the normalized alignment plots in figure 5.7 and 5.9 corresponds to the bending region, while the transition 1-0 corresponds to the recovery region. As the folds bend, the self-intersecting yarns of the stitch come closer together, creating more shorts between fibers of the yarn and within parts of the stitch, which results in a decrease in the resistance of the sensor [46]. The un-insulated simple inner bend of figure 5.7 on the left shows how the short of the stitch with itself at maximum bend results in a drop in the resistance that does not happen for the insulated case, where the linear response of the stitch to bending becomes more visible. This also applies for the hysteresis plots of figure 5.8, where the resistance

decreases with bend for 8 consecutive cycles. In the same way, figures 5.9 and 5.10 show alignment and hysteresis plots for simple outer folds, where there is no short of the stitch at maximum bend, since the stitch faces on the concave surface of the fold. It can be seen from the hysteresis plots, that the resistance values of the insulated case are shifted upward. This is because the resistance of the insulated sensor can only be measured from the two extremes of the sensor, since the remaining sensor is completely insulated.

A large enough number of sensor bends is expected to deteriorate the insulation layer, causing the insulated sensor output to gradually behave as the equivalent un-insulated sensor, especially for the outer type of fold. The insulation of the inner type of fold would need to completely detach from the fabric for the insulated sensor output to behave like the equivalent un-insulated one.

In general, both inner and outer types of fold generate a sensor response at the beginning of the fold, i.e. when the fold starts to bend the sensor. As the sensor starts bending self-intersecting filaments in the stitch come closer together increasing their conductive contact, thus decreasing the sensor output resistance. The inner type of fold in the un-insulated case additionally decreases the output resistance more dramatically when points along the length of the sensor are brought into contact, shorting parts of the sensor.

Part II. Conclusion

The use of conductive yarns has been shown as a promising solution for embedding apparel with electronic sensing capabilities, creating truly wearable garment integrated sensors. The ability to convert standard stitches into sensors able to respond to garment and body movement opens the door to new frontiers for wearable sensing where clothes are the direct transducer for wearable sensing, with no need for major changes in manufacturing processes. Three main stitched sensors

have been used to create sensors able to sense garment stretch: top-thread coverstitched sensor; bottom-thread coverstitched sensor; and, overlock sensor. Stitched sensors have shown to provide repeatable outputs and good linearity properties. Among the three stitched sensors, the bottom thread coverstitch has been shown to be capable of capturing longer elongations and its structure was revealed to be reliably able to sense garment bend. The sensor limitation of output resistance drift was anecdotally justified and reduced by increasing the number of ply's in the conductive thread.

Stretch and Bend have been presented as two promising sensor modalities for capturing garment movement, one more suited than the other depending on the elastomeric properties of the fabric:

- stretch sensing is better adapted to an elastomeric garment, and garments with polyester and spandex content have larger amplitude (peak-to-peak) and hysteresis area in the sensor output, due to the improved stretch ability but compensated by a slower recovery;
- bend sensing is instead the only available option for an un-stretchable garment, where insulation plays a more critical role in the sensor response depending on the effect of the fold concavity by avoiding stitch shorts and affecting flexibility of the fabric by making it more stiff, improving overall sensor reliability.

For the stretch sensing modality, the durability concerns of the sensors was addressed with wash and dry cycles, monitoring the increase in resistance as well as the delamination of the sensor insulation. A similar behavior is expected for the bend sensor. Even though the sensor insulation layer does not allow water to penetrate, it does not render the sensor waterproof. Water can be absorbed through the fabric, reaching the sensor from the opposite side. Insulation has shown to increase the linearity and reduce hysteresis at the expense of smaller peak-to-peak amplitude.

To compare with existing wearable sensing techniques discussed in the background section, the following table 5.2 summarizes the sensors parameters calculated for both stretch and bend stitched sensors, for 25% stretch of a 4-ply bottom-thread sensor and simple inner bend on denim fabric 80833.

Table 5.2. Stitched Stretch and Bend sensors parameters summary

Sensor Properties	Stitched Stretch Bottom-thread	Stitched Bend Bottom thread
Linearity	0.98 Pearson correlation computed for 44% stretch	improves with insulation and stiffest fabrics
Drift	0.2 Ω for both Base Drift and Peak Drift	0 Ω for average Base Drift and .11 Ω for average Peak drift
Speed	2.5inch/min	2.5inch/min
Peak to Peak	4.5 Ω	2.9 Ω (insulated); 19.6 Ω (un-insulated)
Response	with initial bend region of ~10hm bend region prior linearity region for 25% stretch and 3" long sensor	depends on the inner or outer type of fold because of output reduction
Hysteresis	12.63 Ω *in	13.2 Ω *in(insulated); 46.8 Ω *in(un-insulated)
Washability	Resistance increase with washes due to silver coating deterioration, which is negligible after few washes	N/A
Durability	silver coating deterioration due to mechanical stretch and bend forces; delamination of the insulation layer	N/A

Comparing the results in table 5.2 with the literature reviewed: linearity of the sensor shows improvement margins because able to capture longer stretch and the bend linearity can be improved with insulation; the drift of the sensor is improved because it can be controlled by choosing the right number of yarns; the sensing ability at different speeds is also better because the sensor output does not depend by the speed of stretch or bend but by the deformation of the stitch; range of the response is improved because it can be controlled by the length of the stitch; peak-to-peak response is not a plus because of lack of amplitude and it requires an amplifier; hysteresis of the sensor is not a plus either because it strongly depends by the recovery properties of the stretchable fabric or the type of fold; washability and durability are comparable to the literature examples because washes and uses deteriorate the sensor.

Both types of stitched sensors show good linearity that improves when the stretch sensor is pre-stretch, so to remove the initial bend region; or, using insulation on the bend sensor, so to avoid self-shorts and better control the thread movement. The drift is minimal, and it depends from the type of yarn used. Both sensors were tested at the same default speed. However speed was found to not affect the sensor output performance. A consistent and repeatable peak-to-peak response is characterized by a small amplitude due to the dimension of the sensor tested and the conductive yarn used. Hysteresis are of the same order of magnitude, and in general found maximal in the middle of the stretch or bend and depending on fabric properties such us percentage of spandex content or stiffness of the fabric. Washability and thus durability of the sensor were tested for the stretch sensor only. However results are expected to apply for the bend sensor as well because found to be dependent by the yarn and insulation deterioration.

The ability of the sensors to repetitively sense stretch and bend opens to reliable body movement sensing through the clothes worn, preserving perceptibility, appearance, comfort, ease of use and application as will be discussed in the following Part III.

Part III. Evaluation:

Knee Joint Monitoring

Through Garment-Integrated Sensing

Garment-integrated sensing has been presented as a novel methodology to sense garment movement, in terms of garment stretch and garment bend. Garment movement is here considered as composed of fabric stretch and bend resulting from body movement associated with simple everyday actions like walking or sitting and more demanding activities or exercises like running or squatting. Garment elongation and buckling is monitored as a way to provide detailed information on human activities by deducing from the joint movements. The focus is here is on the knee joint in the sagittal plane, in the case of both controlled and uncontrolled knee bends. Knee bend monitoring is commonly done in rehabilitation after knee surgery, but it also offers less critical applications in activity recognition scenarios: for example, learning daily activities (i.e. walking vs seating); or, monitoring athletes training.

Part III. Introduction

Garment-integrated sensing provides an easily accessible method to detect and monitor movements of almost all parts of the human body through everyday clothing without affecting our regular routines, by minimizing the wearer's perceptibility of the garment-integrated wearable technology. Garment-integrated solutions have the potential to overcome most of the typical drawbacks of body sensing applications such as: bulky and/or burdensome devices, networking and interconnections between a large number of sensors, difficulty or annoyance in wearing and/or carrying the device, interference with body movement itself, and psychological and emotional variables related to the visibility and appearance of the wearable device. These drawbacks may generate user discomfort and, therefore, have a direct impact on the effective utility in practice of the wearable solution, because of their effect on the willingness of the user to actually wear the device as well as the quality of the device usage.

A key drawback particularly relevant for non-skin tight approaches to garment integrated sensing is the noise level introduced in the sensing output by the random nature of the movement of the garment: twisting, folding, shifting of the garment over the body surface caused by donning and doffing (i.e., putting clothes on/off) or simply by body movements. In addition, noise can be introduced by the garment production quality: garment integrated solutions usually require standard apparel machinery for integration into the garment which are not as precise as an electronics production cycle and often require direct human intervention to complete the integration process, resulting in a less accurate garment-integration.

The remainder develops and validates a wearable body sensing solution based on a comfortable garment that meets both human and electronics needs. Focus is given to the capability of

measuring and monitoring knee joint movement by integrating stitched sensors as discussed in Part II on the garment area surrounding the knee, which has been identified in Part I as one of the most feasible regions for garment sensing in a pair of pants. Controlled experimental garments and a humanoid robot are used to more precisely evaluate the movement of garments with specific parameters and properties over the body surface. A comparison of the humanoid robot with a human application is also provided. The goal is to contextualize and evaluate the accuracy of this novel garment-integrated sensing method for body movement monitoring, for the specific case of knee bend. A benchmark of wearable sensing applications is provided in the following background section for comparison.

Part III. Background: Wearable Sensing of Joint Position and Movement, Application of Joint Sensing

Smart garment implementations are affected by error introduced from garment size, as well as sensor placement and location. Harms et al. analyzed garment fitting and garment-related orientation error predictions of skin/garment-attached sensors for the classification of ten common shoulder rehabilitation postures with a relative error of 2.5% between simulation and experiments, leading to the conclusion that simulation of skin/garment-attached sensors is a feasible approach to expedite design and development of smart garments [47]. Traditional systems for postural and movement rehabilitation require tight-fitting clothing at specific body locations. Mattmann et al. used a skin tight garment prototype to recognize upper body postures using novel textile strain sensors. The resulting measurement error of 27 static postures is 3.5% over a strain range up to 100% [48]. Clothing as a feasible way to sense the body was used for back posture recognition. By capturing the strain of the fabric from a regular sensor grid distribution, the cloth elongation of more than 20% in a skin tight garment appears on the back and allows to clearly measuring distinguishable elongation patterns in 6 specifically different postures [54]. Garment-integrated skin-tight strain sensors have been used in various array topologies to implement sensing garments to reconstruct shoulder and elbow postures in terms of degree of bend. The estimation error over all experiments performed did not exceed 8% [49].

Garment effects on posture recognition were analyzed and quantified in [50]. Errors of a loose-fitting garment for the recognition of 21 postures, relevant in shoulder and elbow rehabilitation, were compared with skin-attached reference sensors. The posture and movement-sensing platform was a Smart Shirt, designed to provide real-time feedback on body data. Classification results show that posture identification benefits from a tight fitting garment, i.e. improving the

recognition performance, with an average loss in system accuracy of 13% when garment-integrated sensors are used. The movement of the wearable sensor during motion/draping of clothing was already listed between the e-textile design issues [51]. Because most garments do not fit tightly on the human frame, the draping and motion of the cloth in response to the underlying movement of the wearer may also have to be modeled to fully account for the movement of the sensor.

Skin-tight garment-integrated sensors have therefore shown to have the least error. Looser fitting clothing however is supposed to be more comfortable to the user. Comfort and accuracy variables of looser fitting clothes have been investigated. Dunne explores the tradeoff between Comfort and Accuracy by increasing garment ease and measuring the impact on the sensor accuracy of a garment-integrated bend sensor, used to measure the flexion and extension of the knee. A knee-brace application is also evaluated on the same signal parameters in repetitive donning and doffing trials, for consistency between the trials. Results underlined the significant effect of garment movement on sensor performance, identifying the major variable of garment slippage and re-positioning as the error source to analyze in more detailed future research [44].

Gibbs introduces an array of equidistant conductive fiber strain sensors attached into flexible, skin-tight spandex fabrics surrounding the knee joint. Resistance changes across these conductive fibers are used to measure angles through the use of a non-linear predictor after an initial, one-time calibration. During motion, sensors can move and shift over the body surface, and calibration coefficients are dynamically updated by minimizing the average squared error between each sensor's estimate and the average estimate with respect to the sensors offset (self-calibration). The comparison between a reference goniometer and the angle estimated from the sensor response showed an error of 5.4deg for the linear predictor and of 3.2deg for the quadratic predictor [56]. Such strain sensors are thus able to reliably capture the garment stretch of skin-tight pair of pants. However, even if Gibbs' solution provides good accuracy does not consider

user related variables such as comfort, and does not address the ease of integration aspect of the wearable solution. The fiber sensors are spanning across a single axis knee joint attached on top of the garment, looking bulky and cumbersome.

Hyperelastic sensors integrated on a soft motion-sensing suit were used to detect mechanical and electric responses to strain [53]. Two flex sensors have been integrated on the dorsal side of a knee brace like skin-tight textile to develop a wearable system to monitor joint flexion. The change in resistivity of the flex sensors with the knee bend showed a correlation of 0.98, and compared to a goniometer an average bend prediction error of 6.92deg, after fusing the two sensors with Extended Kalman Filter (EKF) [57]. Thus the prediction of hardware sensors compare with correlation and accuracy of fiber/textile-based sensors.

An appropriate design and placement of a wearable computer attaching it to the body depends on its size, shape, weight and weight distribution on the body. Wearability is reached by designing good physiological, biomechanical, and comfort levels for the wearer, to ensure usability and satisfaction [52]. Traditional inertial systems to measure joint angle typically rely on accelerometers, to measure inclination; gyroscopes, to measure rotation speed; and magnetometers, to measure azimuth respect to horizontal reference. Errors were found to be less than 3deg for flexion/extension and abduction/adduction, and up to 9deg for internal/external rotation [55].

Sensing based on body mounted hard-goods has comparable sensing accuracy performance as garment integrated sensors. However the volume and rigidity of such hard-goods interfere with the body movement, and eventually obstructs it without necessarily preserving user wearer comfort.

Chapter 6

Sensing Though Stretch:

The Smart Stretchable Pants

Skin-tight sensors have shown to have the least accuracy error. Also the nature of stretch sensing requires the use of tighter garments in order to ensure that the garment is deformed during movement rather than sliding over the body surface.

Although non-skin-tight garments are optimal in a lot of cases, there remain cases where skin-tight stretchable pants are still “normal” everyday wear. Tight, stretchable pants made out of elastomeric fabrics are commonly used in a variety of physical activities, from running to yoga. Here, the extension of the fabric during body movement is measured by a stitched stretch sensor that stretches with the fabric without affecting elongation or recovery of the fabric properties and without restricting wearer movement. An analysis of the error introduced by different sizes and fabrics is also covered. In the next chapter, looser garments capable of sensing bend rather than stretch are explored.

In Part II, three types of stitches commonly used in apparel have been studied: the bottom-thread coverstitched sensor, with an almost linear inversely proportional analog output response; the top-thread coverstitched sensor, with an output that is a proportional linear response that saturates at ~15% stretch; and the overlock stitched sensor, different than the previous two because it must be integrated on textile edges, with a response that also saturates like the top-thread at similar stretch

percentage but with smaller equivalent resistance amplitude than the top-thread coverstitched sensor.

To recall the output response of the stitched sensors presented, figure 6.1 shows the three stitched stretch sensors responses of 3” long un-insulated sensors when repeatedly stretched and relaxed for about 25% of the sensor length with an INSTRON tensile machine [58]: bottom-thread coverstitched sensor in blue (rhombus); top-thread coverstitched sensor in purple (star); overlock sensor in green (circle). 25% stretch is typically a reference stretch for experiments covered here, meaningful in the stretch capture of a sensor placed across the knee on a pair of skin-tight stretchable pants with a stretch smaller than skin stretch: across the knee, the skin stretches from 35-45% during normal joint movement [45].

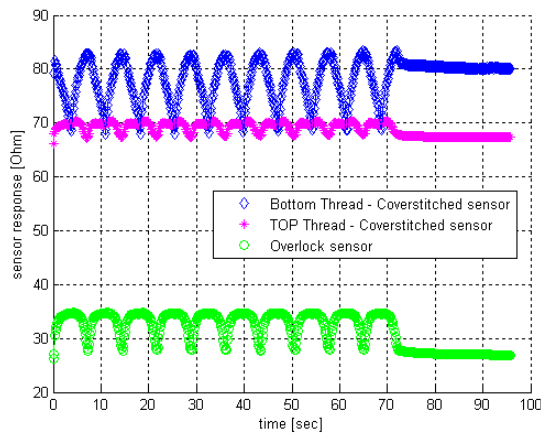


Figure 6.1. Stitched Stretch Sensor responses of 3” long sensors for 25% elongation (.75”)

Both top-thread and overlock stitched sensors exhibit saturation almost immediately, while the bottom-thread sensor keeps decreasing its response until eventually the stitch and/or fabric break due to excessive stretch. This makes the bottom-thread coverstitched sensor more suited to sense

more and larger stretches, for the same stitch length. The bottom-thread coverstitched sensor is used here.

6.1 The Bottom-Thread Coverstitched Sensor Validation

To evaluate variability in sensors due to variables of the stitching process (variations in machine tension, fabric feed, and loop formation within the stitch), three bottom-thread un-insulated coverstitched sensors of identical length (5") were tested in a controlled condition using an INSTRON tensile tester. Each sensor was stretched to 25% of its original length 10 times. Variability in sensor response was evaluated by calculating the variance between the peak-to-peak responses over all trials.

Results of this experiment showed an average standard deviation of 0.39 Ohms. Figure 6.2 shows sensor responses normalized with respect to extension, however variability was computed on non-normalized sensor responses. Peak-to-peak response was 10.06 ohms (average over all cycles/sensors), therefore, a variability of 0.39 Ohms represents 3.88% of the response.

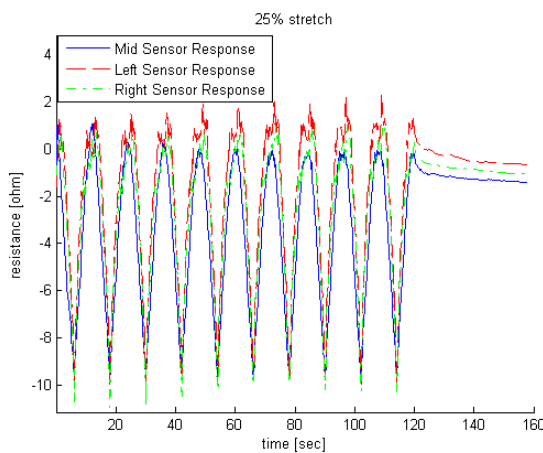


Figure 6.2. Tensile Evaluation of un-insulated Sensor Response

If the total response were mapped to the angular change during knee flexion, this would be 2.85 degrees of the total range of motion. Most goniometers used in practice report error on the order of 2-4 degrees, therefore this can be considered similar performance. In general, knee extension (equivalent to the recovery phase of the sensor) seems to be more prone to error than knee flexion (equivalent to the extension phase of the sensor). This is likely due to hysteresis in the fabric mechanics, as already observed in the fabrics test with overlock sensors discussed in Chapter 4.

6.2 Sample Garments and Sensors Location

The initial positioning of the pants may not be the same for different trials as discussed in Chapter 3, which means that a sensor placed in the center of the knee can instead be horizontally shifted to the left or right of center. To approximate this movement, two additional sensors were integrated $\frac{1}{4}$ " apart on the left and right side of the sensor in the very middle. This approach approximates in some ways (especially with donning/doffing) the effect that might be seen in a looser garment. Moreover, apparel manufacturing techniques used to integrate our garment-integrated stitched stretch sensors are affected by many imprecision variables such as sensor placement, stitch length or stitch structure, as will be discussed in the model analysis next [59].

Figure 6.3 shows the mannequin setup and un-insulated sensors integrated across the knee. The DMM probes were directly clipped on the garment, connected to the sensors leads. The probes connection is not secured on the garment, thus garment movements will introduce noise in the sensors output readings due to the probes movement.



Figure 6.3. From left-to-right: Bottom-thread coverstitched sensors stitched on the frontal side of the left knee of an animatronic mannequin. Alligator clip connection - zoom. Experiment Setup

Consistent knee bends were evaluated using the same animatronic mannequin of Part II. The running mannequin repeats over time the same basic running gait cycle, without completely extending his leg, therefore achieving a maximum extension and flexion of ~ 50 - 120 deg, measured with a traditional manual goniometer. At maximum extension, the maximum pants stretch is located on the very front of the knee and is equal to about 2”.

6.3 Knee angle prediction: Maximum Knee Stretch-based Method

Using the setup illustrated in the previous section 6.2 the garment-integrated sensors in the stretchable pants were evaluated using the animatronic running mannequin, while the sensor resistance was measured using a DMM directly connected to the stitched stretch sensor. A reference measure for joint angle is found using VICON motion capture system with three retroreflective markers placed across the joint [46]. The VICON graph function “angle between three points” was used to compute angle estimates. Because the mannequin performs a reliable,

repeatable gait cycle, the reference joint angles were captured separately with no garment on the mannequin. A reference heel marker was then used to map the mannequin running cycles of the test trials to align the corresponding stretch sensor output with the true joint angle reference capture.

5 consecutive trials were tested with 10 gait cycles each. Each trial starts from the second gait cycle, since the first one was used for alignment between VICON and DMM data. The first maximum resistance value of the trial which corresponds to the fully straight leg position of the mannequin at the second cycle was considered for alignment. Offsets in sensor responses are removed from all trials (i.e., all trials starting from zero ohm). Between trials pants were taken off and put back on the mannequin (Donning and Doffing) to induce variability in sensor output due to initial placement of the garment. The very first trial was used to build a model of the sensor's behavior that maps the sensor's output to knee angle.

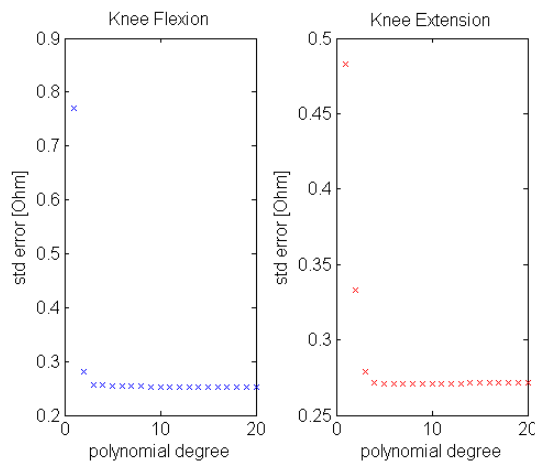


Figure 6.4. The polynomial model std error, for knee bend angle prediction

The model for each sensor's behavior is found by solving in the least square sense the curve fitting problem for knee flexion and extension of the first trial separately. Knee flexion and extension phases are found after alignment with true knee bend angle reconstructed from VICON captures. A polynomial of degree equal to 4 was found to best fit the sensors output data points both knee flexion and extension phases. Figure 6.4 shows an example of the least-squares analysis of the model for the Basic size: for a polynomial of degree 4 the standard error during both knee extension and recovery phases shown in figure 6.4 settles to its minimum, thus the 4th degree polynomial is used to fit the data points resistance [ohm] vs bend angle [deg].

The response of the sensor in the subsequent trials is then compared to the model using an error calculation. For each data point the difference between bend angle predicted by the model and the true knee bend angle for the trial that is known from a parallel VICON capture results in the bend angle error. The bend angle error is in this context the metric to compare sensor responses.

Angle Prediction Error Analysis: Sensors Location Example

To test the accuracy of the method, the three sensors spaced ¼” apart on the very front of the knee were captured by 3 consecutive trials, one trial per sensor. Sensors are about 5” long and integrated on a skin-tight pair of pants, later referred as Base size. The sensor in the middle is used to build the model by solving the curve fitting least square problem to map sensor resistance output to true bend angle estimated with the function “angle between three points” of a VICON system. The model is then used to predict the other two sensors on the sides. Pants are assumed to be in the same location between consecutive trials.

The three front sensors output responses are recorded for 11 consecutive cycles. Removing from each sensor response the offset given by the sensor output value for full knee extension, result in the sensors raw data shown in figure 6.5.

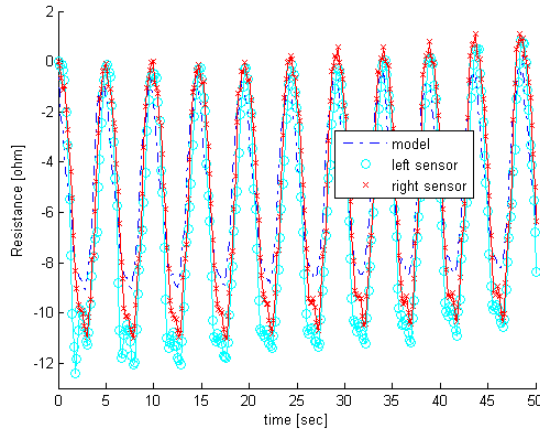


Figure 6.5. Maximum stretch region sensors responses: middle sensor (used as model), sensor spaced ¼” on the left; sensor space ¼” on the right

Using the middle sensor (or model) to map the knee bend angle from lateral sensors responses and the response of the middle sensor itself, the errors in table 6.1 given by the difference between predicted knee angle from the model and true knee angle from the VICON capture are evaluated.

Table 6.1. Knee bend prediction error

Trials no.	Angle Estimation Error
¼” Left Sensor	Flexion = 11.52°; Extension = 8.68°
¼” Right Sensor	Flexion = 7.04°; Extension = 6.31°
Middle Sensor Itself	Flexion = 3.09°; Extension = 2.81°

The angle prediction errors all combined results in an average prediction error of ~ 5.75 deg compared to the true reference angle calculated with VICON for each trial. The error appears larger in the sensor on the left, while the other two sensors were occupying a more central position with the sensor in the middle that has the lowest error for both knee flexion and extension.

The less practical case of normalized resistance where the sensors outputs are normalized by the maximum resistance value recorded over the 11 gait cycles, brings down the average prediction error to ~ 4.95 deg. The normalization has less effect on the error of the sensor in the middle because it was used to build the model thus the output range of the middle sensor between maximum and minimum values is the same as in the model. This shows the impact on the error estimates due to sensor location. A smaller value of the prediction error is evaluated if the normalization is done on a single gait cycle basis.

The estimated errors of the middle sensor reported in table 6.1 show what the error is in the ideal case by building the model from one trial of the sensor (no donning/doffing), and then comparing it to itself. Next sections show the effects of the “inhumanly ideal” case of pinned sensors with different length over donning and doffing cycles and of the donning and doffing cycles alone for three different sizes.

6.4 Variability in Sensor

Just as manufacturing tolerances affect the resulting dimensions of the finished garments, stitched sensors may also be subject to variability due to sewing tolerances. The sensors evaluated here have finished dimensions of 4.5”, 5” and 6”, and are integrated on the frontal side of the knee. To

evaluate the effect of sensor dimension separately from garment dimension, the sensors are evaluated in one trial of 10 gait cycles using the same alignment and offset-removal methodology for the Donning and Doffing trials described in the second paragraph of the previous section 6.3, while pinned directly to the mannequin’s body. Garments are pinned to the same body landmarks on the mannequin, such that they experienced the same stretch and variations in response which could be attributed entirely to variability in the sensor length.

For all three possible combinations using one sensor (in one garment size) to predict the other sensors, an average flexion error overall of 8.16deg and an average extension error of 11.02deg for between-sensors comparisons, and of 4.20deg (flexion) and 4.67deg (extension) for within-sensors comparisons are computed. In Table 6.2, ‘Model’ refers to the length of the sensor used to build the model while ‘Trials’ refers to the length of the sensors used to predict the knee bend angle relying upon the model.

Table 6.2. Knee Bend (pinned) – Between- and Within-sensors Error

Model	Trials	Avg. Flexion Error (deg)	Avg. Extension Error (deg)
4.5”	4.5”	2.60	4.28
4.5”	5”	7.02	10.21
4.5”	6”	10.43	6.93
5”	4.5”	9.01	13.08
5”	5”	6.35	6.57
5”	6”	5.72	12.16
6”	5”	4.63	11.37
6”	4.5”	12.15	12.39
6”	6”	3.66	3.15

When sensors are measured on the body in a restricted position (the pinned case), error is measured on the order of 2-6 degrees, a similar range that also approximates performance of commercial goniometers. This indicates that the sensor itself remains reliable when used to measure joint movements. However, the between-sensors estimation in the pinned sensors case (cross-estimation of angular measurement using a model built from one pinned sensor) showed that differences in sensor lengths have a larger impact on prediction accuracy between sensors than imperfections due to variability in stitching. Variability in length increases the error to the 5-15 degree range, which is greater than the error experienced by off-the-shelf goniometers. While it may remain in the usable range for applications like activity monitoring, it is clear that manufacturing tolerances for sensor length must be far more stringent than those for garment dimensions.

6.5 Variability in Size

Sensors were integrated in the middle of the knee on the frontal side into custom stretchable pants, made of an 82% Nylon/18% Spandex jersey-knit fabric. The base trouser pattern was custom-fitted to the electronic running mannequin precisely, with no wearing ease. Three pairs of trousers were fabricated to simulate variability in sewing tolerances: the “Base” size was fabricated to specifications exactly, the “Small” size was fabricated $-1/4$ ” below the hemi-circumference specifications, and the “Large” size was fabricated $+1/4$ ” above the hemi-circumference specifications. For stretchy garments like these, those tolerances represent a good-quality product. Sewing tolerances for lower-quality products are often much larger.

The results of donning/doffing trials for the three garment sizes are shown in table 6.3. For each size, sensor response is characterized in the initial trial and subsequent trials are compared to that model (sensor error compared to the model of that sensor).

Table 6.3. Knee Bend – Within-sizes Error by Size

Size	Average Flexion Error (Degrees)	Average Extension Error (Degrees)
Small	9.44	9.23
Base	8.55	9.81
Large	8.53	10.70

To simulate the effect of building a model of the sensor in one condition which is then used to translate the response of a different sensor from Ohms to Degrees, the Base size model is used to predict donning/doffing trials of Small and Large sizes, with an average overall error for the Small size of 11.26deg, for the Basic size itself of 9.18deg, and for the Large of 13.50deg, as indicated on table 6.4.

Table 6.4. Knee Bend – Between-sizes Error

Model	Trials	Avg. Flexion Error (Degrees)	Avg. Extension Error (Degrees)
Base	Small	10.21	12.31
	Base	8.55	9.81
	Large	17.09	9.91

Clear differences between “sizes” are not observed, indicating that variability within the scope of sewing tolerances may not have a significant effect on sensor accuracy, and certainly less effect than positioning has. Approaches to garment-integrated goniometry that take into account the potential variability in positioning (such as using redundant sensors and a sensor-selection algorithm) may help in minimizing the effect of positioning error.

6.6 Human Tests

The stretchable pants of figure 6.3 are now tested by a human subject. The response of the stretch sensor located in the region of maximum extension on the frontal side of the knee is recorded using a DMM directly connected to the sensor, similarly to the approach followed in the mannequin captures. Using the same mocap system in the same lab setting seen so far for the mannequin, the human subject is asked to walk at 1 and 2 MPH on a treadmill and to perform some basic knee bends while in place, called here static movements, involving different degrees of knee bend such as knee bends while standing still, sitting on a chair and squatting.[1] The location of the markers is the same as in the mannequin, presented in section 6.3. Thus, using three markers placed across the knee, the true knee bend angle of the subject is computed from the markers location. Figures 6.6 and 6.7 show the raw resistance data collected for different static positions and walk speeds and the corresponding knee bend angle reconstructed from VICON data, on time intervals between 10 and 20 seconds so to allow for the same number of repetitions.

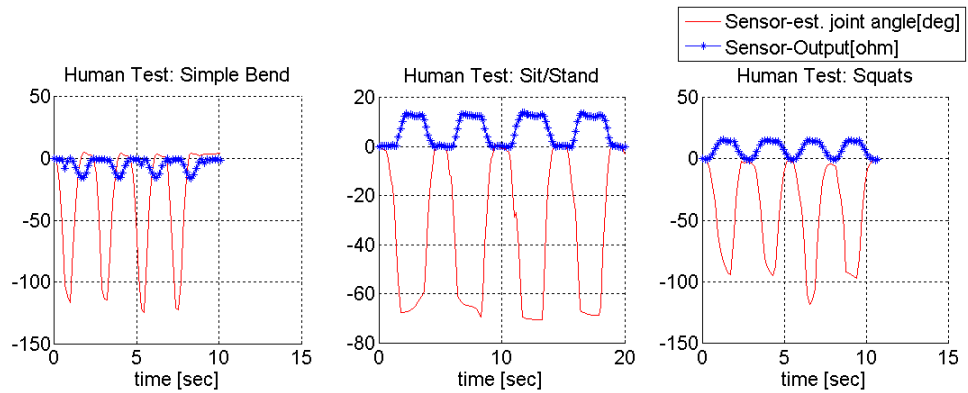


Figure 6.6. Human Squats, Knee Bend, and Sit for 5 knee bend repetitions. Sensor output (dotted blue line) aligned with actual (VICON) angle (red line)

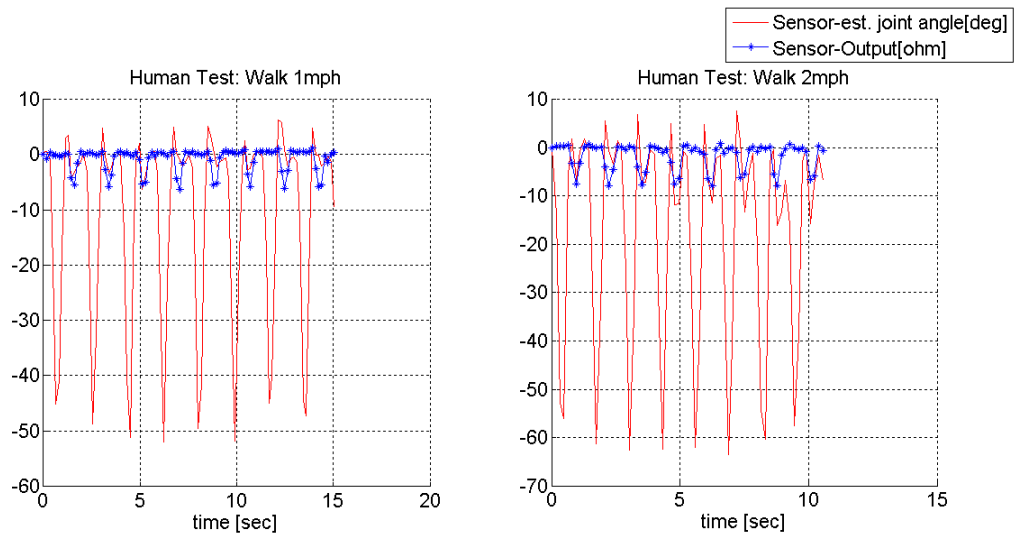


Figure 6.7. Human Walk @ 1MPH and 2MPH for 8 steps Sensor output (dotted blue line) aligned with actual (VICON) angle (red line)

Human Tests Discussion

The method used to reconstruct the knee bend is based on retro-reflective markers captured by VICON Infrared cameras. In the case of human tests, the location of the markers in the space is more variable and potential markers occlusions from the cameras are more likely especially for un-controlled movements, if compared to the mannequin case. This limitation makes the mocap based method used for the mannequin tests not precise to develop the true knee bend angle prediction error type of analysis for the human case. Thus an analysis based on the linear correlation between approximated knee bend angle and sensor output data is conducted. It shows good correlation for values of static positions and less for dynamic walk: $\rho_{\text{SimpleBend}} = -.71$; $\rho_{\text{SitStand}} = -.89$; $\rho_{\text{Squats}} = -.82$; $\rho_{\text{Walk@1MPH}} = -.25$; $\rho_{\text{Walk@2MPH}} = -.29$. Simple bend showed lower correlation among static positions, most likely because it is less controlled and repeatable; both walks showed an even smaller correlation, likely because of the additional larger variability of the markers position in the space during the walk: for example, the reference marker on the left heel is occluded during each step causing misalignment between consecutive steps. Sit/Stand and Squats movement showed the largest correlation with Sit/Stand that showed the largest correlation. The latter is also the most controlled type of movement tested with a chair setting a fixed reference for the knee bend when the subject was seated. For all scenarios tested, as the knee bends (thus the knee bend angle increases) the sensor output decreases because the sensor is stretched. In the Sit/Stand and Squats movements, the trend of the sensor is shown more clearly because of the slower and more controlled speed motion of the transition, compared to the other cases. Simple bend and both walks are characterized by the same transition where the resistance decreases during the bend, and quickly increases when the knee starts to extend again. For the fully flexed knee, markers are occluded and thus the approximated angle reconstruction is smoothed and noisy at the max. Part of the noise in the readings is introduced by the loose

connection between DMM probes and sensor leads, which effect is more visible on the treadmill tests.

Correlations of Sit/Stand and Squats poses suffer less of the method limitation to capture the sensor output, and show sensor output correlation very close to the sensor correlation estimated in the reference case on a one-dimensional linear stretch with INSTRON machine, as computed in section 4.3.

Sensing the knee angle through garment integrated sensing has shown to be a possibility. Relying on a basic approach that does not introduce additional data processing but rely on the sensors raw data to capture the knee bend from corresponding garment stretch, stitched stretch sensors have shown prediction errors on the same order of digital goniometers and other wearable sensing techniques. Pants size to allow for garment stretch after knee bend; sensors placement to absorb the maximum knee bend from the garment stretch; and manufacturing precision so to have reliable sensors identical to the specs are all source of errors that corrupt quality and accuracy of the prediction.

Tight-size pants and central sensor location across the frontal side of the knee are the recommended setting for a reliable solution based on stitched stretch sensor to capture the knee bend, as also justified by the human trials results that ended up being worse than the mannequin. Part of the reason is due to the fact that pants fit tight the mannequin but not as much on the human subjects where instead the pants are looser causing the sensor to move more and to be misplaced from the region of maximum stretch, on the very front of the knee.

6.7 Potential Source of Error

The method used to run the experiment introduces background noise to the data. Figure 6.3 shows how the placement of the DMM probes to measure the sensor is subject to human error to setup the experiment, since probes may not be connected in exactly the same relative position for each sensor. Further, the contact points between probes and conductive thread are not the same because the alligator clip can clamp differently the conductive yarn placed at the extremity of the sensor.

Moreover, applying the sensor on the region of maximum stretch of tight pants results in a bias caused by the body pushing on the sensor during bend. When the knee bends the fabric is stretched and at the same time the knee pushes against the stitch from the inside, compressing the conductive yarn of the stitch and resulting in an additional decrease of the resistance since the conductive filaments in the yarn are brought into closer contact.

A more practical application would probably use a printed board capable to capture the three sensors at the same time scarifying however the calibration precision of the DMM, and would compensate for the additional decrease in resistance due to yarn compression.

Chapter 7

Sensing Through Bend:

The Smart Jeans

Un-stretchable fabrics are often used in clothing items that look and feel looser on the body, but still show correlations with joint and more generally body movement. The fabric folding behavior of a pair of jeans during knee bend is here captured through a garment integrated stitched sensor. Sensor output is shown to be highly correlated with knee bend.

In the previous chapter, tighter garments are needed to sense stretch. However, skin-tight garment may be problematic to wear, for example in the case of elder people. This chapter explores loose-fitting garments that are still capable of sensing joint position by substituting bend for stretch.

7.1 The Folding Method

Human joint bends generate clothes folds and wrinkles. For example, a long sleeve shirt or a pair of pants folds during an elbow or knee flexion whether the garment is skin-tight or not. Likewise as the joint extends folds are recovered. Thus folding reflects information regarding the body movement from whence it is originated. The folding behavior as a means to provide information about the joint bend is here implemented by using the bottom-thread coverstitched sensor

discussed in chapter 5, and evaluated in a controlled scenario based on the repeatable animatronic mannequin run and on a human subject focusing on the knee joint.

7.2 Jeans Preparation

The same jeans model 52735 size +1 of Part I are used in this study. Two un-insulated bottom-thread coverstitched sensors 5" and 6" long were integrated on the dorsal and lateral side of the jeans left leg respectively, centered around the mannequin's knee height as depicted on figure 7.1.

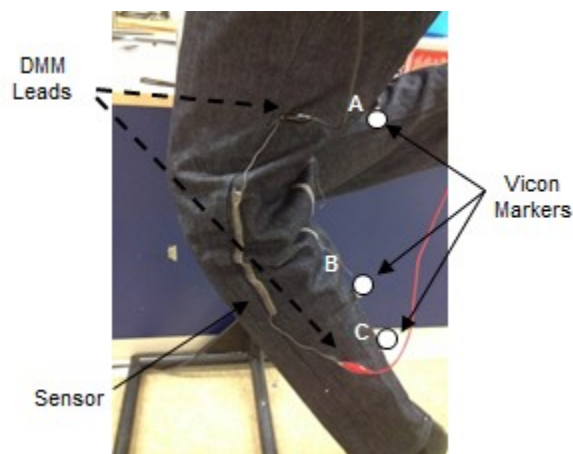


Figure 7.1. Bottom-thread coverstitched sensor integration, and experiment setup

Figure 7.1 shows that the sensor output was captured using the standard approach adopted here of connecting the DMM probes directly to the sensors leads. Using the same approach seen in the previous chapter, three VICON markers were opportunely placed on the dorsal side of the left leg so as to extrapolate an estimate for the knee joint angle computed as a scaled version of two intersecting lines \overline{AB} and \overline{BC} . The dorsal side of the knee was the best location where to locate

the markers to better approximate the knee joint bend, given the movements of the jeans during knee bend. The symmetry between left and right leg of the mannequin allowed the positioning of a reference marker on the right heel to align the repeated gait cycle, while another reference marker placed on the left side of the waist was used to translate the origin of all other markers and to compensate the bouncing effect generated by the metallic arm holding the mannequin, as described in Part I. The left leg of the mannequin has always been the preferred choice for the sensor location because it is more accessible (indeed the entire left side) than the right leg, which faces the metal support arm.

7.2.1 Source of Error

The least stiff fabric was originally chosen prior to the characterization of the bend sensor properties over different fabrics presented in chapter 5 because of its tendency to generate folds, and size +1 was chosen because it was loose enough to allow room for fold generation while maintaining good correlation of folding/unfolding with the knee flexion/extension. However, chapter 5 results suggest that a more stiff fabric would have led to higher average sensitivity and peak-to-peak response, but lower linearity.

7.3 Mannequin Tests

The mannequin gait cycles were captured over 9 consecutive trials, of 5 cycles each. The sensors' output was captured separately using the same method used to measure the pants stretch sensors output, described in the paragraph 6.3. Figure 7.2 shows the knee's true angle reference computed by placing three markers in the locations specified in the previous paragraph but attached directly on the mannequin, aligned with the two lateral and dorsal bend sensors responses over 5

consecutive cycles for 9 distinct trials. Sensors were kept un-insulated because they can generate a larger shorting response when the sensor is self-shortened. This is a great advantage especially for the dorsal sensor which output depends on the sensor shorting with itself.

For both dorsal and lateral sensors mean and standard deviation of 4 metrics are computed: Initial baseline resistance; peak-to-peak; slope of linear response; hysteresis area. All 4 metrics are averaged over the trials.

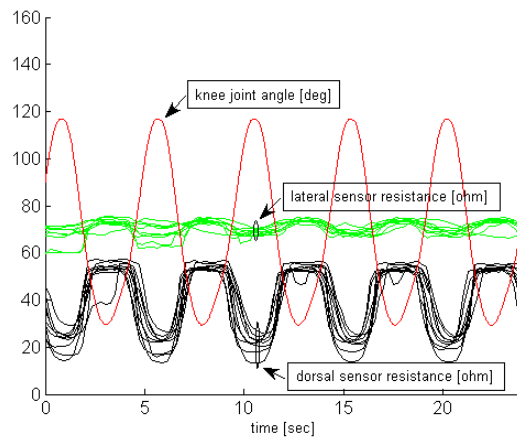


Figure 7.2. Aggregate responses of dorsal and lateral sensors, compared to true knee joint angle

As originally described in the experiment setup of section 4.2.1, DMM and VICON captures are aligned using time-stamps and the higher-frequency VICON's data is reduced to the DMM frequency, in order to allow statistical analysis.

Mannequin Tests Discussion

The peak of the knee joint angle represents maximum flexion, and the trough represents maximum extension. Using the mannequin as reference, the correlation coefficient between the dorsal sensor response and the VICON knee angle is measured at 0.81, and for the lateral sensor is 0.78. The range of resistance output values for the lateral sensor is about 10 Ohms, while for the dorsal sensor is about 45 Ohms [46].

As observed in the previous section, the approach used to connect the DMM to the sensors introduces additional noise in the measured sensors output due to the movements of the alligator clips directly attached on the garment to connect to the sensor leads.

Table 7.1 shows that the dorsal sensor has the largest peak-to-peak sensor response (these are self-intersecting folds). The switch-like behavior during self-intersection is seen in the much larger slope of the linear region of the dorsal sensor's response. The dorsal sensor also shows a much larger hysteresis response (calculated here as the area between the extension and recovery curves), which is likely due to differences in the relationship between joint angle and intersection point of the sensor. The discrepancy in initial resistance is due to the extra 1" length of the lateral sensor [46].

Table 7.1. Sensor characteristic, mannequin tests

Metric	Dorsal Average	Dorsal St Dev	Lateral Average	Lateral St Dev
Initial resistance	54.77 Ω	1.75 Ω	73.78 Ω	1.16 Ω
Peak-to-peak response	33.33 Ω	4.05 Ω	6.20 Ω	1.41 Ω
Slope of linear response	-0.52 Ω/Deg	0.13 Ω/Deg	-0.19 Ω/Deg	0.35 Ω/Deg
Hysteresis area	49.49 $\Omega*\text{Deg}$	34.81 $\Omega*\text{Deg}$	16.70 $\Omega*\text{Deg}$	7.13 $\Omega*\text{Deg}$

The initial hypothesis of this study was that sensor responses would only be evident as binary, switch-like changes in resistance when self-intersecting folds were experienced. The direct answer to that hypothesis is that self-intersection is observed every cycle for the dorsal sensor but no self-intersection for the lateral sensor. Both sensors displayed a detectable response to self-intersecting folds, 100% of the time, simulating donning and doffing effects between the trials to “re-settle” the pants. The dorsal sensor displayed a much more drastic change in resistance, consistent with the switch-like behavior expected, that could be smoothed to a square wave. The sensor never failed to short (by folding along a non-perpendicular axis), even during the highest-activity squat trials. Even in the dorsal sensor the sensor response observed is not fully binary, but include a linear region before the sensor shorts during the self-intersecting portion of the fold. As seen from the lateral sensor, these “bend” deformation effects result in a much smaller resistance range (about 4 times smaller than when shorting across a self-intersection), and are more variable. However, they may still provide a useful input to an activity-recognition system, for instance [46].

7.4 Human Tests

While the mannequin is able to provide a consistent, cyclical movement, humans are not able to repeat movements with this reliability. However, testing on a human subject allows more realistic and varied knee movements to be evaluated. In this study, one human subject was asked to perform five repetitions of three basic movements wearing the jeans illustrated on figure 7.1 [46]:

1. Simple knee bend: from a standing position, the subject is asked to completely flex the knee (standing on one foot) and then to completely extend it again;
2. Sit/Stand: from a standing position and using a chair as reference, the subject is asked to sit and stand up again;
3. Squats: from a standing position, the subject is asked to squat in place, and stand up again.

Sensors output response are recorded and aligned with the knee bend angle data based on VICON measurements of the retro-reflective markers locations on the 3-D space. Markers are placed directly on the jeans.

Figure 7.3 shows the output responses from such basic movements aligned with respect to the estimated knee joint angle.

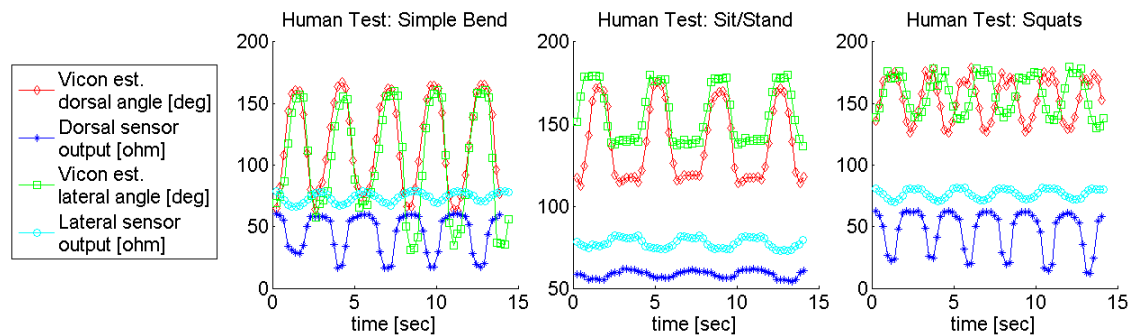


Figure 7.3. Sensor responses and joint angle for human knee bend task, sit/stand task, and squat task

Human Test Discussion

In the human subject trials, for simple knee bends, the correlation coefficient between the VICON angle and the dorsal sensor is 0.88, and for the lateral sensor is 0.85. For the sit/stand trial, these values are 0.75 for the dorsal sensor and 0.88 for the lateral sensor, and for the squat trial, 0.78 for the dorsal sensor and 0.89 for the lateral sensor. Except for the simple knee bend where both sensors have close correlation values, the lateral sensor output shows higher correlation with the VICON angle than the dorsal sensor: sitting on a chair implies dorsal sensor compression between chair and knee, as well as squatting all the way implies dorsal sensor shorting with itself. Such shorting behaviors that are less likely to happen in the simple knee bend (because limited to about 90 deg bend) are attributed as the cause for the lower correlation value of the dorsal sensor in both sit/stand and squat trials.

As observed before, both sensors displayed a detectable response to self-intersecting folds, 100% of the time, both in mannequin tests where the trousers were “re-settled” between trials to simulate effects of donning and doffing, and in human trials where the movement of the garment is less consistent.

Part III. Conclusion

A novel garment-integrated sensing application has been presented. The experiment design reflects the theory developed in the previous chapters. From an initial characterization of the three sensors used, repeated INSTRON gait cycles showed excellent consistency of sensors output with an average standard deviation of 0.39 Ohms. Successfully, strategic locations around the knee are heuristically found for the stitched sensor to fully capture the garment stretch and bend

behavior during body movement. Error sources are found to be related to the fabric properties and the tendency of generate fold. The least stiff fabric is chosen for its ability to generate more folds than a stiffer fabric. Controlled movements are measured using an animatronic mannequin and a human subject. In both cases, repeatable and consistent outputs were measured.

As in Chapter 6, the minimal processing on the sensors output response is referred to the sensors raw data. This process captures and characterizes the accuracy of the sensors when used in the realistic case, i.e. by the human knee joint. The good linearity property of the sensors shows that the sensors are less affected by variability in properties due to manufacturing. The good linearity property of the sensors shows that the sensor response is less affected by variability in properties due to manufacturing. This allows sensor response to be based on relative changes instead of relying on calibrating the sensor, since in some applications it does not matter where the sensor response starts as long as the slope is the same.

The stitched sensors are shown capable to capture the correlation between garment movement and body movement. The stitched stretch sensor integration on the region of maximum pants stretch during knee bend predicted the bend angle with an error that is in the same order of magnitude as the errors of comparable wearable sensing solutions. In the ideal case where the stretch sensor used to build the model is predicted by the model itself, the lowest estimation error was found equal to $\sim 3\text{deg}$, comparable to the ISTRON tests. Adding sensing variability due to the manufacturing process, difference in sizes and the more realistic donning and doffing the knee bend estimation error on average increased anywhere from 1 to 14deg at the most. The stitched bend sensor integrated in the two lateral and dorsal folding regions around the knee reliably captured the folds showing good correlation with the knee bend angle. Both sensor locations showed good accuracy and excellent repeatability in the spectrum of wearable sensing solution.

In the human case, the testing method setup is not suited to capture dynamic movements, such as walking on a treadmill. However, in the human case for controlled types of knee bends (simple bend, squats, sit/stand) for both stretch and bend sensor solutions linear correlations are found between 0.71 and 0.89, comparable with correlation coefficients of Universal and Digital goniometers used by physical therapist in a clinical setting [60] [61]. The potentials of stitched sensors for clinical applications open to less critical application scenarios such as activity recognition where the margins on the prediction error tend in general to be wider: for example to recognize whether a subject is standing or seating rather than knowing in detail the joint bend degree.

Insulated sensors were not considered in the final evaluation for both stretch and bend sensors primarily because of the smaller amplitude of the sensors output which would require additional amplification that was not considered in this context. Moreover, as earlier stated for the case of water, insulation as presented here would not protect from sweat that would penetrate through the fabric to the sensor causing a short in the sensor and yarn deterioration.

Bend sensing is open to the possibility of more comfortable garment-integrated sensing through looser garments. As understood from the beginning, a looser garment will have more variability and randomness in the movement which additionally corrupts the output of the sensor. Additional garment-integrated sensors are thus required, for example an array of stitched sensors, so to correlate the output of many redundant sensors. These additional sensors allow the best prediction based on the best sensors output. Strategies and algorithms are required to collect the sensors data and then decide the best output. Ideally, such strategies and algorithms would need to be garment independent. Garment independence denotes that should work independently from size and fit of the garment. Looser garments are in general more comfortable than skin-tight garment and more likely to be worn for a longer period of time. The need for more accurate,

reliable, and robust garment-integrated sensing through looser clothes is essential to enable comfortable long-term body monitoring.

The accuracy of the sensors is critical to define the type of application, i.e. from activity recognition to medical applications. For example, Drift and hysteresis of the sensors as well as slippage of the garment over the body are factors that affect the quality of the estimates since the sensors output could be off from what expected or different between flexion and extension phases.

Final Conclusion

Clothing is in everyone's life and an important part of how humans perceive and identify themselves. People may want to look professional and stylish at work while they tend to look more comfortable and "less attractive" when home for example. Clothes provide this transformation throughout the week. Clothing promotes feelings of wellbeing depending on the technical and aesthetic concerns of the wearer as well as the social, cultural and health perspective. Acceptance and comfort properties need to be preserved when clothes are used as platforms for wearable technologies. Successful wearable technology works effectively and the wearer is unconditionally willing to use because it is compatible with the physiology of the wearer allowing for desired fit, shape and size, ease of movement and use.

Detecting and measuring human movements is one of the most compelling applications of wearable technology [46]. The ability to capture information through the clothes already worn overcomes barriers related to user acceptance and comfort, while minimizing the application time. The theory and fundamentals of garment-integrated sensing explored in Part I showed that the noise distribution due to the garment movement can be characterized and quantified. Additionally it was specified that in reference to the lower body the hip region should be avoided for body sensing. The novel sensor application introduced in Part II allows for a direct implementation on the garment for body sensing in a comfortable and unnoticeable way. This sensor application also provides for a simplified manufacturing process. The evaluation of the knee bend in Part III showed the same repeatable response of the sensors for heuristic locations. Both sensors exhibited good correlation properties and comparable accuracy with existing wearable sensing solutions.

Future Work

In addition to accuracy and comfort there is an effect on aesthetic and style of the wearable solution. The sensing implementations presented here in the last two chapters (particularly for the cases where stitches are integrated on the frontal and dorsal side of the knee) may require a new concept of style in the garment design with stitches on the front and back side of the pants; or, additional artifacts in the garment structure: for example, an additional fabric layer on the pants to hide the sensors. The effect on garment aesthetics and style open to a new tradeoff between aesthetics “constraints” and garment-integrated sensors design.

Body monitoring potentials of garment-integrated wearable sensing are primarily limited by the difficulties of integration between apparel and electronics. Requirements and expertise are historically defined different between clothes and electronic devices with. These industries have placed different emphasis on various quality requirements: for example comfort vs accuracy, respectively.

Garment integrated sensing using the method presented in this work simplifies and streamlines the manufacturing process. This simplification is possible because stretch and bend stitched sensors are made with conductive yarns that re-use existing stitching machines and methodologies. However, as discussed here this method certainly adds additional limitations related to tolerance and variability during the fabrication process of the sensor. These limitations are countered by the benefit of comfort, perceptibility of the sensors, and an almost unconscious use that benefits the quality of the monitored data.

Wearable technology in this setting becomes truly wearable, because it is a part of the clothing. However, all the research presented here does not define a wearable “product” since it is missing

the basic components to make it practical in a real case, such as a processing unit, connection between sensors and processing unit, and battery for example. The additional listed parts would require new definitions in order to keep the maximal user comfort while preserving the garment aesthetics. New strategies are needed to find batteries of the right size and keep them charged during the day for long term monitoring, ideally. Washability of the fully assembled wearable solution for body monitoring is not a trivial challenge because electronics do not survive wash cycles as clothes do. Thus some sort of insulation or removal would be needed for the processing unit and battery during cleaning of the clothing. Durability now becomes specific to each of the components that are not resistant in the same way to the same type of treatment and usage. In reality all components will generally be under the same conditions at the same time. Thus for a reliable, practical and wearable “product” to be created a significant amount of time and research effort will be needed for success and adoption.

Reference

- [1] L.E. Dunne, S.P. Ashdown, and B. Smyth, "Expanding Garment Functionality Using Embedded Electronic Technology," *Journal of Textiles and Apparel Technology and Management*, 2005, 4:3
- [2] G. Gioberto, "Measuring Joint Movement Through Garment-Integrated Wearable Sensing," *Ubiquitous Computing Adjunct Proc.*, Doctoral School, 2013, Zurich, Switzerland
- [3] E.R. Post, M. Orth, P.R. Russo, and N. Gershenfeld, "E-broidery: Design and fabrication of textile-based computing," *IBM Systems Journal*, IBM, 2000, Vol 39, pp. 840-860.
- [4] T. Martin, M. Jones, J. Edmison, and R. Shenoy, "Towards a design framework for wearable electronic textiles," *7th International Symposium on Wearable Computers*, Oct 21–24, 2003, pp. 190–199
- [5] C. Gopalsamy, S. Park, R. Rajamanickam, and S. Jayaraman, "The Wearable Motherboard™: The first generation of adaptive and responsive textile structures (ARTS) for medical applications," *Springer 1999*, Volume 4, Issue 3, pp 152-168
- [6] J. McCann and D. Bryson, "Smart Clothes and Wearable Technology," *Woodhead Publishing*, February 2009
- [7] D. Meoli, T.M. Plumlee, "Interactive Electronic Textile Development: A Review of Technologies," *Journal of Textile and Apparel, Technology and Management (JTATM)*, Vol.2-2; 2002

- [8] M. Costa, M. Cropley, J. Griffith, and A. Steptoe, "Ambulatory Blood Pressure Monitoring is Associated With Reduced Physical Activity During Everyday Life," *Psychosomatic Medicine*, 61, 806-811.
- [9] K. Bodine, and F. Gemperle, "Effects of Functionality on Perceived Comfort of Wearables," *Wearable Computing, 7th International Symposium on*, 2003, 57-61, White Plains, NY
- [10] K. Tunde, "Multidisciplinary know-how for smart-textiles developers," *Woodhead Publishing*, Cambridge, UK, Philadelphia, PA, 2013
- [11] J. Edmison, M. Jones, T. Lockhart, and T. Martin, "An E-textile System for Motion Analysis," *Proceedings of the International Workshop on New Generation of Wearable Computers for eHealth*, Lucca, Italy, December 2003, pp. 215-223
- [12] L.E. Dunne, P. Walsh, B. Smyth, and B. Caulfield, "Design and Evaluation of a Wearable Optical Sensor for Monitoring Seated Spinal Posture," *10th IEEE International Symposium on Wearable Computers*, Oct 2006, pp.65-68, Montreux
- [13] C. Einsmann, M. Quirk, B. Muzal, B. Venkatramani, T. Martin, and M. Jones, "Modeling a Wearable Full-body Motion Capture System," *9th IEEE International Symposium on Wearable Computers*, 18-21 Oct. 2005
- [14] C.-H. Yang, Z.-S. Lin, C.-L. Hu, Y.-S. Chen, L.-T. Ke, and Y.-R. Chen, "Novel Dynamic Sensing of Wearable Digital Textile Sensor with Body Motion Analysis," *32nd Annual International Conference of the IEEE Engineering in Medicine and Biology Society (EMBC)*, Buenos Aires, Argentina, August, 2010
- [15] Y.-W. Guo, W.-Z. Wang, G.-Z. Liu, G.-R. Zhao, B.-Y. Huang, Z.-Y. Mei, and L. Wang, "Body inertial-sensing platform for wearable 3D gesture analysis," *2011 International Symposium on Bioelectronics and Bioinformatics*, 2011, pp. 259-262, Suzhou

- [16] F. Gemperle, C. Kasabach, J. Stivoric, M. Bauer, and R. Martin, "Design for Wearability," *Digest of Papers. 2nd International Symposium on Wearable Computers*, 19-20 Oct. 1998, Pittsburgh, PA, USA
- [17] G. Gioberto, and L. E. Dunne, "Garment Positioning and Drift in Garment-Integrated Wearable Sensing," in *Proc. of the 16th IEEE International Symposium on Wearable Computers*, Newcastle, UK, 2012.
- [18] I.B. Lee, S.C. Shin, Y.W. Jang, Y.S. Song, J.-W. Jeong, and S. Kim, "Comparison of Conductive Fabric Sensor and Ag-AgCl sensor under Motion Artifacts," *30th International IEEE EMBS Conference*, Aug. 2008, pp 1300 - 1303.
- [19] M. Costa, M. Cropley, J. Griffith, and A. Steptoe, "Ambulatory Blood Pressure Monitoring Is Associated With Reduced Physical Activity During Everyday Life," *Psychosomatic Medicine*, vol. 61, no. 6, pp. 806-811, 1999.
- [20] O. Such and J. Muehlsteff, "The challenge of motion artifacts suppression in wearable monitoring solutions," in *Proc. of the IEEE Engineering in Medicine and Biology Conference*, 2006, pp. 49-52
- [21] K. Kunze and P. Lukowicz, "Dealing with sensor displacement in motion-based onbody activity recognition systems," in *Proc. Of the 10th International Conference on Ubiquitous computing*, NY, USA 2008, pp.20-29
- [22] I. Romero, T. Berset, D. Buxi, L. Brown, J. Penders, S. Kim, and N.V. Helleputte, "Motion artifact reduction in ambulatory ECG monitoring: an integrated system approach," in *Proc. Of the 2nd Conference on Wireless Health*, NY, USA, 2011, pp 11:1-11:8.

- [23] G. Lorussi, W. Rocchia, E. P. Scilingo, A. Tognetti, and D. D. Rossi, "Wearable, redundant fabric-based sensor arrays for reconstruction of body segment posture," *IEEE Sensors Journal*, vol.4, pp.807-818, 2004.
- [24] H. Harms, O. Amft, and G. Troster, "Influence of a loose-fitting sensing garment on posture recognition in rehabilitation," in *IEEE Biomedical Circuits and Systems Conference*, 2008, pp. 353-356.
- [25] H. Harms, O. Amft, and G. Troster, "Estimating Posture-Recognition Performance in Sensing Garments Using Geometric Wrinkle Modeling," *IEEE Transation on Information Technology in Biomedicine*, Brussels, Vol. 14, No. 6, Nov. 2010
- [26] L. E. Dunne, G. Gioberto, and H. Koo, "A Method of Measuring Garment Movement Error for Wearable Sensing," in *Proc. of the 13th IEEE International Symposium on Wearable Computers*, San Francisco, CA, 2011.
- [27] L. E. Dunne, G. Gioberto, V. Ramesh, and H. Koo, "Measuring movement of denim trousers for garment-integrated sensing applications," in *2011 Annual International Conference of the IEEE Engineering in Medicine and Biology Society, EMBC*, 2011, pp. 3990-3993.
- [28] L. Dunne, "Beyond the second skin: an experimental approach to addressing garment style and fit variables in the design of sensing garments," *International Journal of Fashion Design, Technology and Education*, vol.3, Nov. 2012, pp. 109-117.
- [29] A. Lymberis. "Wearable Smart Systems: From technologies to integrated systems," *33rd Annual Conference of IEEE EMBS*, 2011, Boston, MA, USA
- [30] C. Strohrmann, M. Rossi, B. Arnrich, and G. Troster, "A data-driven approach to kinematic analysis using wearable technology," *9th International Conference on Wearable and Implantable Body Sensor Networks*, 2012, London, UK

- [31] J. Edmison, M., Jones, Z. Nakad, and T. Martin, "Using Piezoelectric Materials for Wearable Electronic Textiles," *6th International Symposium on Wearable Computers*, 41-48, October 2002
- [32] M. Stoppa, and A. Chiolerio. "Wearable Electronics and Smart Textiles: A Critical Review," *MDPI Sensors Journal*, July 2014
- [33] C. Mattmann, F. Clemens, and G. Troster, "Sensor for Measuring Strain in Textile," *MDPI Sensors Journal*, 2008
- [34] O. Atalay, and W.R. Kennon, "Knitted strain sensors: Impact of Designing Parameters on Sensing properties," *MDPI Sensors Journal*, 2014
- [35] L. Dunne, S. Brady, B. Smyth, and D. Diamond, "Initial development and testing of a novel foam-based pressure sensor for wearable sensing," *J NeuroEngineering Rehabil*, 2(4), 2005.
- [36] D. De Rossi, F. Carpi, F. Lorussi, A. Mazzoldi, R. Paradiso, E.P. Scilingo, and A. Tognetti, "Electroactive fabrics and wearable biomonitors devices," *AUTEX Research Journal*, vol. 3, no. 4, pp. 180–185, 2003.
- [37] G. Alici, G.M. Spinks, J.D. Madden, Y. Wu, and G.G. Wallace, "Response Characterization of Electroactive Polymers as Mechanical Sensors," *Mechatronics, IEEE/ASME Transactions on*, vol. 13, no. 2, pp. 187 –196, Apr. 2008.
- [38] C. Rovira, S. Coyle, B. Corcoran, D. Diamond, F. Strojescu, and K. Daly, "Integration of textile-based sensors and Shimmer for breathing rate and volume measurement," *International Conference on Pervasive Computing Technologies for Healthcare*, 2011, pp. 238 –241.
- [39] G. Gioberto, L.E. Dunne, "Theory and Characterization of a Top-Thread Coverstitched Stretch Sensor," *IEEE International Conference on System, Man, and Cybernetic (SMC)*, 2012, Seoul, Korea

- [40] O. Atalay, W. R. Kennon, and M. D. Husain, "Textile-Based Weft Knitted Strain Sensors: Effect of Fabric Parameters on Sensor Properties.," *Sensors, MDPI* Aug. 2014
- [41] M.E. Berglund, J. Coughlin, G. Gioberto, and L.E. Dunne, "Washability of E-Textile Stretch Sensors and Sensor Insulation," *18th IEEE International Symposium on Wearable Computers*, Seattle, WA, 2014.
- [42] G. Gioberto, and L.E. Dunne, "Overlock-Stitched Stretch Sensors: Characterization and Effect of Fabric Property," *Journal of Textiles and Apparel Technology and Management (JTATM)*, 2013
- [43] G. Gioberto, and L.E. Dunne, "Garment Integrated Bend Sensor," *Electronics Journal*, Special Issue on Wearable Electronics, 2014.
- [44] L.E. Dunne, "Optical Bend Sensing for Wearable Goniometry: Exploring the Comfort/Accuracy Tradeoff," *Research Journal of Textile and Apparel (RJTA)* 2010, Vol. 14, No. 4
- [45] C.-M. Yang, T.L. Yang, W.T. Huang, C.-H. Chen, S.-H. Hung, C.-M. Cheng, and M.-H. Cheng, "A novel Design and Evaluation of Wearable Digital Sensor for Monitoring Posture," *IEEE EMBS, 30th International Conference*, 2008, Vancouver, Canada
- [46] G. Gioberto, J. Coughlin, K. Bibeau, and L.E. Dunne, "Detecting Bends and Fabric Folds using Stitched Sensors," *17th IEEE International Symposium on Wearable Computers*, Zurich, Switzerland 2013
- [47] H. Harms, O. Amft, and G. Tröster, "Modeling and simulation of sensor orientation errors in garments," in *Proceedings of the Fourth International Conference on Body Area Networks, ICST*, Brussels, Belgium, Belgium, 2009, pp. 20:1–20:8.

- [48] C. Mattmann, O. Amft, H. Harms, G. Troster, and F. Clemens, "Recognizing Upper Body Postures using Textile Strain Sensors," *11th IEEE International Symposium on Wearable Computers*, Boston, MA 2007
- [49] F. Lorussi, W. Rocchia, E.P. Scilingo, A. Tognetti, and D. De Rossi, "Wearable, Redundant Fabric-Based Sensor Arrays for Reconstruction of Body Segment Posture," *IEEE Sensors Journal*, Vol. 4, No. 6, December 2004
- [50] H. Harms, O. Amft, and G. Troster, "Influence of a loose-fitting sensing garment on posture recognition in rehabilitation," *Biomedical Circuits and Systems Conference, Baltimore, MD*, 2008
- [51] T. Martin, M. Jones, J. Edison, T. Sheikh, and Z. Nakad, "Modeling and simulating electronic textile applications," *Conference on Languages, Compilers, and Tools for Embedded Systems*, Washington, DC, 2004
- [52] J.F. Knight, D. Deen-Williams, T.N. Arvantis, C. Baber, S. Sotiriou, S. Anastopoulou, and M. Gargalakos, "Assessing the Wearability of Wearable Computers," *10th IEEE International Symposium on Wearable Computers*, Montreux, 2006
- [53] Y. Menguc, Y.-L. Park, E. Martinez-Villalpando, P. Aubin, M. Zisook, L. Stirling, R.J. Wood, and C.J., Walsh, "Soft Wearable Motion Sensing Suit for Lower Limb Biomechanics Measurements," *IEEE International Conference on Robotics and Automation, Karlsruhe, Germany* 2013
- [54] C. Mattmann, and G. Troster, "Design concept of clothing Recognizing back postures," *3rd International Summer School on Medical Devices and Biosensors*, Cambridge, MA, 2006
- [55] J. Favre, B.M. Jolles, R. Aissaoui, and K. Aminian, "Ambulatory measurement of 3D knee joint angle," *Journal of Biomechanics*, 41, 2008, 1029-1035

- [56] P.T. Gibbs, and H.H. Asada, "Wearable Conductive Fiber Sensor for Multi-Axis Human Joint Angle Measurements," *Journal of NeuroEngineering and Rehabilitation*, March 2005, 2:7
- [57] S. Bakhshi, and M.H. Mahoor, "Development of a Wearable Sensor System for Measuring Body Joint Flexion," *Body Sensor Networks, 2011 International Conference on*, May 2011, 35-40, Dallas, TX, USA
- [58] G. Gioberto, "Garment-Integrated Wearable Sensing for Knee Joint Monitoring," *18th International Symposium on Wearable Computing*, Doctoral School, Seattle, WA 2014
- [59] G. Gioberto, C.H. Min, C. Compton, and L.E. Dunne, "Lower-Limb Goniometry using Stitched Sensors: Effects of Manufacturing and Wear Variables," *18th IEEE International Symposium on Wearable Computers*, Seattle, WA 2014
- [60] L. Brosseau, S. Balmer, M. Tousignant, J.P. O'Sullivan, C. Goudreault, M Goudreault, and S. Gringras, "Intra- and Intertester reliability and criterion validity of the parallelogram and universal goniometers for measuring maximum active knee flexion and extension of patients with knee restrictions," *Physical Medicine and Rehabilitation*, Vol. 82(3), pp. 396-402, 2011
- [61] M.A. Carey, D.E. Laird, K.A. Murray, and J.R. Stevenson, "Reliability, validity, and clinical usability of a digital goniometer," *U.S. National Library of Medicine*, Vol.36(1), pp.55-66, 2010